BEYOND THE STANDARD MODEL WITH SUPERSYMMETRY

BY

Enrico Maria Sessolo

Submitted to the graduate degree program in Physics
and the Graduate Faculty of the University of Kansas
in partial fulfillment of the requirements for the degree of
Doctor of Philosophy.

Danny Marfatia
Chairperson

Committee members:

Hume Feldman

David Lerner

Douglas McKay

John Ralston

Date defended:

The Dissertation Committee for Enrico Maria Sessolo certifies
that this is the approved version of the following dissertation:

BEYOND THE STANDARD MODEL WITH SUPERSYMMETRY

Committee:

Danny Marfatia
Chairperson

Hume Feldman

David Lerner

Douglas McKay

John Ralston

Date approved:

Contents

Chapter 1

Introduction

The Standard Model (SM) of particle physics has been tested to an astonishing degree of accuracy during the years [1], thus providing the definitive theory that describes matter particles and their interactions, up to the electroweak energy scale. Nevertheless, the SM is incomplete. There are both experimental and theoretical arguments that call for an extension of the SM, or for a completely new theory whose "effective representation" at energies below the TeV scale matches the SM predictions. Some of the experimental facts that cannot be explained in the framework of the SM are of recent discovery, like the oscillations of neutrinos observed in solar and atmospherical data. Or the discovery of the accelerated expansion of the Universe, which leads to the need of explaining the "dark energy" that counterbalances the curbing effect of gravity on the rate of expansion. Some other experimental facts have been around for a longer time, like the existence of cold dark matter in the Universe, as it appears from Galaxy rotation and microwave background data. But there are also theoretical arguments for extending the SM, like the presence of a large numbers of parameters. Or the seemingly "ad hoc" choice of the gauge group and of the Higgs potential.

Of a slightly different nature is the so called *Hierarchy* or *Naturalness* problem. The fact that, if there are fundamental scalar fields (like the Higgs) in a chiral gauge theory, radiative corrections to the mass of those fields are quadratic in Λ, the effective

maximum scale of validity of the theory. While this doesn't prevent calculations from having predictive power, as the SM is renormalizable, it nonetheless introduces a "fine tuning" problem. In other words, if we assume $\Lambda = M_{GUT} \sim 10^{16}$ GeV, it is necessary to fine tune the Lagrangian mass parameter m_H^2 to a precision of 10^{-26} to obtain the physical Higgs mass required by unitarity constraints ($\lesssim 1$ TeV).

Supersymmetry (SUSY) is the known symmetry that associates to every fermionic (bosonic) degree of freedom a corresponding bosonic (fermionic) superpartner with the same mass and gauge quantum numbers. SUSY provides an elegant solution to many of the above mentioned problems. For example, the fine tuning problem is solved by introducing new degrees of freedom that manifest themselves at the TeV scale and provide a suitable cancellation of quadratic divergences. Also, under certain reasonable assumptions (like R-parity conservation, which is the subject of Chapter 2), all SUSY theories admit a stable "lightest supersymmetric particle" (LSP), electrically and color neutral, which provides an excellent candidate for cold dark matter.

Weakly interacting massive particles (WIMPs) [2], in particular, are the candidates which have drawn the steadiest efforts from the particle physics community dedicated to solving the mystery of dark matter (DM). These are particles of mass 1-1000 GeV who were produced as thermal relics of the Big Bang, froze-out and naturally have the required relic density at present time. However, it has been recently pointed out that WIMPs are not the only candidates with the correct relic density. As a matter of fact, such property can also be reproduced in the framework of the WIMPless scenario of DM, which is the subject of Chapter 3. This scenario [3, 4, 5, 6, 7] prescribes a *hidden sector* of particles, naturally related to gauge-mediated SUSY breaking (GMSB), which interact with the SM particles through a *connector sector*. Their properties allow them to have the correct thermal relic density without necessarily having either weak scale masses or weak couplings, characteristic of the well

known WIMPs.

In the next pages we briefly introduce some general notions about SUSY, mostly for the purpose of understanding the subsequent notation. We follow Ref. [8] for organization of the material and notation.

1.1 Supersymmetry Algebra

A generic SUSY transformation can be written in terms of SUSY generators as,

$$\mathcal{S} \to \mathcal{S}' = e^{i\bar{\alpha}Q}\mathcal{S}e^{-i\bar{\alpha}Q} \approx \mathcal{S} + [i\bar{\alpha}Q, \mathcal{S}]\,, \tag{1.1}$$

where $\mathcal{S}$ is a generic classical or quantum field, α is a Majorana spinorial parameter and Q is the Majorana spinor generator of SUSY transformations. Given two different transformations Q_1 and Q_2, we can apply the infinitesimal transformation $\delta\mathcal{S} = [i\bar{\alpha}Q, \mathcal{S}]$ twice to obtain,

$$(\delta_2\delta_1 - \delta_1\delta_2)\mathcal{S} = -\bar{\alpha}_{2a}\alpha_{1b}[\{Q_a, \bar{Q}_b\}, \mathcal{S}]\,. \tag{1.2}$$

Infinitesimal SUSY transformations of fermionic (bosonic) fields can be expressed in terms of bosonic (fermionic) fields. The simplest example of such a transformation is the Wess-Zumino model [9].

When Eq. (1.2) is compared to the explicit infinitesimal form a SUSY transformation, one can show that

$$\{Q_a, \bar{Q}_b\} = 2(\gamma^\mu)_{ab}P_\mu\,, \tag{1.3}$$

where γ^μ are Dirac matrices and P_μ is the momentum operator. The fact that the

anticommutator of spinorial charges involves the momentum operator expresses the fact that Supersymmetry can be considered an extension of the Poincaré group. Since anticommutators are involved, this is called a graded Lie algebra.

The complete commutation relations are given by

$$\begin{aligned}
[P_\mu, P_\nu] &= 0 \\
[M_{\mu\nu}, P_\lambda] &= i(g_{\nu\lambda}P_\mu - g_{\mu\lambda}P_\nu) \\
[M_{\mu\nu}, M_{\rho\sigma}] &= -i(g_{\mu\rho}M_{\nu\sigma} - g_{\mu\sigma}M_{\mu\rho} - g_{\nu\rho}M_{\mu\sigma} + g_{\nu\sigma}M_{\mu\rho}) \\
[P_\mu, Q_a] &= 0 \\
[M_{\mu\nu}, Q_a] &= -\left(\frac{1}{2}\sigma_{\mu\nu}\right)_{ab} Q_b \\
\left\{Q_a, \bar{Q}_b\right\} &= 2(\gamma^\mu)_{ab}P_\mu \,,
\end{aligned} \tag{1.4}$$

where the P_μ are the usual generators of translations and the $M_{\mu\nu}$ are the Lorentz group generators in covariant form. Note that the fourth of the above equations implies that the particles and their superpartners must have the same mass.

An explicit representation of the spinorial charges Q_a can be obtained when we consider their action on a *superfield*. The superfield formalism allows to combine operators that transform differently under Lorentz transformations into a single object. Superfields are functions of the four spatial coordinates x^μ as well as four Grassman numbers θ_a. Since $\{\theta_a, \theta_b\} = 0$ for each a and b, every expansion in Grassman variables is necessarily truncated. Due to the Majorana nature of the spinors used in SUSY we need exactly four Grassman numbers to match the fermionic degrees of freedom. We can thus express a general function of the four θs in terms of sixteen

independent bilinears, whose coefficients show explicitly their own Lorentz properties:

$$\begin{aligned}\hat{\Phi}(x,\theta) &= \mathcal{S} - i\sqrt{2}\bar{\theta}\gamma_5\psi - \frac{i}{2}(\bar{\theta}\gamma_5\theta)\mathcal{M} + \frac{1}{2}(\bar{\theta}\theta)\mathcal{N} + \frac{1}{2}(\bar{\theta}\gamma_5\gamma_\mu\theta)V^\mu \\ &\quad + i(\bar{\theta}\gamma_5\theta)[\bar{\theta}(\lambda + \frac{i}{\sqrt{2}}\gamma^\mu\partial_\mu\psi)] - \frac{1}{4}(\bar{\theta}\gamma_5\theta)^2[\mathcal{D} - \frac{1}{2}\Box\mathcal{S}]\,. \end{aligned} \tag{1.5}$$

Eq. (1.5) defines a scalar superfield. $\mathcal{S}$, $\mathcal{M}$, $\mathcal{N}$ and $\mathcal{D}$ are scalar fields, ψ and λ spinor fields, and V^μ is a vector field. When applied to a superfield of the form (1.5), the spinorial charges Q take the differential form,

$$[\bar{\alpha}Q, \hat{\Phi}] = i\bar{\alpha}\left(\frac{\partial}{\partial\bar{\theta}} + i\gamma^\mu\partial_\mu\theta\right)\hat{\Phi}\,. \tag{1.6}$$

Since they "bring θ down or up" when applied on different terms in the superfield expansion, their effect is to change the spin nature of the field.

Under certain assumptions, the superfield multiplets can be reducible, i.e. it is possible to find a subset of the components of Eq. (1.5) that transform into each other under SUSY. Left and Right-Chiral superfield are examples of this reduction procedure.

1.2 Supersymmetric Gauge-invariant Lagrangians

It can be shown that it is possible to write a Lagrangian density that is invariant under SUSY transformations and also under any gauge group of internal symmetries. The procedure is not trivial and its detailed description exceeds the purposes of this work. It generates the so called "master Lagrangian" for SUSY gauge theories. The master Lagrangian is expressed in terms of the kinetic terms for the fields of the theory and their superpartners, including their covariant derivatives with respect to the gauge group of choice. As in the SM, the covariant derivative yields the interaction

of the particles and their superpartners with the intermediate bosons of the gauge group. The Lagrangian is also expressed in terms of a second order expansion of the *superpotential* around the scalar components of the superfields. The superpotential is a SUSY invariant scalar function of the superfields.

The part of the master Lagrangian related to the superpotential reads

$$\mathcal{L} = -\sum_i \left| \frac{\partial \hat{f}}{\partial \hat{\mathcal{S}}_i} \right|^2_{\hat{\mathcal{S}}=\mathcal{S}} - \frac{1}{2} \sum_{i,j} \bar{\psi}_i \left[\left(\frac{\partial^2 \hat{f}}{\partial \hat{\mathcal{S}}_r \partial \hat{\mathcal{S}}_s} \right)_{\hat{\mathcal{S}}=\mathcal{S}} L + \left(\frac{\partial^2 \hat{f}}{\partial \hat{\mathcal{S}}_r \partial \hat{\mathcal{S}}_s} \right)^\dagger_{\hat{\mathcal{S}}=\mathcal{S}} R \right] \psi_j \,, \quad (1.7)$$

where the derivatives of the superpotential $\hat{f}$ are taken with respect to all superfields, and the remaining superfields are set equal to their scalar components. The ψ's are the Majorana fermion fields entering the supermultiplet (Eq. 1.5 or its left-chiral reduction), while $L = (1 - \gamma_5)/2$ and $R = (1 + \gamma_5)/2$ are the chiral projectors.

1.3 Minimal Supersymmetric Standard Model

The smallest supersymmetric extension of the SM, i.e., the one that contains the smallest number of particles and interactions consistent with SM phenomenology, is called Minimal Supersymmetric Standard Model (MSSM). It can be obtained from the master Lagrangian formula described above under the same gauge group of the SM, $SU(3)_C \times SU(2)_L \times U(1)_Y$. The fields of the SM are promoted to left-chiral scalar superfields with exactly the same quantum numbers. The Higgs sector consists of two doublets of left-chiral scalar superfields with opposite hypercharge.

The superpotential of the MSSM is given by,

$$\hat{f} = \mu \hat{H}^a_u \hat{H}_{da} + \sum_{i,j=1,3} \left[(\mathbf{f}_u)_{ij} \epsilon_{ab} \hat{Q}^a_i \hat{H}^b_u \hat{U}^c_j + (\mathbf{f}_d)_{ij} \hat{Q}^a_i \hat{H}_{da} \hat{D}^c_j + (\mathbf{f}_e)_{ij} \hat{L}^a_i \hat{H}_{da} \hat{E}^c_j \right] , \quad (1.8)$$

where $\hat{H}_u = (\hat{h}_u^+, \hat{h}_u^0)^T$ and $\hat{H}_d = (\hat{h}_d^-, \hat{h}_d^0)^T$ are the two Higgs super-doublets, $\hat{L}_i = (\hat{\nu}_i, \hat{e}_i)^T$ and $\hat{Q}_i = (\hat{u}_i, \hat{d}_i)^T$ are the "super" $SU(2)$-doublets for leptons and quarks, while $\hat{E}_i^c$, $\hat{U}_i^c$ and $\hat{D}_i^c$ are the "super" $SU(2)$-singlets. The **f** terms are 3×3 Yukawa coupling matrices with indices $i, j = 1, 2, 3$ labelling the fermion generations, while μ is a dimensionful "mass" parameter.

Since the particles and their superpartners have to have the same mass and, clearly, to the present day none of the superpartners have been experimentally observed, one must deduce that, if it exists, SUSY must be necessarily broken. It is therefore necessary to add to the master Lagrangian of MSSM all the soft SUSY-breaking terms consistent with both gauge invariance and the cancellation of quadratic divergences that solves the fine tuning problem. We will not write them explicitly over here and they can be found in any SUSY textbook. They parametrize our ignorance of the mechanism by which SUSY is broken.

1.4 Outline

As with all new theories, along with an elegant solution to some of the problems of the SM, SUSY introduces some unwanted consequences that origin from the new degrees of freedom that carry the same gauge quantum numbers of ordinary particles, but different spin or mass dimension. One of these is that conservation of baryon or lepton number (B and L) is no longer granted, a fact that can have important phenomenological consequences. In order to restore B and L, one has to introduce an "ad hoc" discrete symmetry called *R-parity*. Due to R-parity's peculiar characteristics, the question arises of whether the size of R-parity violating couplings can be inferred by existing data from precision measurements of the SM. We think it is important to obtain accurate bounds on these parameters in the greatest possible

generality. In Chapter 2 we introduce a new approach to deriving these bounds. We do so by relaxing some of the assumptions that are commonly used in the literature. After reviewing the form of the R-breaking couplings and deriving the effective Lagrangians of interest, we describe the assumptions commonly used in the literature and introduce our extended approach. We derive new bounds on the R-breaking couplings from leptonic and semi-leptonic processes. We use new PDG2008 [10] data to obtain bounds at 2σ that are, in cases where new data has become available, more stringent than the ones existing in the literature.

In Chapter 3 we investigate the prospects of detection of fermion WIMPless DM at the neutrino detectors IceCube and DeepCore. We review general facts about WIMPless DM and describe the properties of the fermion candidate DM particle. We obtain the neutrino spectra arising from the decay of various annihilation products and discuss the predicted event rates at the detector. We add three appendices in which we report the numerical procedure for propagation of neutrino spectra through the solar medium and to the Earth, detail the muon event rate calculation and describe the possible backgrounds.

This work is based on the following published articles,

E. M. Sessolo, F. Tahir and D. W. McKay, "Multi-parameter approach to R-parity violating SUSY couplings," Phys. Rev. D **79**, 115010 (2009),

V. Barger, J. Kumar, D. Marfatia and E. M. Sessolo, "Fermion WIMPless Dark Matter at DeepCore and IceCube," Phys. Rev. D **81**, 115010 (2010).

Chapter 2

Multiparameter Approach to R-parity Violation

It is well known that the SM admits some "accidental" symmetries such as the separate conservation of B and L. In other words, the requirement of gauge-invariance and renormalizability of the operators that appear in the Lagrangian does not allow the presence of terms that violate baryon or lepton number conservation. In the framework of the MSSM this is no longer true. In this model, operators that carry the same baryon and lepton number of the SM, but different spin or mass dimension (the superpartners), violate B and L conservation, which can be enforced by hand with the introduction of R-parity. This additional discrete symmetry of the spinorial charges allows the LSP to remain stable and is defined as [11]:

$$R = (-1)^{3(B-L)-2S}, \tag{2.1}$$

with S being the spin quantum number. All the standard model particles have $R = 1$, while their superpartners have $R = -1$.

The phenomenological signatures of an unstable LSP have been investigated extensively in a variety of papers, both at lepton [12, 13] and hadron [14] colliders. Generally the signatures are the consequences of new interaction terms that arise in the superpotential or in the soft SUSY breaking part of the Lagrangian when the

assumption of R-parity is lifted. Wide attention has been given to extracting bounds on these new couplings from precision tests of the standard model and from cosmological constraints. The extent of the literature on the subject is daunting: we refer the reader to Ref. [15] and references therein for a comprehensive review.

2.1 R-parity Violating Couplings and Low Energy Effective Lagrangians

There is no theoretical argument that prevents the superpotential from having the following bilinear or trilinear terms [8]:

$$\hat{f}_T = \lambda_{ijk}\epsilon_{ab}\hat{L}_i^a\hat{L}_j^b\hat{E}_k^C + \lambda'_{ijk}\epsilon_{ab}\hat{L}_i^a\hat{Q}_j^b\hat{D}_k^C + \lambda''_{ijk}\epsilon_{lmn}\hat{U}_i^{Cl}\hat{D}_j^{Cm}\hat{D}_k^{Cn} \tag{2.2}$$

and

$$\hat{f}_B = \mu'_i\epsilon_{ab}\hat{L}_i^a\hat{H}_u^b\,, \tag{2.3}$$

where the carets label the superfields corresponding to the standard model fields, the indices $i, j, k = 1, 2, 3$ label the fermionic generations, $a, b = 1, 2$ are $SU(2)$-doublet indices, while $l, m, n = 1, 2, 3$ are $SU(3)$-triplet indices. The λ_{ijk} couplings are antisymmetric in i, j due to the antisymmetry in a, b, imposed by $SU(2)$, while the λ''_{ijk} are antisymmetric in j, k due to the complete antisymmetry of ϵ_{lmn}, required by $SU(3)$. One can see that the first and second terms in Eq. (2.2), and Eq. (2.3) violate L conservation, while the third term in Eq. (2.2) violates B conservation. On the other hand, phenomenological considerations show that the trilinear terms in λ_{ijk} and λ''_{ijk} cannot be simultaneously present with values large enough to affect the processes we study here, otherwise squark-exchange would lead to unacceptable rates for proton decay [16, 17].

Eqs. (2.2) and (2.3) introduce 48 new complex parameters to the MSSM: 3 dimensionful parameters from the bilinear couplings, and $9+27+9=45$ dimensionless parameters from the trilinear. Along with the superpotential terms, B and L can also be violated by 51 additional soft SUSY-breaking terms in the Lagrangian. Since they are not pertinent to the following discussion we will not write them explicitly here. They can be found in Ref. [15], along with a discussion of the choice of bases in which the bilinear term in the $\not{R}$ superpotential, Eq. (2.3), is rotated away by an $SU(4)$ transformation, so that the sneutrinos acquire a vacuum expectation value under electroweak symmetry breaking [18, 19, 20].

Consistent with the existing literature on trilinear $\not{R}$ bounds as reviewed in Ref. [15], here we choose to work in the mass basis, assume all bilinear $\not{R}$ terms in the tree-level Lagrangian are absent and base our analysis solely on the trilinear terms.

Since R-parity violating terms are neither forbidden by gauge invariance nor by renormalizability, but rather depend on phenomenological consistency, one can wonder to what extent R-parity could be broken, i.e. how big are the couplings appearing in Eqs. (2.2) and (2.3). Restricting our discussion to Eq. (2.2), determinations of the couplings' size are generally obtained in the literature by comparing an effective Lagrangian expressed in terms of the λ, λ' and λ'' couplings with the neutral and charged current interaction effective Lagrangian that describes fundamental tests of the standard model. We largely confine ourselves in this paper to flavor-conserving cases, to keep the presentation focused. The most general effective Lagrangian for fermion-fermion neutral current interactions $\bar{l}l \to \bar{f}f$ at low energies reads:

$$\mathcal{L} = -4\sqrt{2}G_F \bar{l}\gamma^\mu[(g_L^l+\epsilon_L^l)L + (g_R^l+\epsilon_R^l)R]l\bar{f}\gamma_\mu[(g_L^f+\epsilon_L^f)L + (g_R^f+\epsilon_R^f)R]f\,, \quad (2.4)$$

where $G_F = \sqrt{2}g^2/(8M_W^2)$ is the Fermi coupling constant, $L = (1-\gamma_5)/2$ and $R = (1+\gamma_5)/2$ are the chiral projectors, g_L and g_R are the coupling to the chiral components of the fundamental spinors, and the ϵ's describe the "non-standard" part of the interactions. One requires that the R-breaking contributions do not exceed the limit imposed by the precision of the experimental measurements, thus obtaining bounds on the couplings.

As we have mentioned above, the simultaneous presence of leptonic and hadronic R-parity violating couplings is tightly constrained experimentally by the stability of the proton. One may then choose to consider either λ_{ijk} couplings, or λ''_{ijk} couplings to be negligible. In this paper we deal strictly with processes that involve λ and λ', as their corresponding experimental signatures are clearer and the reported uncertainties are smaller.

An effective four-fermion Lagrangian, applicable to processes at energies small compared to the weak scale, can be obtained from the superpotential of Eq. (2.2):

$$\mathcal{L} \ni -\frac{1}{2}\sum_{r,s}\left[\left(\frac{\partial^2 \hat{f}}{\partial\hat{\mathcal{S}}_r\partial\hat{\mathcal{S}}_s}\right)_{\hat{\mathcal{S}}=\mathcal{S}}\bar{\psi}_r L\psi_s + \left(\frac{\partial^2 \hat{f}}{\partial\hat{\mathcal{S}}_r\partial\hat{\mathcal{S}}_s}\right)^{\dagger}_{\hat{\mathcal{S}}=\mathcal{S}}\bar{\psi}_r R\psi_s\right], \tag{2.5}$$

where r, s span the superfields $\hat{\mathcal{S}}$ of the superpotential, and $\psi_{r,s}$ are the Majorana fermion fields entering the supermultiplets. The part involving semi-leptonic interactions is given by the second term in Eq. (2.2):

$$\hat{f} \ni \lambda'_{ijk}(\hat{\nu}_i\hat{d}_j\hat{D}^C_k - \hat{e}_i\hat{u}_j\hat{D}^C_k)\,. \tag{2.6}$$

Application of Eq. (2.5) to this term yields

$$\begin{aligned}\mathcal{L} \ \ni \ & -\lambda'_{ijk}(\tilde{d}^{\dagger}_{Rk}\bar{\psi}_{\nu_i}L\psi_{d_j} - \tilde{d}^{\dagger}_{Rk}\bar{\psi}_{e_i}L\psi_{u_j} + \tilde{\nu}_i\bar{\psi}_{d_j}L\psi_{D^C_k} - \tilde{e}_{Li}\bar{\psi}_{u_j}L\psi_{D^C_k} \\ & + \tilde{d}_{Lj}\bar{\psi}_{\nu_i}L\psi_{D^C_k} - \tilde{u}_{Lj}\bar{\psi}_{e_i}L\psi_{D^C_k}) + \text{ h.c.} \end{aligned} \tag{2.7}$$

The vertices can be obtained by defining Dirac spinors as

$$d(u,e) \equiv L\psi_{d(u,e)} + R\psi_{D^C(U^C,E^C)} \qquad d^C(u^C,e^C) \equiv R\psi_{d(u,e)} + L\psi_{D^C(U^C,E^C)}\,, \tag{2.8}$$

$$\nu \equiv L\psi_{\nu} \qquad \nu^C \equiv R\psi_{\nu}\,, \tag{2.9}$$

so that one gets for the interaction part of the Lagrangian,

$$\begin{aligned}\mathcal{L}_{\lambda} \ = \ & -\lambda'_{ijk}[\tilde{d}^{\dagger}_{Rk}\bar{\nu^C_i}Ld_j + \tilde{d}_{Lj}\bar{d}_kL\nu_i + \tilde{\nu}_i\bar{d}_kLd_j - \tilde{d}^{\dagger}_{Rk}\bar{e^C_i}Lu_j \\ & -\tilde{e}_{Li}\bar{d}_kLu_j - \tilde{u}_{Lj}\bar{d}_kLe_i] - \lambda'^{*}_{ijk}[\tilde{d}_{Rk}\bar{d}_jR\nu^C_i + \tilde{d}^{\dagger}_{Lj}\bar{\nu}_iRd_k \\ & +\tilde{\nu}^{\dagger}_i\bar{d}_jRd_k - \tilde{d}_{Rk}\bar{u}_jRe^C_i - \tilde{e}^{\dagger}_{Li}\bar{u}_jRd_k - \tilde{u}^{\dagger}_{Lj}\bar{e}_iRd_k]\,. \end{aligned} \tag{2.10}$$

The effective Lagrangian for scalar mediated four-fermion interactions can be obtained by combining the vertices of Eq. (2.10) and applying Fierz identities to the result:

$$\begin{aligned}\mathcal{L}^{sl}_{eff} \ = \ & \frac{|\lambda'_{ijk}|^2}{2}\left[\frac{1}{m^2_{\tilde{d}_{Rk}}}(\bar{\nu}_i\gamma^{\mu}L\nu_i)(\bar{d}_j\gamma_{\mu}Ld_j) + \frac{1}{m^2_{\tilde{d}_{Rk}}}(\bar{e}_i\gamma^{\mu}Le_i)(\bar{u}_j\gamma_{\mu}Lu_j)\right. \\ & -\frac{1}{m^2_{\tilde{d}_{Rk}}}(\bar{\nu}_i\gamma^{\mu}Le_i)(\bar{d}_j\gamma_{\mu}Lu_j) - \frac{1}{m^2_{\tilde{d}_{Lj}}}(\bar{\nu}_i\gamma^{\mu}L\nu_i)(\bar{d}_k\gamma_{\mu}Rd_k) \\ & -\frac{1}{m^2_{\tilde{\nu}_{Li}}}(\bar{d}_j\gamma^{\mu}Ld_j)(\bar{d}_k\gamma_{\mu}Rd_k) - \frac{1}{m^2_{\tilde{e}_{Li}}}(\bar{u}_j\gamma^{\mu}Lu_j)(\bar{d}_k\gamma_{\mu}Rd_k) \\ & \left.-\frac{1}{m^2_{\tilde{u}_{Lj}}}(\bar{e}_i\gamma^{\mu}Le_i)(\bar{d}_k\gamma_{\mu}Rd_k)\right]\,. \end{aligned} \tag{2.11}$$

The effective Lagrangian of Eq. (2.11) introduces 135 independent parameters: 9 combinations in any two of the indices times 3 combinations in the remaining index which runs through the families of 5 possible exchanged sparticles. The leptonic interaction effective Lagrangian is obtained by applying the same procedure to the first term in Eq. (2.2):

$$\hat{f} \ni \lambda_{ijk}(\hat{\nu}_i \hat{e}_j \hat{E}^C_k - \hat{e}_i \hat{\nu}_j \hat{E}^C_k)\,. \tag{2.12}$$

One gets [13]

$$\begin{aligned}\mathcal{L}^{lep}_{eff} \;=\; & \frac{|\lambda_{ijk}|^2}{2}\left[\left(\frac{1}{m^2_{\tilde{e}_{Rk}}}(\bar{\nu}_i\gamma^\mu L\nu_i)(\bar{e}_j\gamma_\mu Le_j) - \frac{1}{m^2_{\tilde{e}_{Rk}}}(\bar{e}_i\gamma^\mu L\nu_i)(\bar{\nu}_j\gamma_\mu Le_j)\right.\right. \\ & \left.\left. -\frac{1}{m^2_{\tilde{\nu}_{Li}}}(\bar{e}_j\gamma^\mu Le_j)(\bar{e}_k\gamma_\mu Re_k) - \frac{1}{m^2_{\tilde{e}_{Li}}}(\bar{\nu}_j\gamma^\mu L\nu_j)(\bar{e}_k\gamma_\mu Re_k)\right) \\ & +(i \leftrightarrow j)\right]\,,\end{aligned} \tag{2.13}$$

where $i < j$ is understood in Eq. (2.13). The same antisymmetry in the i and j indices of the λ couplings reduces the number of effective independent couplings encompassed in Eq. (2.13) with respect to the semileptonic case. There are 45: 3 free parameters in a 3×3 antisymmetric matrix multiply 3 possibilities for the remaining free index that carries the dependence on the $m_{\tilde{e}_{Rk}}$; plus, there are 6×3 possibilities with left-handed sneutrino exchange and 18 more possibilities with left-handed selectron exchange.

The limits in the literature are obtained under the assumption that a single coupling dominates the R-parity violating contributions to a process (SCD). This assumption rests on the premise that some hierarchy exists between the leptonic, semileptonic and hadronic couplings, or between different fermionic families. Besides, the couplings often enter as sums of squares, so that one might guess the most conservative bounds follow from this hypothesis. We found that in most cases this is not so.

It is an open question whether such a hierarchy does indeed exist. In the absence

of a theoretical guide, we apply a "multi-parameter" approach to placing bounds, to explore new regions of parameter space. In Secs. 2.2 and 2.3 we give examples of our approach and contrast the results to those of the SCD simplification.

2.1.1 Notation and Conventions

We think it is important at this point to clarify our notation, as the originality of our contribution rests in making explicit use of some properties of $\not{R}$-couplings that are often overlooked in the literature, partly because the established notation bears some elements of ambiguity. As far as SCD is concerned, the concept was originally formulated by Dimopoulos and Hall [12]. As generally applied, one assumes that a single coupling (or a single product of couplings) is much larger than the others which, therefore, can be neglected when placing bounds. As is the case in most of the corrections to the SM that involve R-parity violating couplings, more than one coupling is present and often this simultaneous presence is not clear in the notation. For example, when the process at hand involves the four-fermion interactions described by Eqs. (2.11) and (2.13), the initial and final states of the scattering or decay are supposed to be completely known, whereas the exchanged sparticle, whether a squark or a slepton, can be of any generation. Thus, since this flavor is unknown, one has always to sum over the families of the sparticles compatible with the relevant vertices. So, it is important to understand that a bound that reads, for example, $|\lambda_{12k}| \leq 0.15(\tilde{e}_{Rk})$ can be taken to mean either

$$|\lambda_{12k}| \leq 0.15 \left(\frac{m_{\tilde{e}_{Rk}}}{100 \text{ GeV}}\right) , \qquad \text{(strong version)} \tag{2.14}$$

for each $k = 1, 2, 3$, or

$$\sqrt{\sum_k \left(\frac{|\lambda_{12k}|}{m_{\tilde{e}_{Rk}}}\right)^2} \leq 0.0015 \text{ GeV}^{-1}\,. \qquad \text{(weak version)} \tag{2.15}$$

As in Eqs. (2.14) and (2.15), we adopt the standard 100 GeV scaling of sfermion masses throughout. One of the ways of implementing the SCD convention consists in setting all but one λ_{12k} in Eq. (2.15) to zero, thus effectively obtaining Eq. (2.14). The strong version produces bounds that are obviously more conservative than the weak one, so we will display the form (2.14) every time we place a new bound on a coupling, with the caveat that the reader can interpret it in the form of Eq. (2.15). We will state explicitly when we make an exception to this rule.

If the initial and final states of the four-fermion process involve the same vertices, the R-breaking couplings enter the process only through their modulus squared. In the literature it is then customary to express the corrections to the SM as functions of simplified quantities: $r_{ijk}(\tilde{l}_i)$ (but also $r_{ijk}(\tilde{l}_j)$, $r_{ijk}(\tilde{l}_k)$) or $r'_{ijk}(\tilde{f}_i)$ (but also $r'_{ijk}(\tilde{f}_j)$, $r'_{ijk}(\tilde{f}_k)$). In light of what we have explained above, we want to make clear that these are symbols that stand in full for:

$$r_{ijk}(\tilde{l}_i) = \sum_i \frac{|\lambda_{ijk}|^2}{4\sqrt{2}G_F m^2_{\tilde{l}_i}} \quad \text{and} \quad r'_{ijk}(\tilde{f}_i) = \sum_i \frac{|\lambda'_{ijk}|^2}{4\sqrt{2}G_F m^2_{\tilde{f}_i}}\,, \tag{2.16}$$

where the scaling factor $4\sqrt{2}G_F$ comes from the general form, Eq. (2.4). Thus, they admit a sum over the flavors of the exchanged sfermion $\tilde{f}_i$ (or $\tilde{f}_j$, $\tilde{f}_k$) which, depending on the case, can be a slepton ($\tilde{l}_i$) or a squark ($\tilde{q}_i$). It is also clear that the value of the mass of the exchanged sparticle is always left unknown. If, instead, the SUSY process involves different vertices, then the correction to the standard model is expressed as a function of a product of couplings, of the kind $\lambda_{ijk} \cdot \lambda_{rsk}$ (equivalently, $\lambda'_{ijk} \cdot \lambda'_{rsk}$ or

$\lambda_{ijk} \cdot \lambda'_{rsk}$). In these cases too, a sum over k needs to be considered. Analyses that return one product as dominant are a common extension of the SCD.

We have decided to label the fermion (sfermion) generations by a number index i (or j or k) $= 1, 2, 3$ whenever the families are summed over, as in Eqs. (2.15) and (2.16), or when one of the indices is free to take any values, as in Eq. (2.14). But, for clarity's sake, if the bound involves just one single particular coupling we will label the generation by name so that, for example, $\tilde{e}_{R1} \leftrightarrow \tilde{e}_R$, $\tilde{\nu}_{L2} \leftrightarrow \tilde{\nu}_{\mu L}$, $\tilde{u}_{L3} \leftrightarrow \tilde{t}_L$, and so on.

We have mentioned above that implementation (2.14) of the SCD produces bounds that are more conservative. In most cases, though, a physical process cannot be expressed in terms of only one combination of couplings such as (2.16). The bounds from experiment are placed generally on a function of combinations

$$F\left(r_{ijk}(\tilde{l}_i), r_{rst}(\tilde{l}_s), r'_{lmn}(\tilde{q}_n), ...\right) . \tag{2.17}$$

It is a common approach in the literature to set all the r's of Eq. (2.17) but one to zero, so as to place bounds on the surviving combination of couplings. Moreover, one term at a time of the combination is then assumed to dominate. It is this particular implementation of the SCD that we find excessively severe, as it reduces the dimensionality of the allowed regions of parameter space thus missing any information on the combined action of different couplings embedded in the function F. In the next two sections we show that allowing the full dependence on F does indeed give more information and in some cases also extends the allowed bounds on the couplings.

2.2 Leptonic Case

In order to show how our approach works, we start with some classical examples in the leptonic case [13, 15]. We begin with constraints required by universality in muon and tau decays, then take up the constraints from $\nu_\mu e$, $\nu_e e$, and $\bar{\nu}_e e$ elastic scattering cross section measurements.

2.2.1 Muon and Tau Decays

Let us consider the two following ratios:

$$R_{\tau\mu} = \frac{\Gamma(\tau^- \to \mu^- \bar{\nu}_\mu \nu_\tau)}{\Gamma(\mu^- \to e^- \bar{\nu}_e \nu_\mu)} \tag{2.18}$$

and

$$R_\tau = \frac{\Gamma(\tau^- \to e^- \bar{\nu}_e \nu_\tau)}{\Gamma(\tau^- \to \mu^- \bar{\nu}_\mu \nu_\tau)}\,, \tag{2.19}$$

which are sensitive to violation of lepton universality. By comparing the tree-level effective Lagrangian of Eq. (2.13) with the SM, one can derive bounds on some of the λ-couplings. The SUSY processes that contribute to the decay (2.18) are shown in Fig. 2.1. Those for (2.19) can be obtained by replacing $j = 2 \to 3$ in Fig. 2.1b.

Besides, one also needs to consider the λ-dependence of the Fermi coupling constant G_F [12]. As is well known, G_F is experimentally determined from measurements of the muon lifetime. Therefore, when dealing with R-parity violating SUSY, G_F receives a correction from the SUSY processes that contribute to μ-decay, Fig. 2.1b. The correction is given by [13]:

$$\frac{G_F}{\sqrt{2}} = \frac{g^2}{8M_W^2}\left(1 + \frac{M_W^2}{g^2 m^2_{\tilde{e}_{Rk}}}|\lambda_{12k}|^2\right) \equiv \frac{g^2}{8M_W^2}\left[1 + r_{12k}(\tilde{e}_{Rk})\right]\,. \tag{2.20}$$

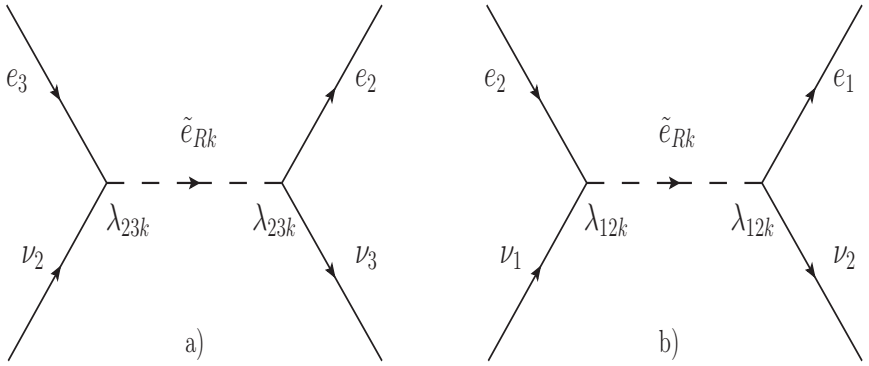

Figure 2.1: a) R-breaking contribution to $\tau^- \to \mu^- \bar{\nu}_\mu \nu_\tau$. b) R-breaking contribution to $\mu^- \to e^- \bar{\nu}_e \nu_\mu$.

where a sum over repeated indices is intended, as explained in Sec. 2.1.1. We have also used the notation introduced in Eq. (2.16).

Taking into account the processes of Fig. 2.1, Eqs. (2.18) and (2.19) can be expressed in terms of their SM expressions and yield, to first order in R-breaking couplings [13],

$$R_{\tau\mu} = R_{\tau\mu}^{SM} \left\{1 + 2\left[r_{23k}(\tilde{e}_{Rk}) - r_{12k}(\tilde{e}_{Rk})\right]\right\} \tag{2.21}$$

and

$$R_{\tau} = R_{\tau}^{SM} \left\{1 + 2\left[r_{13k}(\tilde{e}_{Rk}) - r_{23k}(\tilde{e}_{Rk})\right]\right\} , \tag{2.22}$$

again, with the conventions of Eq. (2.16). As explained in the discussion preceding and following Eq. (2.17), if we were to use the SCD at this point, we would consider one r-combination at a time and obtain a bound on each of them when the remaining couplings are put to zero. By using the measured values of $R_{\tau\mu}$ and R_τ [10] and the standard model values after radiative corrections ([21, 22] and References therein) for $R_{\tau\mu}^{SM}$ and R_τ^{SM}, we would obtain at 2σ: $|\lambda_{23k}| \leq 0.063$ $(\tilde{e}_{Rk})$ and $|\lambda_{12k}| \leq 0.045$ $(\tilde{e}_{Rk})$ from $R_{\tau\mu}$, $|\lambda_{23k}| \leq 0.051$ $(\tilde{e}_{Rk})$ and $|\lambda_{13k}| \leq 0.048$ $(\tilde{e}_{Rk})$ from R_τ, where the dominant uncertainty is the one on the τ lifetime, and we have used the conventions introduced

in the discussion preceding Eq. (2.14). In principle, though reasonably well motivated and not inconsistent, *there is no theoretical justification for considering one coupling at a time*, or a sum over families at a time. As Fig. 2.2 shows, the full dependence on the couplings presents a richer structure.

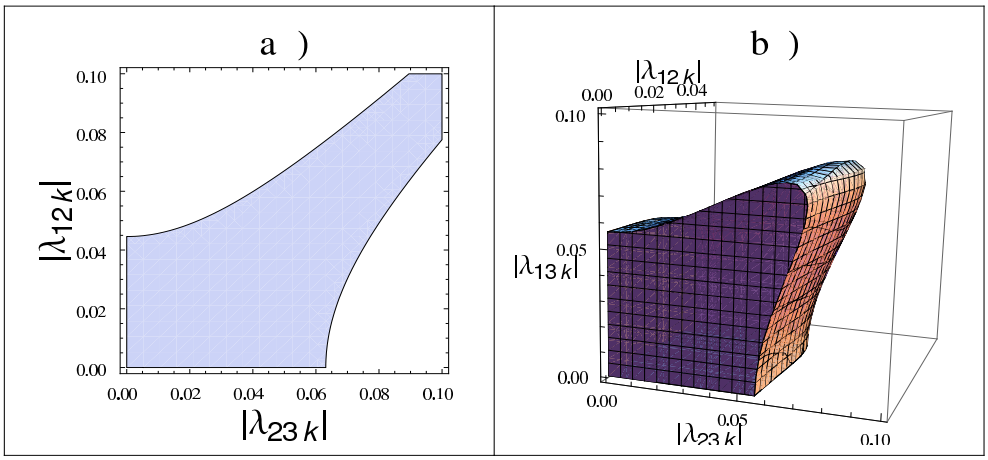

Figure 2.2: a) $|\lambda_{23k}|$ and $|\lambda_{12k}|$ are underconstrained at 2σ if one takes solely into account $R_{\tau\mu}$, Eq. (2.21). b) 2σ bound region on $\lambda_{23k}(\tilde{e}_{Rk})$, $\lambda_{12k}(\tilde{e}_{Rk})$ and $\lambda_{13k}(\tilde{e}_{Rk})$ from $R_{\tau\mu}$, R_τ and muon lifetime combined data. The allowed region can be enclosed in a box of size $\{|\lambda_{23k}|(\tilde{e}_{Rk}), |\lambda_{12k}|(\tilde{e}_{Rk}), |\lambda_{13k}|(\tilde{e}_{Rk})\} \leq \{0.075, 0.043, 0.082\}$.

Figure 2.2a shows that Eq. (2.21) admits degeneracies on the couplings. When taken together, $|\lambda_{23k}|$ and $|\lambda_{12k}|$ can be taken arbitrarily large, consistent with the underlying perturbation expansion, since they cancel each other. A similar picture holds for R_τ, as Eq. (2.22) has the same form as Eq. (2.21). Thus, an approach extended beyond SCD consists in trying to limit and reduce those degeneracies by combining different experiments that involve the same couplings.

In particular, the measurement of the muon lifetime can be used to determine a first bound on the sum of couplings λ_{12k}, when a right-handed charged slepton is exchanged, Eq. (2.20). The result is dependent on radiative corrections and on the renormalization scheme. Expressions for $\lambda_{12k}/m^2_{\tilde{e}_{Rk}}$ can be derived in the *on shell*,

Scheme	$\sin^2\theta_W$	Δr	$\hat{\rho}$
On shell (o.s.)	$1-\frac{M_W^2}{M_Z^2}$	$1-\frac{\alpha}{\hat{\alpha}(M_Z)}-\frac{\rho_t}{\tan^2\theta_W\vert_{\rm o.s.}}$	1
$\overline{MS}$	$\left(1+\frac{\rho_t}{\tan\theta_W\vert_{\rm o.s.}}\right)\left(\sin^2\theta_W\vert_{\rm o.s.}\right)$	$1-\frac{\alpha}{\hat{\alpha}(M_Z)}+...$[24]	1.01023(22)
NOV	$\frac{1}{2}-\left(\frac{1}{4}-\frac{\pi\alpha(M_Z)}{\sqrt{2}G_F M_Z^2}\right)^{1/2}$	$1-\frac{\alpha}{\alpha(M_Z)}$	1

Table 2.1: Analytic expressions for $\sin^2\theta_W$, Δr and $\hat{\rho}$ in the *on shell*, $\overline{MS}$ and NOV renormalization schemes. $\rho_t = 3G_F m_t^2/8\sqrt{2}\pi^2$. We use the following average values at 1σ [10]: $\sin^2\theta_W|_{\overline{MS}} = 0.23119(14)$; $\hat{\alpha}^{-1}(M_Z) = 127.925(16)$; $\alpha^{-1}(M_Z) = 128.91(2)$; $\sin^2\theta_W|_{\rm NOV} = 0.23108(5)$; $\Delta r|_{\rm o.s.} = 0.0369(14)$; $\Delta r|_{\overline{MS}} = 0.06962(12)$. The ellipsis indicates non-leading order terms that can be found in [24].

$\overline{MS}$ and Novikov-Okun-Vysotsky (NOV) renormalization schemes [23], and are given by

$$\frac{|\lambda_{12k}|^2}{m^2_{\tilde{e}_{Rk}}} = \frac{8G_F}{\sqrt{2}}\left[\frac{M_Z^2\sqrt{2}G_F\hat{\rho}|_{\rm scheme}(\sin^2\theta_W\cos^2\theta_W)|_{\rm scheme}(1-\Delta r|_{\rm scheme})}{\pi\alpha}-1\right], \tag{2.23}$$

where the scheme dependence of $\hat{\rho}$, $\sin^2\theta_W$ and Δr can be found in Table 2.1. According to the different renormalization scheme, we find the 1σ-bounds on λ_{12k} obtained from the muon lifetime:

$$\textit{(on shell)} \qquad |\lambda_{12k}| \text{ is excluded} \tag{2.24}$$

$$(\overline{MS}) \qquad |\lambda_{12k}| \leq 0.029\left(\frac{m_{\tilde{e}_{Rk}}}{100\ \text{GeV}}\right) \tag{2.25}$$

$$(\text{NOV}) \qquad |\lambda_{12k}| \leq 0.011\left(\frac{m_{\tilde{e}_{Rk}}}{100\ \text{GeV}}\right). \tag{2.26}$$

And at 2σ:

$$\textit{(on shell)} \qquad |\lambda_{12k}| \leq 0.031 \left(\frac{m_{\tilde{e}_{Rk}}}{100\ \text{GeV}}\right) \tag{2.27}$$

$$(\overline{MS}) \qquad |\lambda_{12k}| \leq 0.037 \left(\frac{m_{\tilde{e}_{Rk}}}{100\ \text{GeV}}\right) \tag{2.28}$$

$$\text{(NOV)} \qquad |\lambda_{12k}| \leq 0.015 \left(\frac{m_{\tilde{e}_{Rk}}}{100\ \text{GeV}}\right) . \tag{2.29}$$

We can therefore decide to use this bound to limit the degeneracies present in $R_{\tau\mu}$ and R_τ. Figure 2.2b shows the 2σ-allowed region of parameter space in λ_{23k}, λ_{12k} and λ_{13k} when the PDG2008 data for $R_{\tau\mu}$, R_τ and muon lifetime are combined. We use the $\overline{MS}$ bound, Eq. (2.28), on λ_{12k}. One can see that the λ-parameters undergo a extension up to a factor of two with respect to the value obtained using the SCD. When scaled to the masses of the exchanged sleptons the 2σ region shown in Fig. 2.2b can be enclosed in a box of size $\{|\lambda_{23k}|(\tilde{e}_{Rk}), |\lambda_{12k}|(\tilde{e}_{Rk}), |\lambda_{13k}|(\tilde{e}_{Rk})\} \leq \{0.075, 0.043, 0.082\}$. The 2σ bounds are:

$$|\lambda_{23k}| \leq 0.066 \left(\frac{m_{\tilde{e}_{Rk}}}{100\ \text{GeV}}\right) \tag{2.30}$$

and

$$|\lambda_{13k}| \leq 0.071 \left(\frac{m_{\tilde{e}_{Rk}}}{100\ \text{GeV}}\right) . \tag{2.31}$$

The other schemes yield similar values. Note that the new bound on λ_{13k} does not include λ_{133}, since this coupling is separately and more severely bounded by the ν_e mass [12]. Similarly, there exist strong bounds on many pair-wise products of the couplings above, coming from experimental bounds on decays disallowed in the SM [15, 25]. However, there are always combinations of λ_{12k}, λ_{13k} and λ_{23k} that are still unconstrained by the bounds on products. This comment applies to all the cases that we are considering. To list the detailed conditions takes us beyond the aim of this paper, so we leave them as implicit.

2.2.2 Neutrino-electron Scattering

We now turn to the flavor diagonal neutrino - electron scattering processes $\nu_\mu + e \rightarrow \nu_\mu + e$ and $\nu_e + e \rightarrow \nu_e + e$. In the $\nu_\mu e$ and $\nu_e e$ examples, the energy is always large enough to neglect the electron mass in the kinematics, while in the $\bar{\nu}_e e$ case, the neutrino energies are in the MeV range, which requires us to keep the electron mass effects in the kinematics. The individual left -and right-handed couplings or, equivalently, axial and vector couplings, have been extracted individually in the experiments on the $\nu_\mu e$ case [26], making the analysis of bounds on R-parity violating parameters quite straightforward; we begin with this process.

$\nu_\mu + e \rightarrow \nu_\mu + e$

Neglecting the terms proportional to the electron mass, the total cross sections for $\nu_\mu + e \rightarrow \nu_\mu + e$ and $\overline{\nu}_\mu + e \rightarrow \overline{\nu}_\mu + e$ can be written as

$$\sigma(\nu_\mu e) = \frac{G_F^2 s}{\pi}\left(g_L^2 + \frac{1}{3}g_R^2\right) \tag{2.32}$$

and

$$\sigma(\overline{\nu}_\mu e) = \frac{G_F^2 s}{\pi}\left(g_R^2 + \frac{1}{3}g_L^2\right) . \tag{2.33}$$

The direct-channel Mandelstam variable $s = 2m_e E_\nu$ in the target-electron rest frame. We can write g_L and g_R in terms of the weak angle and the R-parity violating parameters (Fig. 2.3) as

$$g_L = g_L^{SM} - (1 + g_L^{SM}) r_{12k}(\tilde{e}_{Rk}) \tag{2.34}$$

and

$$g_R = g_R^{SM} + r_{121}(\tilde{e}_L) + r_{231}(\tilde{\tau}_L) - g_R^{SM} r_{12k}(\tilde{e}_{Rk}) , \tag{2.35}$$

where $x_W \equiv \sin^2\theta_W$, and $g_L^{SM} = x_W - \frac{1}{2}$ and $g_R^{SM} = x_W$ are the SM expressions for the L and R couplings.

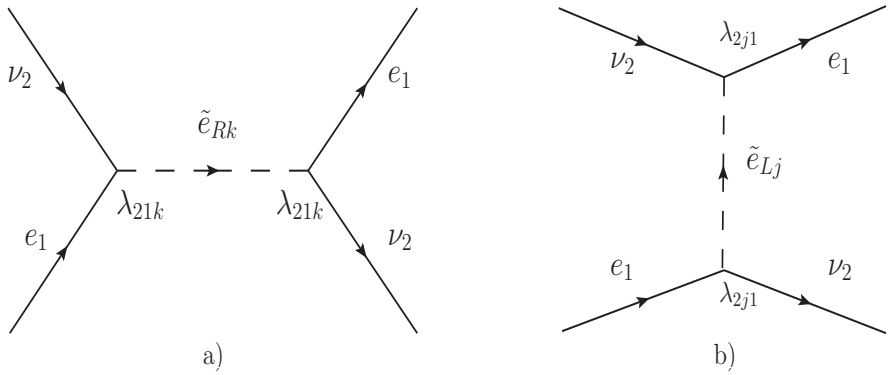

Figure 2.3: a) SUSY R-breaking process contributing to g_L and g_R. b) SUSY process contributing to g_R. Here gauge invariance requires $j = 1, 3$.

Since the experimental averages, with errors, are reported by the Particle Data Group [10] for $g_A = g_L - g_R$ and $g_V = g_L + g_R$, we use these forms to obtain the bounds on the R-parity violating couplings:

$$g_A = g_A^{SM}\left[1 - r_{12k}(\tilde{e}_{Rk})\right] - r_{121}(\tilde{e}_L) - r_{231}(\tilde{\tau}_L) - r_{12k}(\tilde{e}_{Rk}) = -0.507 \pm 0.014 \quad (2.36)$$

and

$$g_V = g_V^{SM}\left[1 - r_{12k}(\tilde{e}_{Rk})\right] + r_{121}(\tilde{e}_L) + r_{231}(\tilde{\tau}_L) - r_{12k}(\tilde{e}_{Rk}) = -0.040 \pm 0.015\,, \quad (2.37)$$

where $g_V^{SM} = -0.0397 \pm 0.0003$ and $g_A^{SM} = -0.5064 \pm 0.0001$. The values quoted for the g-parameters are taken from the 2008 Particle Data Group, who point out that the CHARM II results [26] dominate the average values.

Including $\lambda_{12k}(\tilde{e}_{Rk})$, Eq. (2.28), in the 2σ joint bounds, we find the corresponding

upper bound to be:

$$\sqrt{\left[|\lambda_{121}|\left(\frac{100\text{ GeV}}{m_{\tilde{e}_L}}\right)\right]^2+\left[|\lambda_{231}|\left(\frac{100\text{ GeV}}{m_{\tilde{\tau}_L}}\right)\right]^2}\leq 0.130\,. \tag{2.38}$$

To put Eq. (2.38), a bound on the sum of squares of couplings divided by scaled masses, in the context of other bounds, we can use the bound from [25], updated to 2008 data [10]:

$$\left|\lambda_{121}\left(\frac{100\text{ GeV}}{m_{\tilde{\nu}_{\mu L}}}\right)\times\lambda_{231}\left(\frac{100\text{ GeV}}{m_{\tilde{\nu}_{\mu L}}}\right)\right|\leq 3.0\times 10^{-4}\,. \tag{2.39}$$

The bound in Eq. (2.39) combines the experimental bound on the decay rate for $\tau\to ee\overline{e}$ with its representation in the "double coupling dominance convention" for R-parity violating trilinear couplings [25]. The representation of the decay involves the sum of squares of five coupling products, and the convention, in this case, serves to place the weakest bound on each product by assuming all the others are effectively zero. This example, though not in line with our restriction to flavor-conserving processes, allows us to discuss the implications for sfermion masses that follow from $\not{R}$ bounds. Because three unknown masses appear in Eqs. (2.38) and (2.39), what one can say about the implications of the bounds for the λ parameters is limited, even if the individual $\not{R}$ couplings entering the two equations are the same. Concisely put, one can say that whenever the sneutrino mass satifies

$$m_{\tilde{\nu}_{\mu L}}\geq\frac{0.130}{\sqrt{2\times 3.0\times 10^{-4}}}\sqrt{m_{\tilde{e}_L}\times m_{\tilde{\tau}_L}}\approx 5.3\sqrt{m_{\tilde{e}_L}\times m_{\tilde{\tau}_L}}\,, \tag{2.40}$$

the bound of Eq. (2.38) is more restrictive than that of Eq. (2.39), which becomes irrelevant. If, instead, Eq. (2.40) is not satisfied, the above bounds have to be considered together, because the hyperbola described by Eq. (2.39) will cut through the

elliptical region defined by Eq. (2.38), and part of the region allowed by Eq. (2.38) will be prohibited by Eq. (2.39).

Unless we invoke some theoretical prejudice about the relative mass scales, we cannot conclude more than that. Only if one of the inequalities includes a lower bound, does the combination of bounds lead to a general condition on the masses. We will see an illustration of this situation below, when considering the combined bounds on $\nu_e e$ and $\overline{\nu}_e e$ scattering at 1σ.

$\nu_e + e \to \nu_e + e$

Turning to the implications of data on the scattering processes $\nu_e + e \to \nu_e + e$ and $\overline{\nu}_e + e \to \overline{\nu}_e + e$ [27, 28, 29], we must consider both high energy data, $E_\nu \gg m_e$, and low energy data, $E_\nu \sim m_e$. General, model independent analyses of bounds on non-standard interactions from these and related neutrino and electron data have recently been carried out for both non-universal and flavor-changing new physics interactions [30, 31, 32]. We focus here on the bounds on $\not{R}$ trilinear coupling parameters provided by flavor diagonal elastic $\nu_e e$ accelerator data at tens of MeV [28] and elastic $\overline{\nu}_e e$ reactor data at several MeV [27].

The LSND Collaboration provides a measurement of the total cross section for elastic scattering of the electron neutrinos off electrons. Assuming that the final state neutrinos are also electron-type, we can use their reported value and the general expression for left handed neutrinos scattering of unpolarized electrons to set a limit. The general expression for a $(V-A)\bigotimes[g_L(V-A)\bigoplus g_R(V+A)]$ four-fermion interaction differential cross section reads

$$\frac{d\sigma}{dT} = \frac{2G_F^2 m_e}{\pi}\left[g_L^2 + g_R^2\left(1-\frac{T}{E_\nu}\right)^2 - g_L g_R \frac{m_e T}{E_\nu^2}\right], \tag{2.41}$$

and for the total cross section

$$\begin{aligned}\sigma_{\nu e} &= \frac{2m_e E_\nu G_F^2}{\pi}\left(g_L^2+\frac{1}{3}g_R^2-\frac{1}{2}\frac{m_e}{E_\nu}g_L g_R\right)\\ &= (10.1\pm 1.5)\times 10^{-42}E_\nu(\mathrm{GeV})\ \mathrm{cm}^2\,,\end{aligned} \tag{2.42}$$

where E_ν is the neutrino energy in the rest frame of the target electron, and T is the kinetic energy of the recoil electron. In view of the low precision of the experimental uncertainties, we have not included radiative corrections. For a study discussing radiative corrections and future possibilities for precision measurements, see [33]. The $\bar{\nu}_e e$ cross sections follow by interchanging g_L and g_R in Eqs. (2.41) and (2.42). When $E_\nu \gg m_e$, as in the case of the LSND experiment, m_e/E_ν is ignorable, and the expression for the cross section simplifies to the familiar high energy form. Including the $\not{R}$ trilinear parameters in the expressions for the g_L and g_R coupling coefficients, we find

$$g_L^{\nu_e e} = \left(\frac{1}{2}+x_W\right)\left[1-r_{12k}(\tilde{e}_{Rk})\right] \tag{2.43}$$

$$g_R^{\nu_e e} = x_W\left[1-r_{12k}(\tilde{e}_{Rk})\right]+r_{121}(\tilde{\mu}_L)+r_{131}(\tilde{\tau}_L)\,, \tag{2.44}$$

where we have considered a SUSY process like the one depicted in Fig. 2.3b, in which $\nu_2 \equiv \nu_\mu$ has to be replaced by $\nu_1 \equiv \nu_e$, $\lambda_{2j1} \to \lambda_{1j1}$, and $j = 2, 3$, while the λ_{12k}-dependence is given by the correction to G_F, Eq. (2.20). In our study of the bound on $r_{12k}(\tilde{e}_{Rk})$ that follows from the precision measurement of muon decay and the renormalized expression for the muon decay formula, we found the bounds of Eqs. (2.25) and (2.28) respectively at the 1σ and 2σ C.L. The corresponding values of $r_{12k}(\tilde{e}_{Rk})$ are so small that it can be dropped from further discussion. The coupling coefficient g_L then has its SM value, and g_R is modified from the SM value by the

terms that depend on λ_{121} and λ_{131}. Referring to Eq. (2.42) and (2.44), we find the bound on the region of trilinear couplings we are after:

$$\sqrt{\left(|\lambda_{121}|\frac{100\text{ GeV}}{m_{\tilde{\mu}_L}}\right)^2+\left(|\lambda_{131}|\frac{100\text{ GeV}}{m_{\tilde{\tau}_L}}\right)^2}\leq 0.66\,, \tag{2.45}$$

at 2σ.

Before discussing the tie-in of Eq. (2.45) with other limits, we look next at the independent limits set by the results for $\overline{\nu}_e + e \rightarrow \overline{\nu}_e + e$ from reactor data. In this case, the electron mass-dependent terms are important and must be kept. The cross section expression in Eq. (2.42) is modified by interchange of g_L and g_R for application to the $\overline{\nu}_e e$ case.

$\overline{\nu}_e + e \rightarrow \overline{\nu}_e + e$

The highest statistics experiment $\overline{\nu}_e + e \rightarrow \overline{\nu}_e + e$ is still that of Reines, Gurr and Sobel [27]. The results are presented as dimensionless factors times the SM charged current, $V-A$ expression σ_{V-A}, for the cross section for each of two kinetic energy bins. The cross section for a given recoil electron energy range is evidently the result of folding the differential cross section with respect to electron energy with the $\overline{\nu}_e$ flux [34], integrating over neutrino energies and then integrating over the recoil kinetic energy. The experimental cross sections reported are $\sigma_{\text{exp}} = (0.87 \pm 0.25)\sigma_{V-A}$ (1.5 MeV $\leq T \leq$ 3.0 MeV) and $\sigma_{\text{exp}} = (1.70 \pm 0.44)\sigma_{V-A}$ (3.0 MeV $\leq T \leq$ 4.5 MeV). The quantity thus calculated is a function of the $\not{R}$ parameters, which enter through the coupling $g_R^{\nu_e e}$, Eq. (2.44).

The theoretical expressions for electron-neutrino and antineutrino scattering involve the same $\not{R}$ couplings. Thus, in the spirit of our multi-parameter, multi-experiment approach, we can combine data from LSND [28] and Irvine [27] results

for both ΔT bins in a way similar to what we did for $R_{\tau\mu}$ and R_τ in Sec. 2.2.1. The resulting constraint at the 2σ level is:

$$\sqrt{\left(|\lambda_{121}|\frac{100\text{ GeV}}{m_{\tilde{\mu}_L}}\right)^2+\left(|\lambda_{131}|\frac{100\text{ GeV}}{m_{\tilde{\tau}_L}}\right)^2}\leq 0.38\,. \tag{2.46}$$

At first glance it is surprising that the $\overline{\nu}_e$ data, with larger uncertainty, produces tighter constraints than the ν_e data. The source of the added resolving power is the $g_L g_R$ term in the cross section expressions, which plays a significant role in the low energy analysis and increases the sensitivity to the variation with respect to the $\not{R}$ parameters.

Though the bound Eq. (2.46) is consistent with zero at 2σ, at the 1σ level, given current values for g_L and g_R, it is not. This in itself is not of special significance, but it affords the opportunity to illustrate added implications when "new $\not{R}$-physics" is needed to fill a gap between SM and experiment. The joint bound from LSND and Irvine at 1σ yields:

$$0.14\leq\sqrt{\left(|\lambda_{121}|\frac{100\text{ GeV}}{m_{\tilde{\mu}_L}}\right)^2+\left(|\lambda_{131}|\frac{100\text{ GeV}}{m_{\tilde{\tau}_L}}\right)^2}\leq 0.34\,. \tag{2.47}$$

Projected onto each parameter one finds,

$$0.20\leq|\lambda_{121}|\frac{100\text{ GeV}}{m_{\tilde{\mu}_L}}\leq 0.32\qquad\left(0.11\leq|\lambda_{121}|\frac{100\text{ GeV}}{m_{\tilde{\mu}_L}}\leq 0.35\right)\,, \tag{2.48}$$

at 1σ (1.65σ), and similarly for $\lambda_{131}(\tilde{\tau}_L)$.

Now we have the interesting situation that, taking the bound Eq. (2.47) at face value, we can ask under what conditions are they consistent with stringent bounds on related parameters, coming from more recent data. Examples we have already

studied are the bound $|\lambda_{121}|(100\text{ GeV})/m_{\tilde{e}_R} \leq 0.037$, Eq. (2.28), and the bound $|\lambda_{131}|(100\text{ GeV})/m_{\tilde{e}_R} \leq 0.071$, Eq. (2.31). We assumed here a variant of the SCD assumption, corresponding to the largest possible range for individual parameters, $|\lambda_{12k}| \to |\lambda_{121}|$ and $|\lambda_{13k}| \to |\lambda_{131}|$.

From Eq. (2.47), scaling by $m_{\tilde{e}_R}$, we can now map out regions of $(m_{\tilde{\mu}_L}, m_{\tilde{\tau}_L})$ space where the constraints from Eqs. (2.47), (2.28) and (2.31) are all satisfied, ignoring for present purposes the mixing of 1σ and 2σ constraints. The result of this analysis is displayed in Fig. 2.4. To satisfy the lower bound shown in Eq. (2.47), we see that at least one of the masses must be less than the mass $m_{\tilde{e}_R}$. This mass pattern, if it were borne out by future experimental constraints, would contradict models that predict $m_{\tilde{e}_R} < m_{\tilde{e}_L}$, as is the case in minimal supergravity, for example [35]. The smaller the mass becomes, the larger the other must be to satisfy the inequalities. This mass information can *only* be obtained if the strict SCD approach is relaxed, as we have done here.

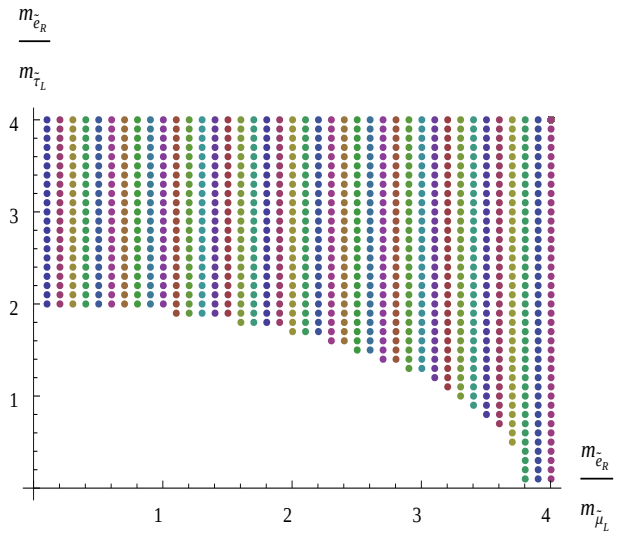

Figure 2.4: The darkened region shows the values of $m_{\tilde{e}_R}/m_{\tilde{\mu}_L}$ and $m_{\tilde{e}_R}/m_{\tilde{\tau}_L}$ allowed by simultaneous application of bounds shown in Eqs. (2.47), (2.28) and (2.31).

Alternatively, taking the bounds one at a time, Eq. (2.48), we find $m_{\tilde{\mu}_L} \leq 0.185$ (0.34) $m_{\tilde{e}_R}$ or $m_{\tilde{\tau}_L} \leq 0.355$ (0.65) $m_{\tilde{e}_R}$ at 1σ (1.65σ).

The preceding discussion, summarized in Fig. 2.4, is offered to illustrate the added power that multi-parameter analysis provides to probe $\not{R}$ parameters. Experiments delivering data with high statistics at energies of a MeV or so to study $\overline{\nu}_e e$ scattering would sharpen the picture, clarifying the possible role of $\not{R}$ SUSY in this sector of neutrino physics. Here we are considering only low energy processes, where the four-fermion effective interactions apply, but at high energies the non-local effects of the exchanged particle must be included, directly probing the sfermion masses. This possibility is afforded by $e^+e^- \to \nu\overline{\nu}\gamma$ results from LEP [36] and, in the future, possibly 100 GeV range $\nu_\mu e \to \nu_\mu e$ and $\nu_\mu e \to \nu_e \mu$ scattering experiments such as those proposed by NuSOnG [37].

This concludes our exploration of the multi-parameter effects in purely leptonic processes. Next we consider some important constraints from semi-leptonic physics.

2.3 Semi-leptonic Case

When R-parity violating interactions are taken into account, charge current and neutral current interaction generally involve more than one coupling at a time, and in some cases these couplings can be large and cancel each other. The lesson we take from the leptonic case is that such degeneracies can be removed by considering a subset of experiments characterized by the same R-parity couplings. Then one bounds the couplings by considering the experimental uncertainties on this subset altogether. This is even more evident when we analyze processes that involve the semi-leptonic couplings λ'_{ijk} of Eq. (2.11). Contrary to the leptonic and hadronic cases, the couplings λ'_{ijk} are not required by gauge invariance to have any symmetry in their indices.

As a consequence, the number of effective couplings entering the Lagrangian is much greater than those appearing in Eq. (2.13), as we have mentioned in Sec. 2.1. There are thus more processes that must be used simultaneously to bound the couplings. What this also means is that, due to the amazing overall accuracy of the SM predictions and the great number of tests, there are many more ways to cut down the allowed regions of parameter space. As we will see in the following standard examples, when the availability of experiments from which we can draw bounds on a particular coupling increases, the bound on the coupling tends to approach the one obtained under the SCD.

2.3.1 Universality in Pion and Tau Decay

In the cases of semi-leptonic couplings, we can obtain behavior similar in nature to the one depicted in Fig. 2.2a. The ratio

$$R_{\tau\pi} = \frac{\Gamma(\tau^- \to \pi^- \nu_\tau)}{\Gamma(\pi^- \to \mu^- \bar{\nu}_\mu)} = R_{\tau\pi}^{SM} \frac{|V_{ud} + r'_{31k}(\tilde{d}_{Rk})|^2}{|V_{ud} + r'_{21k}(\tilde{d}_{Rk})|^2} \tag{2.49}$$

would give in the SCD the 2σ bounds $|\lambda'_{31k}| \leq 0.092$ $(\tilde{d}_{Rk})$ and $|\lambda'_{21k}| \leq 0.032$ $(\tilde{d}_{Rk})$. Here, again, the uncertainty on the τ lifetime is comparable in magnitude to the one on the branching fraction to pions, and has to be taken into account. As in the leptonic case, the simultaneous presence of both couplings introduces a two-fold degeneracy. Such degeneracy can be removed by considering the ratio [13]

$$R_\pi = \frac{\Gamma(\pi^- \to e^- \bar{\nu}_e)}{\Gamma(\pi^- \to \mu^- \bar{\nu}_\mu)} = R_\pi^{SM} \left\{ 1 + \frac{2}{V_{ud}} \left[r'_{11k}(\tilde{d}_{Rk}) - r'_{21k}(\tilde{d}_{Rk}) \right] \right\} . \tag{2.50}$$

For the purpose of illustrating our multidimensional approach, it is convenient in this case to follow the restriction mentioned in [13], so we use Eq. (2.50) to effectively place

two alternative 2σ bounds. Note here that Eq. (2.51) implies a sum over couplings and exchanged particles. Neutrinoless double-beta decay places a strong independent bound on λ'_{111}, which applies to $\tilde{d}_R$- and $\tilde{u}_L$-exchange equally [38]. Either

$$|\lambda'_{11k}| \leq 0.051 \left(\frac{m_{\tilde{d}_{Rk}}}{100 \text{ GeV}}\right) , \tag{2.51}$$

or

$$|\lambda'_{21k}| \leq 0.040 \left(\frac{m_{\tilde{d}_{Rk}}}{100 \text{ GeV}}\right) . \tag{2.52}$$

As we have done in Sec. 2.2.1, we can combine Eqs. (2.49) and (2.50) to place 2σ bounds on the region spanned by λ'_{31k} and λ'_{21k}. The result is shown in Fig. 2.5a. The

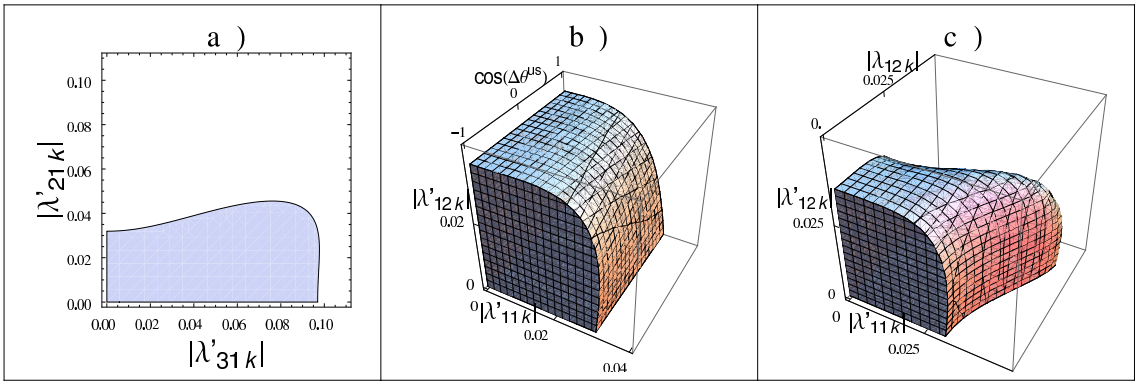

Figure 2.5: a) 2σ bound region on $\lambda'_{31k}(\tilde{d}_{Rk})$, $\lambda'_{21k}(\tilde{d}_{Rk})$ from $R_{\tau\pi}$ and R_π combined data, Eqs. (2.49-2.50). The allowed region can be enclosed in a box of size $\{|\lambda'_{31k}|(\tilde{d}_{Rk}), |\lambda'_{21k}|(\tilde{d}_{Rk})\} \leq \{0.098, 0.045\}$. b) 2σ bound region on $\lambda'_{11k}(\tilde{d}_{Rk})$, $\cos(\Delta\theta^{us}_k)$, $\lambda'_{12k}(\tilde{d}_{Rk})$ from R_π, CKM unitarity (Eq. (2.55), $\lambda_{12k} = 0$) and FB asymmetry combined data. c) 2σ bound region on λ'_{11k} $(\tilde{d}_{Rk})$, λ_{12k} $(\tilde{e}_{Rk})$ and λ'_{12k} $(\tilde{d}_{Rk})$. $|\lambda'_{12k}|$ is bounded by the FB asymmetry while $|\lambda_{12k}|$ by μ decay in the $\overline{MS}$ scheme. $\cos(\Delta\theta^{us}_k) = -1$. The allowed region can be enclosed in a box of size $\{|\lambda'_{11k}|(\tilde{d}_{Rk}), |\lambda_{12k}|(\tilde{e}_{Rk}), |\lambda'_{12k}|(\tilde{d}_{Rk})\} \leq \{0.047, 0.042, 0.036\}$.

allowed region, rescaled to the masses of the exchanged squarks, can be enclosed in a box of size $\{|\lambda'_{31k}|(\tilde{d}_{Rk}), |\lambda'_{21k}|(\tilde{d}_{Rk})\} \leq \{0.098, 0.045\}$. The resulting 2σ bound on

λ'_{31k} reads:

$$|\lambda'_{31k}| \leq 0.092 \left(\frac{m_{\tilde{d}_{Rk}}}{100 \text{ GeV}}\right) , \tag{2.53}$$

exactly equal to the one obtained by SCD.

2.3.2 Unitarity of the CKM Matrix and Forward-backward Asymmetry

The Cabibbo-Kobayashi-Maskawa (CKM) matrix elements are experimentally determined by comparing the rates of decays that involve quarks in the initial state to the rate of muon decay. In general, nuclear beta decay is used to determine the value of $|V_{ud}|$, while the rates for $s \to ul\bar{\nu}_l$ and $b \to ul\bar{\nu}_l$ in K and charmless B decay are used to determine $|V_{us}|$ and $|V_{ub}|$. The R-breaking processes involved in these decays are shown in Fig. 2.6.

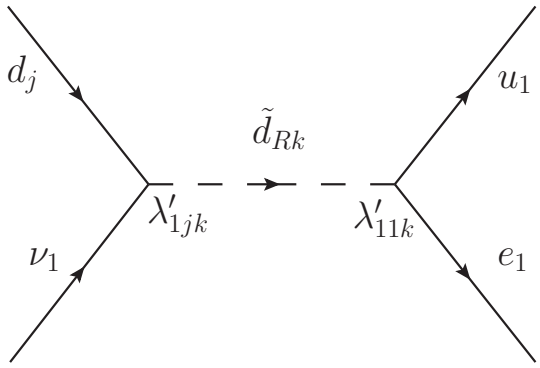

Figure 2.6: SUSY processes involved in $d \to ue\bar{\nu}_e$ ($j = 1$), $s \to ue\bar{\nu}_e$ ($j = 2$), and $b \to ue\bar{\nu}_e$ ($j = 3$).

The unitarity constraint can be imposed on the CKM matrix elements, together with the effective Lagrangian of Eq. (2.11) and a similar one, constructed from Eq. (2.10), involving the product of different couplings. One gets [15]:

$$\sum_{i=1}^{3}|V_{ud_i}|^2 = \frac{1}{|1+r_{12k}(\tilde{e}_{Rk})|^2}\left(\left|V_{ud}+r'_{11k}(\tilde{d}_{Rk})\right|^2+\left|V_{us}+\sum_k\frac{\lambda'^{*}_{11k}\lambda'_{12k}}{4\sqrt{2}G_F m^2_{\tilde{d}_{Rk}}}\right|^2 + \left|V_{ub}+\sum_k\frac{\lambda'^{*}_{11k}\lambda'_{13k}}{4\sqrt{2}G_F m^2_{\tilde{d}_{Rk}}}\right|^2\right) , \tag{2.54}$$

which becomes at leading order in R-parity breaking,

$$\sum_{i=1}^{3}|V_{ud_i}|^2 = 1-2r_{12k}(\tilde{e}_{Rk})+2r'_{11k}(\tilde{d}_{Rk})\,|V_{ud}|+2\left(\sum_k\frac{|\lambda'_{11k}||\lambda'_{12k}|\cos(\Delta\theta^{us}_k)}{4\sqrt{2}G_F m^2_{\tilde{d}_{Rk}}}\right)|V_{us}| +2\left(\sum_k\frac{|\lambda'_{11k}||\lambda'_{13k}|\cos(\Delta\theta^{ub}_k)}{4\sqrt{2}G_F m^2_{\tilde{d}_{Rk}}}\right)|V_{ub}| , \tag{2.55}$$

where $\cos(\Delta\theta^{us}_k)\equiv\cos(\theta_{us}+\theta_{12k}-\theta_{11k})$ and $\cos(\Delta\theta^{ub}_k)\equiv\cos(\theta_{ub}+\theta_{13k}-\theta_{11k})$ are the relative phases between the CKM matrix elements and the complex R-parity violating couplings. Using Eq. (2.55) we can place bounds on the λ' couplings involved by separation between the right- and left-hand side. One can substitute the most recent experimental determination of the central values of the CKM matrix element on the right, and use the errors on the unitarity bound on the left at the desired level of precision.

In the literature, Eq. (2.55) is treated in the SCD, with the additional constraint that R-parity couplings and CKM matrix elements are treated as real. With these assumptions we find that the most recent data [10] result in the following bounds at 2σ: $|\lambda'_{11k}|\leq 0.027$ $(\tilde{d}_{Rk})$ and $|\lambda_{12k}|\leq 0.028$ $(\tilde{e}_{Rk})$.

In Eqs. (2.54) and (2.55) the notation of Eq. (2.16), to express the sum of moduli squared, has been used, together with the correction to G_F from the muon lifetime, Eq. (2.20). As can be seen, the full dependence on the CKM and R-parity violating

phases is also indicated. We have adopted the Wolfenstein parametrization [39] to express the CKM matrix elements. In this parametrization V_{us} is real, while V_{ub} is not. Nonetheless, measurements of the absolute values of the CKM elements give $|V_{ub}| \sim 0.004$, approximately two orders of magnitude smaller than $|V_{ud}| \sim 0.974$ and $|V_{us}| \sim 0.226$. Thus, the behavior of Eq. (2.55) is almost independent of λ'_{13k}, as $|V_{ub}|$ can be neglected. Taking into account the fact that V_{us} is real and $|V_{ub}|$ is tiny, and neglecting for the moment the SUSY correction to G_F, Eq. (2.55) implies 2σ bounds on a three dimensional parameter space spanned by $|\lambda'_{11k}|$, $|\lambda'_{12k}|$ and $\cos(\theta_{12k} - \theta_{11k})$. λ'_{11k}, can be bounded by π-decay, Eq. (2.50). λ'_{12k} can be bounded by the forward-backward (FB) asymmetry in fermion pair production reactions $e^-e^+ \to f\bar{f}$, which we treat in detail in the next subsection. The 2σ-bound region is shown in Fig. 2.5b. Note that, contrary to the other cases in the paper, here the index k has to be common to the three axes in the picture. One can see that, in spite of the fact that the phases are allowed to take on any values, the λ' parameters are allowed a slightly larger region when $\cos(\Delta\theta^{us}_k) = -1$. We come back to this point at the end of this section.

Forward-backward Asymmetry

The forward-backward asymmetry in fermion pair production has been studied at PEP, PETRA, TRISTAN, LEP, and SLC. In order to bound $\lambda'_{12k}(\tilde{d}_{Rk})$ we need charm production, $e^-e^+ \to c\bar{c}$. The SUSY diagram that contributes to this process is depicted in Fig. 2.7a, with $u_1 \to u_2$, $\lambda'_{11k} \to \lambda'_{12k}$. We assume that the right-handed down squark mass is far enough above the Z-pole that we can retain our effective Lagrangians, Eqs. (2.11) and (2.13), and use the data in [10], dominated by Z-pole measurements.

The SM expression for the charm FB asymmetry reads [40]:

$$A_{FB}^{SM} = \frac{A_1}{\frac{8}{3}A_0}\,, \tag{2.56}$$

where

$$\begin{aligned} A_0 &= Q_c^2 - \frac{Q_c}{2}\Re(r)\left(g_L^e g_L^c + g_R^e g_R^c + g_L^e g_R^c + g_R^e g_L^c\right) \\ &\quad + \frac{1}{4}|r|^2\left[(g_L^e g_L^c)^2 + (g_R^e g_R^c)^2 + (g_L^e g_R^c)^2 + (g_R^e g_L^c)^2\right], \qquad (2.57) \\ A_1 &= -Q_c\Re(r)\left(g_L^e g_L^c + g_R^e g_R^c - g_L^e g_R^c - g_R^e g_L^c\right) \\ &\quad + \frac{1}{2}|r|^2\left[(g_L^e g_L^c)^2 + (g_R^e g_R^c)^2 - (g_L^e g_R^c)^2 - (g_R^e g_L^c)^2\right], \qquad (2.58) \end{aligned}$$

where $g_{L,R}$ are the usual chiral couplings, $Q_c = 2/3$ is the charge of the charm and

$$r = \frac{4\sqrt{2}G_F M_Z^2}{s - M_Z^2 + iM_Z\Gamma_Z}\left(\frac{s}{e^2}\right) \tag{2.59}$$

parametrizes the $\gamma - Z$ interference. The R-parity contribution is obtained by the substitution:

$$g_L^e g_L^c \longrightarrow g_L^e g_L^c - \frac{r'_{12k}(\tilde{d}_{Rk})}{2}\,. \tag{2.60}$$

So the correction to the SM reads at lowest order,

$$A_{FB} = A_{FB}^{SM}\left[1 - \frac{r'_{12k}(\tilde{d}_{Rk})F(r)}{2}\left(\frac{1}{2A_0} - \frac{1}{A_1}\right)\right], \tag{2.61}$$

where

$$F(r) = Q_c\Re(r) - |r|^2 g_L^e g_L^c \tag{2.62}$$

and r has to be calculated at the Z-pole. By using the standard $SU(2)\times U(1)$ expressions for g_L and g_R, and adopting the $\overline{MS}$ scheme value of $\sin^2\theta_W$ for definiteness,

one gets the values: $g_L^e = -0.2688$, $g_R^e = 0.2312$, $g_L^c = 0.3459$, $g_R^c = -0.1541$. We obtain the bound at 2σ:

$$|\lambda'_{12k}| \leq 0.027 \left(\frac{m_{\tilde{d}_{Rk}}}{100 \text{ GeV}}\right) . \tag{2.63}$$

As mentioned above, Fig. 2.5b shows that allowing for the λ'_{11k} and λ'_{12k} couplings to have opposite complex phases ($\cos \Delta\theta_k^{us} = -1$) slightly extends the allowed regions of parameter space with respect to the SCD. Furthermore, such an extension becomes significant when we also introduce the leptonic coupling λ_{12k}, bounded by the experimental limits on the muon liftime in the $\overline{MS}$ scheme, Eq. (2.28). The 2σ-allowed region in λ'_{11k}, λ_{12k} and λ'_{12k} obtained by simultaneous combination of the data from CKM unitarity, FB asymmetry in charm production and muon decay in the $\overline{MS}$ renormalization scheme is shown in Fig. 2.5c. It is enclosed in a box of size $\{|\lambda'_{11k}|(\tilde{d}_{Rk}), |\lambda_{12k}|(\tilde{e}_{Rk}), |\lambda'_{12k}|(\tilde{d}_{Rk})\} \leq \{0.047, 0.042, 0.036\}$, thus allowing roughly factor of two extensions of the parameters with respect to the SCD bounds. The combined analysis furnishes a new 2σ bound on λ'_{11k}. As mentioned above, λ'_{111} is tightly bounded by neutrinoless double-beta decay [38]. We get,

$$|\lambda'_{11k}| \leq 0.039 \left(\frac{m_{\tilde{d}_{Rk}}}{100 \text{ GeV}}\right) . \tag{2.64}$$

This striking situation, where three parameters are all allowed to be non-zero and larger than their SCD values, is obscured when only one parameter at a time is considered, i.e. SCD is assumed uniformly. In principle the second row of the CKM

matrix could be used in a similar fashion to bound $|\lambda'_{21k}|$ and $|\lambda'_{22k}|$:

$$\sum_{i=1}^{3}|V_{cd_i}|^2 = 1-2r_{12k}(\tilde{e}_{Rk})+2\left(\sum_k \frac{|\lambda'_{21k}||\lambda'_{22k}|\cos(\Delta\theta_k^{cd})}{4\sqrt{2}G_F m^2_{\tilde{d}_{Rk}}}\right)|V_{cd}|+2\sum_i r'_{22k}(\tilde{d}_{Rk})\,|V_{cs}|\ , \tag{2.65}$$

where $\cos(\Delta\theta_k^{cd}) \sim \cos(\theta_{21k}-\theta_{22k})$ in the Wolfenstein parametrization. $|\lambda'_{21k}|$ ($\tilde{d}_{Rk}$) can be bounded by pion decay, Eq. (2.50). The dependence on λ_{12k} ($\tilde{e}_{Rk}$) comes from the bounds on universality of the Fermi constant in muon decay. We use, again, the $\overline{MS}$ bound at 2σ, Eq. (2.28). The weakest bound consistent with both these constraints is obtained when $\cos(\Delta\theta_k^{cd}) = -1$ and reads, at 2σ,

$$|\lambda'_{22k}| \leq 0.14\left(\frac{m_{\tilde{d}_{Rk}}}{100\ \text{GeV}}\right)\ . \tag{2.66}$$

A caveat is necessary at this point, in the sense that Eq. (2.65) is derived for processes involving the production of charmed particles in deep inelastic ν_μ-nucleon scattering, with the assumption of lepton flavor conservation. This is the standard textbook process used for the determination of the CKM couplings $|V_{cd}|$ and $|V_{cs}|$ [41]. Such a choice is reflected by the $i = 2$ index of the λ'_{ijk} couplings entering Eq. (2.65). The use of recent PDG2008 data for the uncertainty affecting the unitarity constraint and for the central values of the CKM matrix elements is not fully consistent with this idealized picture. The most recent and precise values given in [10] are obtained through a weighted average of different processes, some of which involve external particles of the first or third lepton generation. It is clear that the robustness of the bound given in Eq. (2.66) depends strongly on the amount and nature of the weighting involved. Because such detailed knowledge and extensive analysis in this regard goes beyond the purposes of this paper, we limit ourselves to presenting the bound above, recommending caution in its interpretation. As we will see in Sec. 2.3.4,

D^0 decay alone places bounds on the same (sum of) couplings. We consider those bounds more robust.

Finally, Eq. (2.55) has the nice feature that it involves the phases of the R-breaking couplings. In general such phases are associated with CP violating effects. So we can envisage a strategy that would combine additional experiments in the CP violating sector with those that can place bounds on the moduli of $\not{R}$-couplings like the two above, so that a more thorough restriction of parameter space takes place. However we did not find in the literature [15], nor were we able to create a specific example that would help us bound the phases of the couplings involved in this case, namely the product $\lambda'^{*}_{11k}\lambda'_{12k}$ ($\tilde{d}_{Rk}$), in terms of CP violating processes. Some asymmetries in fermion pair production at leptonic colliders ($l^+l^- \to f_J\bar{f}_{J'}$) on and above the Z-pole [42] can be expressed in term of non trivial combinations of R-breaking phases like $\Im(\lambda'^{*}_{1Jk}\lambda'_{1J'k}\lambda'_{ijJ}\lambda'^{*}_{ijJ'})/|\lambda'^{*}_{i'1J}\lambda'_{i'1J'}|^2$, with obvious summation over dummy indices. A detailed and comprehensive study of such processes would probably shed light on the phenomenological constraints on CP violating phases. Nonetheless, due to the great number of couplings involved, such a study would have to take into account a large number of interactions, many of which cannot be treated as "low energy" processes. This clearly exceeds the purposes of this paper, requiring an extensive, separate investigation.

As anticipated above, and shown in Fig 2.5b, we have tried to constrain the phase difference $\cos(\theta_{11k} - \theta_{12k})$ by using Eq. (2.55), where all the absolute values are bounded by some other experiments. We have also tried to constrain the phase $\cos(\theta_{21k} - \theta_{22k})$ with the second row, Eq. (2.65). We found no handle to constrain parameters, as any possible values of the phases are allowed by CKM unitarity.

2.3.3 Atomic Parity Violation

We can follow the same technique, and use the bounds on λ'_{11k} obtained by CKM unitarity and the bounds on λ_{12k} obtained in the $\overline{MS}$ renormalization scheme to place bounds on λ'_{1j1} from atomic parity violation (APV). In the SM the Z-exchange between the electrons and atomic nuclei leads to parity violating transitions between particular atomic levels. This has been observed for example in the $6S \to 7S$ transitions of $^{133}_{55}$Cs [43, 44]. The SM contributions are encapsulated in the weak charge Q_W^{SM}, which is defined as [10]

$$Q_W^{SM} = -2\left[(A+Z)\,C_1^{SM}(u) + (2A-Z)\,C_1^{SM}(d)\right]\,, \tag{2.67}$$

where Z is the atomic number, A the atomic mass, and the coefficients $C_1(i)$ are given at tree level by

$$C_1^{SM}(u) = -\frac{1}{2} + \frac{4}{3}x_W \quad \text{and} \quad C_1^{SM}(d) = \frac{1}{2} - \frac{2}{3}x_W\,. \tag{2.68}$$

The corresponding experimental quantities can be expressed in terms of the SM contributions and the $\not{R}$ processes depicted in Fig. 2.7 [13]:

$$C_1(u) = C_1^{SM}(u)\,[1 - r_{12k}\,(\tilde{e}_{Rk})] - r'_{11k}(\tilde{d}_{Rk}) \tag{2.69}$$

$$C_1(d) = C_1^{SM}(d)\,[1 - r_{12k}\,(\tilde{e}_{Rk})] + r'_{1j1}(\tilde{u}_{Lj})\,, \tag{2.70}$$

where we have assumed the R-parity correction to the Fermi constant, Eq. (2.20). The most recent determination of the difference $\delta Q_W = Q_W^{\rm exp} - Q_W^{SM}$ for cesium can

be found in [10] and its expression in terms of $\not{R}$-couplings reads:

$$\delta Q_W = -Q_W^{SM} r_{12k}(\tilde{e}_{Rk}) + 376 r'_{11k}(\tilde{d}_{Rk}) - 422 r'_{1j1}(\tilde{u}_{Lj})\,. \tag{2.71}$$

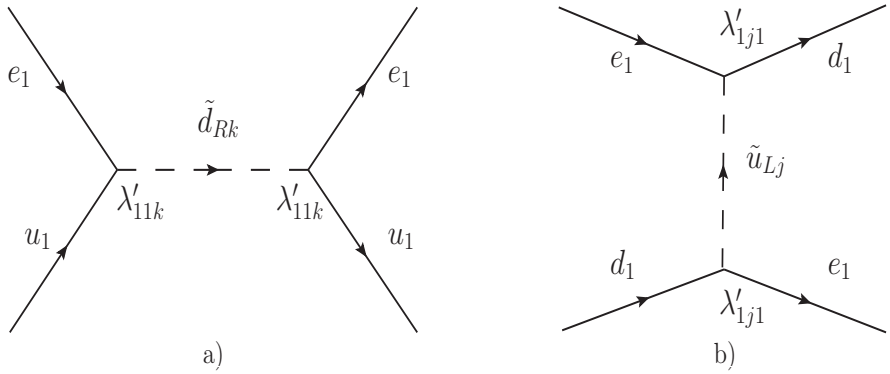

Figure 2.7: SUSY processes involved in Atomic Parity Violation.

Again, we can first determine the 2σ bounds on the semi-leptonic couplings that one can obtain by use of the SCD: $|\lambda'_{11k}| \leq 0.051$ $(\tilde{d}_{Rk})$ and $|\lambda'_{1j1}| \leq 0.024$ $(\tilde{u}_{Lj})$. When both semi-leptonic couplings are considered, the region of parameter space that is bounded is two dimensional and its shape is similar to that of Fig. 2.2a. The dependence of δQ_W on the leptonic coupling λ_{12k} $(\tilde{e}_{Rk})$ due to G_F-correction introduces an additional direction in parameter space, which becomes three dimensional. μ decay in one of the renormalization schemes described in Sec. 2.2 can be used to place bounds on λ_{12k}, while pion decay, Eq. (2.50), can be used to place bounds on λ'_{11k}. The weakest bound is obtained in the $\overline{MS}$ scheme, Eq. (2.28). As we have explained extensively in Sec. 2.3.1, by simultaneously considering these three processes we can delimit a 2σ bounded region of parameter space, which we present in Fig. 2.8a. It can be enclosed in a box of size $\{|\lambda'_{1j1}|(\tilde{u}_{Lj}), |\lambda_{12k}|(\tilde{e}_{Rk}), |\lambda'_{11k}|(\tilde{d}_{Rk})\} \leq \{0.055, 0.043, 0.059\}$, thus allowing only marginal extension with respect to the SCD for the λ'_{11k} and λ_{12k}

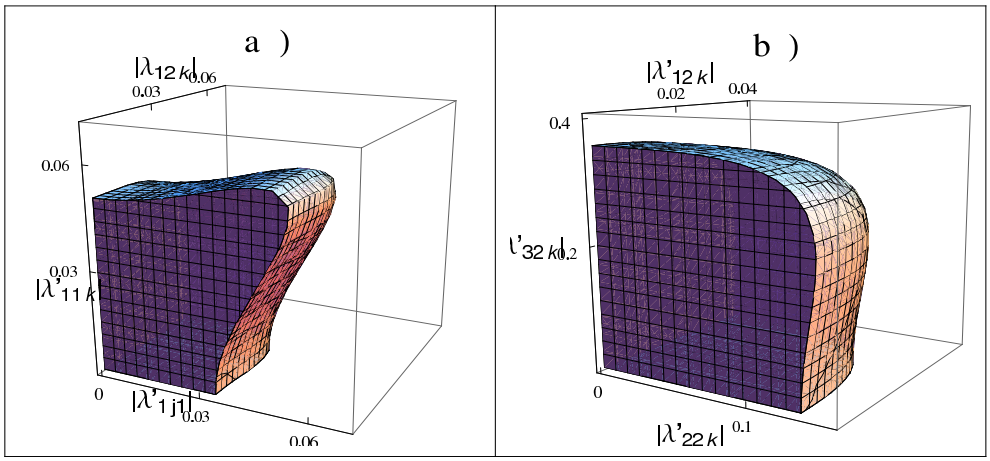

Figure 2.8: a) 2σ bound region on $\lambda'_{1j1}(\tilde{u}_{Lj})$, $\lambda_{12k}(\tilde{e}_{Rk})$ and $\lambda'_{11k}(\tilde{d}_{Rk})$ from APV, μ decay in the $\overline{MS}$ renormalization scheme and R_π combined. The allowed region can be enclosed in a box of size $\{|\lambda'_{1j1}|(\tilde{u}_{Lj}), |\lambda_{12k}|(\tilde{e}_{Rk}), |\lambda'_{11k}|(\tilde{d}_{Rk})\} \leq \{0.055, 0.043, 0.059\}$. b) 2σ bound region on $\lambda'_{22k}(\tilde{d}_{Rk})$, $\lambda'_{12k}(\tilde{d}_{Rk})$ and $\lambda'_{32k}(\tilde{d}_{Rk})$ from D_0 decay, FB asymmetry and D_s decay combined. The allowed region can be enclosed in a box of size $\{|\lambda'_{22k}|(\tilde{d}_{Rk}), |\lambda'_{12k}|(\tilde{d}_{Rk}), |\lambda'_{32k}|(\tilde{d}_{Rk})\} \leq \{0.140, 0.034, 0.359\}$.

parameters, but roughly a factor of two for the λ'_{1j1} parameter. The 2σ bound on λ'_{1j1} we gather from the combined analysis reads,

$$|\lambda'_{1j1}| \leq 0.045 \left(\frac{m_{\tilde{u}_{Lj}}}{100 \text{ GeV}}\right) . \tag{2.72}$$

2.3.4 *D* Decays

For our last examples, let us now consider D- and D_s-meson decays. We can implement our procedure of taking processes that involve one or more of the couplings we have bounded in the previous cases, together with others which are at the moment unbounded, and then use the known bounds to restrict the boundaries of the allowed multidimensional parameter space to obtain bounds on the remaining couplings. Again we use the averages from experimental data as reported in PDG2008 and present bounds at the 2σ level.

We consider the following ratios of branching fractions: $R_{D^+} = B(D^+ \to \bar{K}^0 \mu^+ \nu_\mu)/B(D^+ \to \bar{K}^0 e^+ \nu_e)$ and $R_{D^0} = B(D^0 \to K^- \mu^+ \nu_\mu)/B(D^0 \to K^- e^+ \nu_e)$. Their expression in terms of R-breaking semileptonic couplings is given by

$$\frac{R_{D^+}}{R_D^{SM}} = \frac{R_{D^0}}{R_D^{SM}} = \frac{\left|V_{cs} + r'_{22k}(\tilde{d}_{Rk})\right|^2}{\left|V_{cs} + r'_{12k}(\tilde{d}_{Rk})\right|^2}\,. \tag{2.73}$$

$R_D^{SM} = 1/1.03$ is the reduction due to muon phase-space [45, 15]. The bidimensional parameter space for $|\lambda'_{12k}|$ vs. $|\lambda'_{22k}|$ presents a degeneracy very similar to the one depicted in Fig. 2.2a, where the maximum values obtained on the axis correspond to simple use of the SCD: $|\lambda'_{22k}| \leq 0.32$ $(\tilde{d}_{Rk})$, $|\lambda'_{12k}| \leq 0.20$ $(\tilde{d}_{Rk})$ for D^+ decay, and $|\lambda'_{22k}| \leq 0.10$ $(\tilde{d}_{Rk})$, $|\lambda'_{12k}| \leq 0.21$ $(\tilde{d}_{Rk})$ for D^0 decay.

It is clear that, of the two ratios we have considered, D^0 decay places a tighter bound on these couplings. On the other hand, we can bound separately λ'_{12k} by means of the FB asymmetry, Eq. (2.61). The bound is tight enough to cut the bidimensional degeneracy almost entirely. We get, as a consequence,

$$|\lambda'_{22k}| \leq 0.090 \left(\frac{m_{\tilde{d}_{Rk}}}{100\ \text{GeV}}\right)\,, \tag{2.74}$$

ten percent stronger than that obtained by SCD.

Turning to the $D_s^- \to \ell^- + \overline{\nu}_\ell$ decays for further constraints, we can bound λ'_{32k} in the same way, starting from the ratio

$$\frac{R_{D_s}(\tau\mu)}{R_{D^-}^{SM}} = \frac{\Gamma(D_s^- \to \tau^- \bar{\nu}_\tau)}{R_{D^-}^{SM} \times \Gamma(D_s^- \to \mu^- \bar{\nu}_\mu)} = \frac{\left|V_{cs} + r'_{32k}(\tilde{d}_{Rk})\right|^2}{\left|V_{cs} + r'_{22k}(\tilde{d}_{Rk})\right|^2}\,, \tag{2.75}$$

where $R_{D^-}^{SM} = 9.76$ accounts for the phase-space suppression. One would get, by

SCD use, $|\lambda'_{22k}| \leq 0.27$ $(\tilde{d}_{Rk})$ and $|\lambda'_{32k}| \leq 0.34$ $(\tilde{d}_{Rk})$. The combined analysis of D_0 decay, Eq. (2.73), and Eqs. (2.75) and (2.61) yields the 2σ region depicted in Fig. 2.8b, whose margins are given by the box $\{|\lambda'_{22k}|(\tilde{d}_{Rk}), |\lambda'_{12k}|(\tilde{d}_{Rk}), |\lambda'_{32k}|(\tilde{d}_{Rk})\} \leq \{0.140, 0.034, 0.359\}$, with only slight extension beyond the bounds obtained by assuming SCD. This translates to the 2σ bound

$$|\lambda'_{32k}| \leq 0.29 \left(\frac{m_{\tilde{d}_{Rk}}}{100 \text{ GeV}}\right) . \tag{2.76}$$

This bounds is, again, roughly ten percent stronger than that obtained by SCD [46].

2.4 Summary

In this chapter, we limited our attention to experimental results from a set of standard leptonic and semi-leptonic processes and allowed $\not{R}$ parameters to vary together, constrained by data at the 2σ level, to place bounds on their values. We compared the resulting bounds with those obtained from the long-standing procedure of allowing only one parameter to be non-zero at a time, which has produced a long, useful list of bounds in the literature over the past twenty years or so. Using our different approach, we showed that a joint analysis of different experiments involving the same subset of couplings can explore regions of parameter space where the bounds are weakened compared to the value set by the SCD procedure. More importantly, the 2σ bounds on individual couplings obtained by the combined approach are generally different from those obtained by strict SCD. This is due to the fact that almost all processes can by expressed in terms of more than one parameter, thus introducing correlations between the couplings and degeneracies in the allowed regions of parameter space. The combined-experiments approach helps eliminate these degeneracies

λ(scale)	Experiment	Bound(2σ)	Corr. λ	SCD Bound
$\lambda_{12k}(m_{\tilde{e}_{Rk}})$	G_μ	0.037	none	NA
$\lambda_{121}(m_{\tilde{\mu}_L})$	$\nu_e(\overline{\nu}_e)e$	0.36	$\lambda_{131}(m_{\tilde{\tau}_L})$	0.33
$\lambda_{121}(m_{\tilde{e}_L})$	$\nu_\mu e$	0.118	$\lambda_{231}(m_{\tilde{\tau}_L})$	0.138
$\lambda_{13k}(m_{\tilde{e}_{Rk}})$	R_τ	0.071	$\lambda_{12k}(m_{\tilde{e}_{Rk}}), \lambda_{23k}(m_{\tilde{e}_{Rk}})$	0.048
$\lambda_{131}(m_{\tilde{\tau}_L})$	$\nu_e(\overline{\nu_e})e$	0.36	$\lambda_{121}(m_{\tilde{\mu}_L})$	0.33
$\lambda_{23k}(m_{\tilde{e}_{Rk}})$	R_τ	0.066	$\lambda_{12k}(m_{\tilde{e}_{Rk}}), \lambda_{13k}(m_{\tilde{e}_{Rk}})$	0.051
$\lambda_{231}(m_{\tilde{\tau}_L})$	$\nu_\mu e$	0.118	$\lambda_{121}(m_{\tilde{e}_L})$	0.138
$\lambda'_{11k}(m_{\tilde{d}_{Rk}})$	$CKM_{unitary}$	0.039	$\lambda_{12k}(m_{\tilde{e}_{Rk}}), \lambda'_{12k}(m_{\tilde{d}_{Rk}})$	0.027
$\lambda'_{12k}(m_{\tilde{d}_{Rk}})$	$A_{FB}(c\overline{c})$	0.027	none	NA
$\lambda'_{22k}(m_{\tilde{d}_{Rk}})$	D_0 decay	0.090	$\lambda'_{12k}(m_{\tilde{d}_{Rk}})$	0.10
$\lambda'_{21k}(m_{\tilde{d}_{Rk}})$	$(\pi/\tau)_{universal.}$	0.040	$\lambda'_{31k}(m_{\tilde{e}_{Rk}})$	0.032
$\lambda'_{31k}(m_{\tilde{d}_{Rk}})$	$(\pi/\tau)_{universal.}$	0.092	$\lambda'_{21k}(m_{\tilde{e}_{Rk}})$	0.092
$\lambda'_{1j1}(m_{\tilde{u}_{Lj}})$	APV	0.045	$\lambda_{12k}(m_{\tilde{e}_{Rk}}), \lambda'_{11k}(m_{\tilde{d}_{Rk}})$	0.024
$\lambda'_{32k}(m_{\tilde{d}_{Rk}})$	D_s decay	0.29	$\lambda'_{22k}(m_{\tilde{d}_{Rk}}), \lambda'_{12k}(m_{\tilde{d}_{Rk}})$	0.34

Table 2.2: Summary of constraints on λ values with their corresponding mass scale in parenthesis. The "Experiment" column gives the measured quantities that are the source of the multi-variable bound, the "Bound" column. The "Corr. λ" column gives the most directly correlated λ determining the constraint, while the final column, "SCD bound" gives the value of the bound when all the relevant λ couplings but the one in the first column are set to zero. The note "none" in a column means that only one coupling appears in the relevant expression to compare to experiment. The note "NA" means that there is no other coupling to set to zero for the case in this row.

and at the same time maintains the full parameter space structure. These features provide qualitatively different information from that available in the literature, whose results are almost exclusively limited to isolating parameters and considering them one at a time. New bounds obtained with our approach are given in Table 2.2, where we present a summary of the results described in the preceding sections.

In the $\bar{\nu}_e e$ case, we found that the requirement that certain trilinear couplings were non-zero, combined with simultaneous constraints involving the same couplings but different sfermion masses, we could extract hierarchical relationships among these masses. We illustrated this situation in Fig. 2.4, where the 1σ allowed area in the space of "mass ratios" is displayed, and in the paragraphs following Eq. (2.48), where

individual 1σ and 1.65σ mass bounds are shown. To the best of our knowledge, this is the first effort, in the context of purely phenomenological bounds on $\not{R}$ parameters, to find constraints among the sfermion masses.

In conclusion, we can say that, overall, a richer, more complex picture of parameter space and, in most cases weaker bounds on $\not{R}$ parameters result from a multi-parameter, multi-process analysis, compared to the analysis of each parameter in isolation. This conclusion is non-trivial when, as the case in expressions we consider, parameters enter as sums of squares, suggesting that dropping all parameters but one provides the most conservative limit on each. Nonetheless, since we found the allowed ranges of parameters were larger by at most a factor two, we conclude that the SCD approach is a reliable order of magnitude estimate of the upper bounds on the individual parameters. At the same time, we conclude that fuller analyses, as exemplified here, are needed to search for hints that data are showing R-parity violation in a region of parameter space where several parameters are non-zero. Finally, such analyses are needed to explore mass relations among sparticle masses, which requires disentangling couplings and masses by comparisons of theory with data.

Chapter 3

Indirect Signatures of Fermion WIMPless Dark Matter

There has long been interest in the use of neutrino experiments for indirect dark matter (DM) detection, with a particular focus on neutrino signals from DM annihilation in the Sun. The basic idea is that DM particles can be captured by the Sun if they lose sufficient kinetic energy through elastic scattering from solar nuclei. This leads to an enhanced DM number density in the solar core, where DM can annihilate to standard model (SM) products. These products in turn decay, producing a neutrino flux which can be detected by Earth-based detectors. Because the Sun is (for most models under consideration) in equilibrium, the DM capture rate is equal to twice the annihilation rate. Thus, the neutrino flux on Earth is determined by the capture rate, which in turn is determined (up to a few $\mathcal{O}(1)$ factors related to solar physics) by the DM mass m_χ and the DM-nucleon scattering cross section σ. This is one of the key advantages of neutrino-based indirect searches for DM: the event rate is directly related to the scattering cross section, without many of the astrophysical uncertainties which attend other indirect detection strategies. Moreover, it is in principle possible to directly compare search results at neutrino experiments with those at direct-detection experiments, which also measure the DM-nucleon scattering cross section; for a recent discussion, see [47]. This allows one to corroborate a signal at one type of experiment with a signal at a very different type of experiment, which is

desirable.

The downside, however, is that for much of the (m_χ, σ)-parameter space, sensitivities for current and future neutrino detectors have already been surpassed by direct-detection bounds, implying that neutrino detectors may have difficulty providing new input to DM studies. However, there are two scenarios where neutrino experiments are expected to shine. One is at low-mass ($m_\chi \sim 4 - 10$ GeV). In this mass range, bounds from direct-detection experiments tend to become significantly worse because the nuclear recoil energies often fall below the experimental threshold. Experiments such as Super-Kamiokande (Super-K) and other proposed water Cherenkov or liquid scintillator-type detectors can provide the best bounds in this range [48], and could be sensitive to spin-independent (SI) scattering cross sections $\sigma_{SI} \sim 10^{-5}$ pb. DM in this range can potentially explain the annual modulation signal seen by the DAMA experiment ([49], though see also [50]), as well as unexplained events recently reported by the CDMS and CoGeNT Collaborations [51, 52, 53]. There is thus considerable interest to cross-check these results with neutrino detectors.

Another scenario for which neutrino experiments can excel is for models where the DM-nucleon scattering is largely spin-dependent (SD), rather than SI [54]. The reason is that DM can then be captured by SD scattering from hydrogen in the Sun, leading to significant neutrino fluxes. Current direct-detection experiments provide much less sensitivity to SD scattering and the best bounds are set by indirect detection experiments, even at large m_χ. This has been the focus of large neutrino detectors, such as AMANDA or IceCube. For example, with 1800 live days of running, IceCube could be sensitive to $\mathcal{O}(100$ GeV) DM with $\sigma_{SD} \sim 10^{-5}$ pb [55]. Although the relatively high threshold energy of these detectors limits their utility in studying the low-mass DM, their large size makes them ideal for studying higher-mass DM ($m_\chi \geq 100$ GeV) with $\sigma_{SD} \gg \sigma_{SI}$.

Direct detection is much more sensitive to σ_{SI} due to the possibility of coherent scattering in the nucleus. Direct-detection experiments, including CDMS and XENON100, currently have a sensitivity to σ_{SI} in the $\mathcal{O}(100$ GeV) mass range of about 3 orders of magnitude [51, 56] greater than the IceCube projected 1800 d sensitivity to σ_{SD}. But for models with $\sigma_{SI} \ll \sigma_{SD}$, complementary coverage from neutrino detectors becomes important. This complementary coverage is especially important if one goes beyond models of weakly interacting massive particles (WIMPs). The recently proposed WIMPless model of dark matter [3, 4] is notable because it provides a very generic hidden sector DM candidate which naturally has about the right relic density to match astronomical observations, regardless of the mass of the DM particle or the details of the hidden sector. This versatility suggests the possibility of specific WIMPless models with almost exclusively SD scattering, for which the best detection prospects would lie at neutrino detectors.

We present a model of WIMPless dark matter where the DM candidate is a Majorana fermion in the hidden sector. At tree level, it will exhibit only SD scattering with SM nuclei. We find that significant neutrino fluxes on Earth arise from models where DM annihilates either to tau, stau, or sneutrino pairs. We consider the detection prospects for this type of model at DeepCore and IceCube.

3.1 WIMPless Dark Matter

Here we briefly review the WIMPless DM scenario [3]. This scenario is closely related to GMSB [57]. Our theory consists of a SUSY-breaking sector, the visible MSSM sector and a hidden sector, plus a *connector* sector which we introduce in the next subsection. We assume there is at least one chiral superfield S in the SUSY-breaking sector, and there are messenger fields Φ, $\bar{\Phi}$ between the SUSY-breaking and MSSM

sectors and Φ_χ, $\bar{\Phi}_\chi$ between the SUSY-breaking and hidden sector. S is coupled to the messenger fields through Yukawa couplings in the superpotential $W = \lambda\bar{\Phi}S\Phi + \lambda_\chi\bar{\Phi}_\chi S\Phi_\chi$. The effect of GMSB on the MSSM sector is well-known: the chiral field S acquires a vacuum expectation value (VEV) $\langle S\rangle = M + \theta^2 F$. The Yukawa couplings generate messenger mass terms of order $m_{mess} \sim \lambda M$ and messenger mass-splittings of order $F_{mess} = \lambda F$. Once the heavy gauge messengers are integrated out, the low-energy effective theory has a new SUSY-breaking soft scale m_{soft} which is generated by diagrams with the messengers running in the loops,

$$m_{soft} \sim \frac{g^2}{(4\pi)^2}\left(\frac{F_{mess}}{m_{mess}}\right) = \frac{g^2}{(4\pi)^2}\frac{F}{M}\,, \tag{3.1}$$

where g is the largest relevant gauge coupling. The effect in the hidden sector is qualitatively the same, and we assume that some unbroken symmetry stabilizes a particle in the hidden sector at the soft SUSY-breaking scale, whatever it may be. The soft SUSY-breaking scale in the hidden sector is then given by

$$m_\chi \sim \frac{g_\chi^2}{(4\pi)^2}\left(\frac{F_{mess\chi}}{m_{mess\chi}}\right) = \frac{g_\chi^2}{(4\pi)^2}\frac{F}{M}\,, \tag{3.2}$$

where $F_{mess\chi} = \lambda_\chi F$ and $m_{mess\chi} \sim \lambda_\chi M$. Because the ratio F/M is determined by the dynamics of the SUSY-breaking sector, it appears in the same way in the soft scale in both the hidden sector and MSSM sector. We thus find

$$\frac{g_\chi^4}{m_\chi^2} \sim \frac{g^4}{m_{soft}^2} \propto \left(\frac{M}{F}\right)^2. \tag{3.3}$$

The ratio g^4/m^2 sets the annihilation cross-section for a particle of mass of order m through gauge interactions of strength g, and the cross-section in turn determines the thermal relic density, ($\Omega \propto \langle\sigma v\rangle^{-1}$ [58]). To obtain a thermal relic density which

matches astronomical observations, a DM candidate would need an annihilation cross-section $\langle \sigma v \rangle \sim 1$ pb. The "WIMP Miracle" is the amazing fact that, when calculated at the electroweak scale, the ratio g^4_{weak}/m^2_{weak} yields an annihilation cross-section which is in fact close to 1 pb. But we see from Eq. (3.3) that the annihilation cross-section for a stable particle at the hidden sector soft SUSY-breaking scale will be approximately the same; this DM candidate will thus automatically have approximately the right relic density. Most importantly, the scale m_χ of the DM is a free parameter, thus motivating DM searches over a wide range of masses.

3.1.1 Fermionic Model

In the WIMPless scenario, DM is stabilized by a hidden sector symmetry (which may be discrete). We let $\hat{X}_{L,R}$ be chiral supermultiplets in the hidden sector, with a fermionic mass eigenstate of $X_{L,R}$ (henceforth denoted as X) being the lightest particle charged under the stabilizing symmetry. WIMPless DM interacts with the SM through Yukawa couplings, which permit the exchange of exotic "connector" particles. Consider the interaction superpotential,

$$\begin{aligned} W &= \lambda_{Li}\hat{X}_L\hat{Y}_L\hat{Q}_{Li} + \lambda_{Ri}\hat{X}_R\hat{Y}_R\hat{Q}_{Ri} + m_Y\hat{Y}_L\hat{Y}_R \\ &\quad + \lambda'_{Lj}\hat{X}_L\hat{Y}^{lep.}_L\hat{L}_{Lj} + \lambda'_{Rj}\hat{X}_R\hat{Y}^{lep.}_R\hat{L}_{Rj} + m_{Y^{lep.}}\hat{Y}^{lep.}_L\hat{Y}^{lep.}_R, \end{aligned} \tag{3.4}$$

where $\hat{Q}_{Li,Ri}$ are MSSM chiral quark multiplets, $\hat{L}_{Li,Ri}$ are MSSM chiral lepton multiplets, and $\hat{Y}_{L,R}$ and $\hat{Y}^{lep.}_{L,R}$ are the exotic connector particles which are charged under both the MSSM and the hidden sector symmetry. Gauge-invariance requires the $\hat{Y}_{L,R}$ to be chiral under the MSSM, so their fermion components behave like exotic fourth generation quarks (similarly, the fermions of $\hat{Y}^{lep.}_{L,R}$ are exotic fourth generation leptons). The mass terms m_Y, $m_{Y^{lep.}}$ are thus set by electroweak symmetry breaking,

and are determined by the Higgs VEV and Yukawa couplings.

The mass of the exotic quarks is constrained by perturbativity and precision electroweak data to the range $m_Y \lesssim 600\,\text{GeV}$ [59, 60, 61]. Since the DM particle X is the lightest particle charged under the stabilizing hidden sector symmetry, it is constrained to be lighter than any of the exotic connectors.

Since the exotic squarks $\tilde{Y}_{L,R}$ can get mass terms which are decoupled from electroweak symmetry breaking, there is no relevant upper bound on $m_{\tilde{Y}_{L,R}}$. But $m_{\tilde{Y}_{L,R}}$ can be bounded from below by direct searches at colliders. The exotic squarks can be pair produced through QCD processes, with each decaying via $\tilde{Y}_{L,R} \to X + u, d$. The signal at a hadron collider would be exclusive dijet production with missing transverse energy, which is the same signature as that of leptoquark pair production, with decay to a quark and neutrino. A CDF collaboration search for this signature [62] places a bound on the leptoquark mass at $m_{LQ} > 187$ GeV. Since, in our case, the missing energy arises from a relatively heavy DM particle X (as opposed to a nearly massless neutrino), the lower bound on the mass of the exotic squark will be even weaker, and for our analysis it will not be constraining.

The DM candidate X can be either a Dirac or Majorana fermion. We thus see that DM-nucleon scattering can arise from s- or u-channel exchange of the Y multiplets, as represented in Fig. 3.1. After a Fierz transformation, we can write the DM-parton scattering matrix element in terms of an effective operator,

$$\mathcal{O} = \frac{\lambda_{Li}^2}{2(m_X^2 - m_{\tilde{Y}_L}^2)^2}(\bar{q}_i\gamma^\mu P_L q_i)(\bar{X}\gamma_\mu P_R X) + \frac{\lambda_{Ri}^2}{2(m_X^2 - m_{\tilde{Y}_R}^2)^2}(\bar{q}_i\gamma^\mu P_R q_i)(\bar{X}\gamma_\mu P_L X)\,. \tag{3.5}$$

We assume from here on that the scalars from the Y_L and Y_R multiplets have degenerate mass; $m_{\tilde{Y}_L} = m_{\tilde{Y}_R} = m_{\tilde{Y}}$. If we only retain terms which provide a velocity-

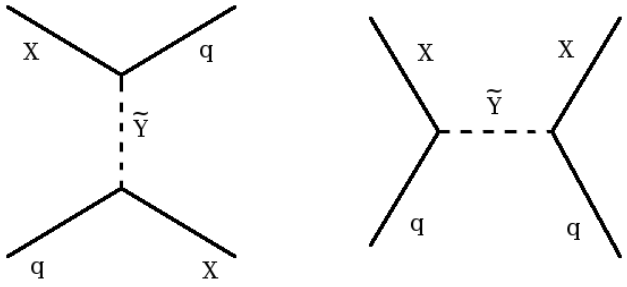

Figure 3.1: The u- and s-channel Feynman diagrams for Xq-scattering.

independent contribution to DM-nucleon scattering, we can write this operator as

$$\mathcal{O} \approx \frac{\lambda_{Li}^2 + \lambda_{Ri}^2}{8(m_{\tilde{Y}}^2 - m_X^2)}[(\bar{q}_i\gamma^\mu\gamma_5 q_i)(\bar{X}\gamma_\mu\gamma_5 X) - (\bar{q}_i\gamma^\mu q_i)(\bar{X}\gamma_\mu X)]\,. \tag{3.6}$$

We find that if X is a Dirac fermion, then

$$\begin{aligned}
\sigma_{SI} &= \frac{1}{4}\frac{m_r^2}{64\pi(m_{\tilde{Y}}^2 - m_X^2)^2}\left[\sum_i(\lambda_{Li}^2 + \lambda_{Ri}^2)(ZB_i^p + (A-Z)B_i^n)\right]^2 \\
\sigma_{SD} &= \frac{1}{4}\frac{m_r^2}{4\pi(m_{\tilde{Y}}^2 - m_X^2)^2}\frac{J+1}{J}\left[\sum_i(\lambda_{Li}^2 + \lambda_{Ri}^2)(\langle S_p\rangle\Delta_i^{(p)} + \langle S_n\rangle\Delta_i^{(n)})\right]^2,
\end{aligned} \tag{3.7}$$

where the 1/4 factor accounts for the fact that the DM is not its own antiparticle, so only the s- or u-channel will contribute to $Xq \to Xq$ scattering. $m_r = m_X M_n/(m_X + M_n)$ is the reduced mass of the DM-nucleus system. The vector-vector part of the effective operator generates σ_{SI}, while the axial-axial part generates σ_{SD}. The $B_i^{(p,n)}$ parametrize the quark content of the nucleon, and the $\Delta_i^{(p,n)}$ its quark spin content. The $\langle S_{p(n)}\rangle$ are the expectation values of the spin content of the proton (neutron) group in the nucleus. The numerical values of Δ_i^p corresponding to structure functions

including next-to-next-to-leading order QCD corrections are [63],

$$\Delta_u^p = 0.78 \pm 0.02\,, \quad \Delta_d^p = -0.48 \pm 0.02\,, \quad \Delta_s^p = -0.15 \pm 0.02\,. \tag{3.8}$$

As noted in Ref. [64], uncertainties in quark spin contents can lead to substantial variations in σ_{SD}.

If the DM is Dirac, then a σ_{SD} which is potentially detectable at DeepCore would already be ruled out by direct detection constraints on σ_{SI}. We therefore focus on the case where X is a Majorana fermion which is stabilized by a Z_2 symmetry (so $CXC = X$). The vector-vector part of the effective operator is then identically zero and the scattering cross-section is necessarily SD ($\sigma_{SI} = 0$), and we find

$$\sigma_{SD} \;=\; \frac{m_r^2}{4\pi(m_{\tilde{Y}}^2 - m_X^2)^2}\frac{J+1}{J}\left[\sum_i(\lambda_{Li}^2 + \lambda_{Ri}^2)(\langle S_p\rangle\Delta_i^{(p)} + \langle S_n\rangle\Delta_i^{(n)})\right]^2\,, \tag{3.9}$$

since now both s- and u-channels contribute. Note that we have only included the velocity-independent terms, and only at tree-level. Since the bounds on σ_{SI} are ~ 4 orders of magnitude stronger than the expected IceCube bounds on σ_{SD}, one might wonder if this model could be probed by direct detection experiments via velocity-dependent or loop-induced spin-independent effective operators. One would expect velocity-dependent operators to be suppressed by at least 10^{-6}. Also, loop-induced SI effective operators would be suppressed by $(\alpha/4\pi)^2 \sim 10^{-6}$. Thus, with further improvements, direct detection probes of σ_{SI} induced by one-loop diagrams may be comparable to probes of σ_{SD} at tree-level by IceCube. This is an interesting subject for future study, but is beyond the scope of the present work.

In our model, DM can have axial-vector couplings to the light and/or the heavy quarks. Scalar DM coupling to heavy quarks was studied in detail in [65], but no such

study has been performed in the case of axial-vector coupling. Instead, we consider the case where DM couples to light quarks; if DM couples to more than one quark generation, then there is a potential for dangerous flavor-changing neutral currents. As a simple solution to this constraint, we assume that the only DM-quark coupling is to the first generation. We take $\lambda \equiv \lambda_{Lu} = \lambda_{Ru} = \lambda_{Ld} = \lambda_{Rd}$, and $\lambda_{Ls} = \lambda_{Rs} = 0$.

3.1.2 Annihilation

In WIMPless DM models, the annihilation cross-section to hidden sector particles is naturally $\langle \sigma_{ann.} v \rangle \sim 1$ pb at the time of decoupling. From the form of the Yukawa couplings, we see that DM can also annihilate to MSSM matter multiplets. The annihilation cross-section to MSSM particles should not be very much larger than 1 pb, or else annihilation will dilute the relic density and ruin the WIMPless miracle. But in order to get a significant flux at neutrino detectors, it is necessary for the annihilation branching fraction to MSSM particles to be comparable to unity.

Since we are considering the case where the DM is Majorana, annihilation to light fermions is chirality/p-wave suppressed. Also, in order to obtain SD scattering without inducing dangerous flavor-changing neutral currents, we assume that the only quark multiplets which the DM couples to are the first generation multiplets. So DM annihilation to quarks will be suppressed; if the DM annihilation to the hidden sector is not suppressed at current times, then the branching fraction for DM in the Sun to annihilate to quarks will be very small. One caveat to this statement is that if the light hidden sector particles are also fermions, then annihilation to the hidden sector is also chirality/p-wave suppressed. This does not significantly suppress the annihilation cross-section at decoupling, but may suppress the annihilation cross-section to hidden sector particles in the Sun by enough to allow the branching fraction to quarks to be

sizable. In this case, DM annihilation to quarks in the Sun can be a significant source of neutrinos observed at IceCube. But if there are light vectors or scalars (perhaps

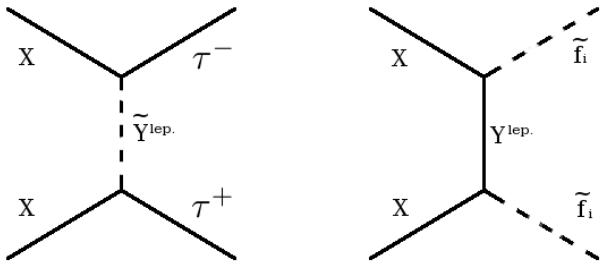

Figure 3.2: Feynman diagrams for DM annihilation into $\tau^-\tau^+$ and into $\tilde{f}_i\bar{\tilde{f}}_i$.

Goldstone bosons) in the hidden sector, then annihilation to these products is not suppressed, and the cross-section for hidden sector annihilation would be expected to be $\sim 1\,\text{pb}$. To get an annihilation cross-section to SM particles of comparable magnitude, one must either consider squark final states, or make use of Yukawa couplings to SM leptons. Then, the only relevant MSSM annihilation products are τ, $\tilde{l}_{L,R}$ and the first generation squarks $\tilde{u}_{L,R}$ and $\tilde{d}_{L,R}$. These annihilation cross-sections are given by

$$\begin{aligned}
\sigma_{XX\to\tau\bar{\tau}}v &= \frac{(\lambda'^2_{L\tau}+\lambda'^2_{R\tau})^2 m_\tau^2}{32\pi(m^2_{\tilde{Y}^{lep.}}+m_X^2)^2}\sqrt{1-\frac{m_\tau^2}{m_X^2}}\left[1+\frac{1}{3}\frac{\overrightarrow{p}^2}{m_\tau^2}\right] \\
\sigma_{XX\to\tilde{f}_i\tilde{f}_i^*}v &= \frac{(\lambda'^2_{Li}+\lambda'^2_{Ri})^2}{16\pi}\sqrt{1-\frac{m^2_{\tilde{f}_i}}{m_X^2}}\frac{m_X^2-m^2_{\tilde{f}_i}}{(m^2_{Y^{lep.}}+m_X^2-m^2_{\tilde{f}_i})^2}\,,
\end{aligned} \tag{3.10}$$

and the corresponding diagrams are shown in Fig. 3.2. We set $\lambda'_\tau \equiv \lambda'_{L\tau} = \lambda'_{R\tau}$ and $\lambda'_i \equiv \lambda'_{Li} = \lambda'_{Ri}$.

DM-annihilation to squarks requires the squark masses to be lighter than the DM mass, which in turn is lighter than the connector, which is bounded by precision

electroweak data and perturbativity to be lighter than 600 GeV. Generally though, in GMSB-inspired models the squarks are heavier than the sleptons due to the hierarchy of the gauge couplings. Thus, such light squark masses are not natural. Besides, the cascade products of heavy squarks and the resulting neutrino spectra are extremely model dependent, being determined by the features of the sparticle spectrum. For these reasons we decide to avoid the treatment of annihilation to squarks and focus on the channels dominated by leptonic Yukawa couplings.

3.2 Annihilation Products and Propagation

3.2.1 DM Annihilation in the Sun

The time dependence of the number of DM particles in the Sun is determined by the balance of capture and annihilation. A massive particle can be gravitationally captured by the Sun from the galactic halo at a rate $C_\odot$. On the other hand, annihilation at the center of the Sun will decrease the number of particles at a rate Γ_A. Thus, the time evolution of the number of DM particles in the Sun N is given by the solution to the differential equation [2],

$$\frac{dN}{dt} = C_\odot - C_A N^2 \,, \tag{3.11}$$

where $C_A = 2\Gamma_A/N^2$.

Assuming that the number of collisions DM particles undergo inside the Sun during the Sun's lifetime is large enough for them to thermalize [66], the number density of DM particles at a distance r from the solar core can be expressed in terms of the DM mass m_X, the temperature of the Sun T and the gravitational potential

$\phi(r) = 2\pi\rho r^2/(3M_{Pl}^2)$:

$$n(r) = n_0 e^{-\phi(r)\frac{m_X}{T}} = n_0 e^{-\frac{2\pi\rho r^2}{3M_{Pl}^2}\frac{m_X}{T}} , \tag{3.12}$$

where n_0 is the DM number density at the center of the Sun, ρ is the average density of the Sun and $M_{Pl} = 1.22 \times 10^{19}$ GeV is the Planck mass. C_A is then a constant that depends only on ρ, T and the annihilation cross section $\langle\sigma_A v\rangle$ averaged over the velocity distribution in the limit $v \to 0$:

$$C_A = \frac{\int n(r)^2 \langle\sigma_A v\rangle d^3r}{(\int n(r) d^3r)^2} = \langle\sigma_A v\rangle \left(\frac{3M_{Pl}^2 T}{m_X \rho}\right)^{-\frac{3}{2}} . \tag{3.13}$$

Equation (3.11) admits the solution,

$$N(t) = \sqrt{\frac{C_\odot}{C_A}} \tanh\left(\frac{t}{\tau}\right) , \tag{3.14}$$

where $\tau \equiv 1/\sqrt{C_A C_\odot}$ is the characteristic time necessary to reach equilibrium. For $t \sim 4.5\,\mathrm{Gyr}$ and $\langle\sigma_{ann.} v\rangle \sim 1\,\mathrm{pb}$ (as is the case for WIMPless dark matter) and $\sigma_{SD} \gtrsim 10^{-6}$ pb (the range of interest for IceCube/DeepCore), it is known [2, 66] that $t/\tau \gg 1$ for the range $150\,\mathrm{GeV} < m_X < 600\,\mathrm{GeV}$ considered here. Since $\Gamma_A = C_A N^2/2 = C_\odot \tanh^2(t/\tau)/2$, one can easily see that when $t \gg \tau$, $\Gamma_A \to \Gamma_{eq} \equiv C_\odot/2$.

This limit simplifies the calculations, as it relates the event rate to the DM-nucleon scattering cross section, thus bypassing all the astrophysical uncertainties related to the solar model. However, the condition of equilibrium is not guaranteed. For example, in Ref. [67] it was recently shown that there are regions of mSUGRA parameter space for which the annihilation rate is far below the capture rate. Moreover, since DM can annihilate to hidden sector particles as well as MSSM particles, the annihilation rate relevant for neutrino detection is scaled by the branching fraction to MSSM

decay products, $\Gamma_A^{MSSM} = \Gamma_A B_F^{MSSM}$. In the figures presented in Sec. 3.3, we account for these uncertainties by scaling the muon event rates at the detector by the parameter $\xi \equiv \Gamma_A^{MSSM}/\Gamma_{eq} = B_F^{MSSM} \tanh^2(t/\tau)$. However, our discussion assumes $\xi = 1$, as this choice allows us to draw quantitative conclusions. Event rates at conditions away from equilibrium can be obtained by simply choosing a lower value for ξ.

3.2.2 Capture Rate

If WIMPless DM is Majorana, it has only SD scattering. This property presents the advantage of not being tied to the direct-detection bounds on the SI cross section. The corresponding capture rate is [2, 68],

$$C_\odot \simeq 3.35 \times 10^{20}\ \mathrm{s}^{-1} \left(\frac{\sigma_{SD}}{10^{-6}\ \mathrm{pb}}\right) \left(\frac{100\ \mathrm{GeV}}{m_X}\right)^2 , \tag{3.15}$$

where we have taken the local DM density to be 0.3 GeV/cm^3, and the root-mean-square of the velocity dispersion in the halo to be 270 km/s. For SD scattering in the Sun, the only relevant nucleus with spin is hydrogen.

3.2.3 Neutrino Spectra

We limit our consideration to the cases of DM particles annihilating to taus, staus and sneutrinos of all three families. For the cases where DM annihilates to sparticles, we assume that the annihilation product is the next-to-next-to-lightest SUSY particle (NNLSP), and the lightest neutralino is the next-to-lightest SUSY particle (NLSP); in GMSB the LSP is the gravitino. Such a choice is consistent with generic sparticle spectra originating from GMSB.

In Figs. 3.3a, 3.3b and 3.3c, we show the neutrino energy spectra dN/dE_ν for an annihilation of WIMPless particles of mass $m_X = 150$ GeV into taus, $X\bar{X} \rightarrow$

$\tau^-\tau^+$. The corresponding antineutrino spectra are shown in Figs. 3.3d, 3.3e and 3.3f. Figures 3.3a and 3.3d show the spectra at the origin; Figs. 3.3b and 3.3e at the surface of the Sun and Figs. 3.3c and 3.3f at the detector. Similar spectra are obtained for annihilation into taus for the other two benchmark DM masses we consider in this paper: $m_X = 300$ GeV and $m_X = 400$ GeV. In Fig. 3.4 we show the neutrino and antineutrino spectra from annihilation into staus ($X\bar{X} \to \tilde{\tau}_1^-\tilde{\tau}_1^+$) of a $m_X = 300$ GeV DM particle. In Fig. 3.5, the neutrino and antineutrino spectra from $m_X = 400$ GeV DM-annihilation into $\tilde{\nu}_{eL}\tilde{\nu}_{eL}$, $\tilde{\nu}_{\mu L}\tilde{\nu}_{\mu L}$ and $\tilde{\nu}_{\tau L}\tilde{\nu}_{\tau L}$ with equal branching fractions are shown. The spectral shapes for $m_X = 150$, 400 GeV DM-annihilation into staus are similar to those in Fig. 3.4, while those for $m_X = 150$, 300 GeV DM-annihilation into sneutrinos are similar to Fig. 3.5.

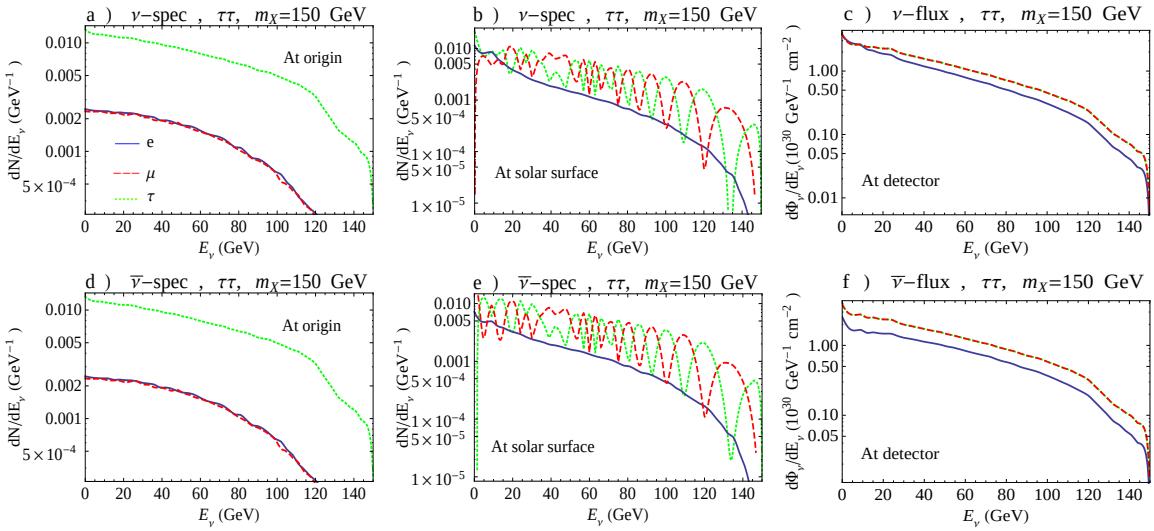

Figure 3.3: Neutrino spectra and fluxes for all three flavors per $X\bar{X} \to \tau^-\tau^+$ annihilation with $m_X = 150$ GeV, a) at production, b) at the surface of the Sun, c) flux $\Phi_\nu \equiv N/4\pi R_{SE}^2$ at Earth. d), e), f) $\bar{\nu}$ spectra and fluxes.

We obtain the neutrino spectra by cascading the annihilation products with PYTHIA 6.4 [69]. In the cases of Figs. 3.4 and 3.5 we consider a typical GMSB spectrum, like the one given in Ref. [70]. We assume $m_{\tilde{\tau}_1} = 137$ GeV and $m_{\tilde{Z}_1^0} = 94.5$ GeV, corre-

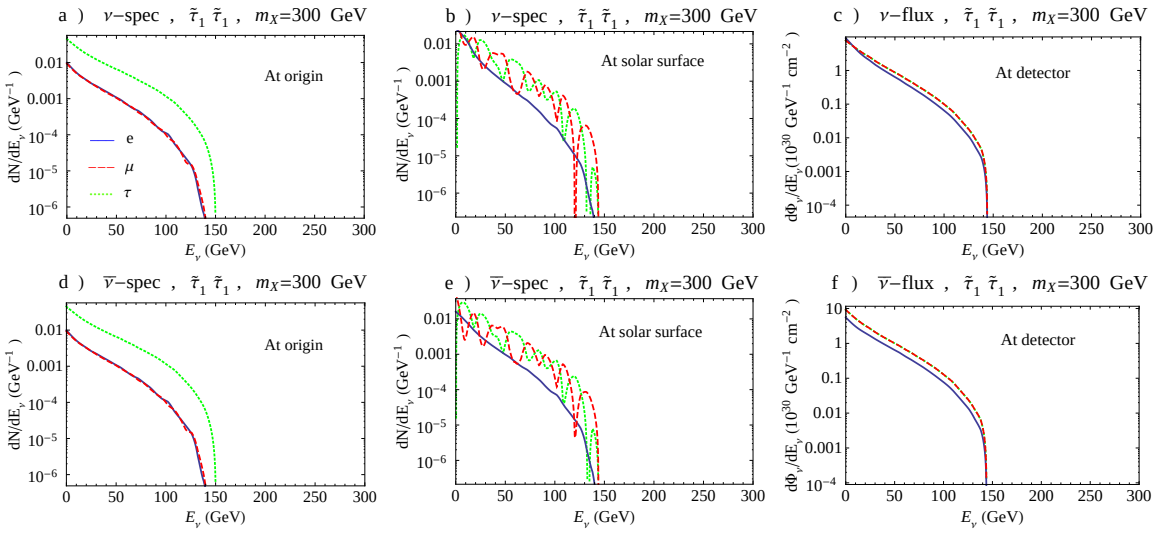

Figure 3.4: Similar to Fig. 3.3 for $X\bar{X} \to \tilde{\tau}_1^- \tilde{\tau}_1^+$ with $m_X = 300$ GeV.

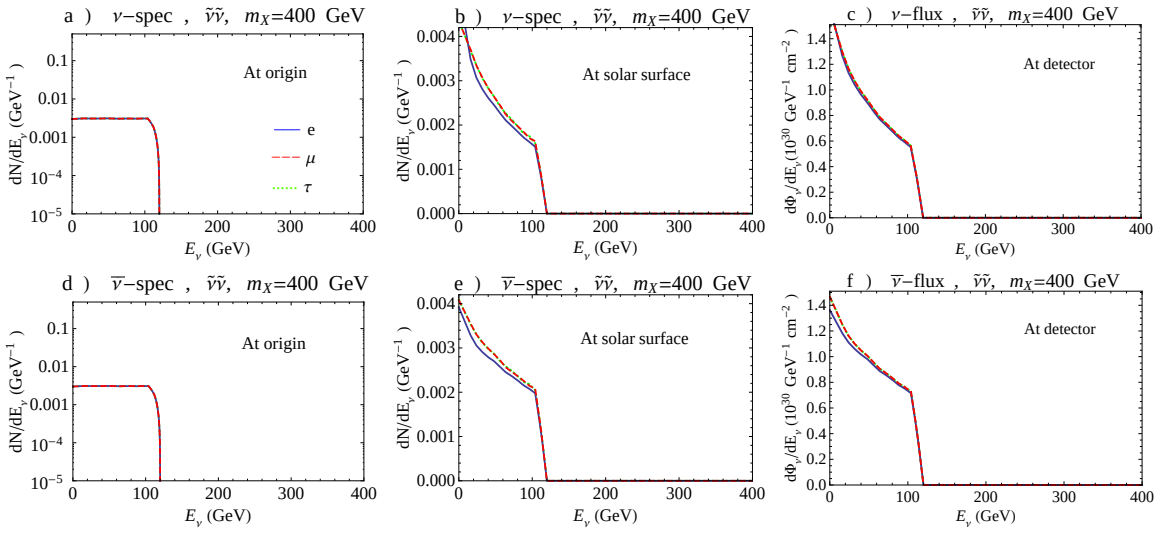

Figure 3.5: Similar to Figs. 3.3, 3.4 for $X\bar{X} \to \tilde{\nu}_{e(\mu,\tau)}\tilde{\nu}_{e(\mu,\tau)}$ with equal branching fractions and $m_X = 400$ GeV.

sponding to $\tan\beta \sim 10$. The cascade proceeds primarily through $\tilde{\tau}_1^{-(+)} \to \tilde{Z}_1^0 \tau^{-(+)}$, hence the higher number of ν_τs and $\bar{\nu}_\tau$s at the origin in Figs. 3.4a and 3.4d.

In the case where the DM candidate annihilates primarily into sneutrinos (Fig. 3.5), we assumed for simplicity that the three sneutrino masses are degenerate ($m_{\tilde{\nu}} = 111.5$ GeV) and that the couplings to the three flavors are identical, so that the pro-

duction spectra for the three neutrino families are the same, $\tilde{\nu}_{eL(\mu L,\tau L)} \rightarrow \tilde{Z}_1^0 \nu_{e(\mu,\tau)}$. As in the previous case we have $m_{\tilde{Z}_1^0} = 94.5$ GeV, corresponding to $\tan\beta \sim 10$. Note that since WIMPless DM particles only annihilate leptonically into SM particles or the NNLSP, the neutrino spectra have the same shape whether X is heavier or lighter than the top quark. Notice that the spectra from tau decays are broader than in the stau and sneutrino cases. This is expected because of the influence of the neutralino mass on kinematics. As a matter of fact, the steep drop in the neutrino spectra arising from annihilation to sparticles will have important consequences for detection at IceCube and DeepCore, as we discuss in Sec. 3.3.

The propagation of neutrinos produced at the center of the Sun through the solar medium and to the Earth is detailed in the appendices. We take into account neutrino oscillations and the effects of neutral-current (NC) and charged-current (CC) interactions and tau regeneration. In Figs. 3.3b, 3.3e and corresponding panels of Figs. 3.4 and 3.5 we show the neutrino and antineutrino fluxes after propagation to the surface of the Sun. They present expected features: for example, an accumulation of events at lower energies is visible, due to energy losses of the neutrinos undergoing NC- and CC-scattering inside the Sun. Tau-regeneration, too, has the effect of increasing the low energy neutrino flux. Furthermore, we see that flavor mixing affects the ν_μ and ν_τ spectra but leaves the ν_e spectra unaltered, since $\theta_{23} = 45°$, $\theta_{13} = 0°$ (Eq. 18 of Appendix A). Figs. 3.3c, 3.3f and corresponding panels of Figs. 3.4 and 3.5 show the fluxes at the Earth after our averaging procedure, described in Appendix A. We define the flux $\Phi_\nu \equiv N/(4\pi R_{SE}^2)$, with $R_{SE} \sim 1$ AU being the Sun-Earth distance. Our results are in very good agreement with those of Ref. [71]. Notice that almost all modulation is washed out.

The flux of high energy neutrinos produced by DM annihilation can be detected

by neutrino telescopes like IceCube [72]. The IceCube detector at the South Pole is an array of 80 strings uniformly spaced 125 m from one another, each with 60 digital optical modules. It is deployed at a depth between 1450 m and 2450 m, and the instrumented volume of ice covers 1 km^3. When muon-neutrinos undergo CC-scattering on nucleons in ice they produce a muon that propagates through the ice. These muons leave a trail of Cherenkov radiation that can be detected by the optical modules. We are therefore interested in determining the muon and antimuon flux in and near the detector, taking into account possible energy losses due to the propagation in ice. DeepCore [73], an extension of IceCube, is a denser (72 m spacing) array of six strings surrounding one of the central strings of IceCube, most of them placed below the "dust layer", at a depth of 2100 m. As detailed in Appendix B, DeepCore's denser strings lower the neutrino energy threshold with respect to IceCube and thus allow detection of neutrinos from annihilation of DM particles of a lower mass. Besides, DeepCore is designed to use the outer instrumented volume of IceCube as a veto on atmospheric muons from above the horizon to a level of one part in 10^6, thus drastically reducing the background. Such properties make it a perfect instrument to test the WIMPless scenario in the case of Majorana DM.

DeepCore's muon effective volume becomes insignificant below muon energies of 10 GeV [74]. At energies between 10 and 35 GeV DeepCore cannot provide directional information, since only one or two optical modules will be triggered. Very good directional information is needed to track the Sun throughout the year, so we fix DeepCore's energy threshold at $E_{min} = 35$ GeV [75]. For IceCube we consider the very optimistic threshold $E_{thr} = 100$ GeV.

3.3 Results

In this section we investigate the prospects for DM detection at IceCube and DeepCore. We consider a 3σ-detection as

$$\text{“}3\sigma\text{-detection”} \leftrightarrow \frac{N_\mu}{\sqrt{N_{BG}}} = 3\,, \tag{3.16}$$

where N_μ is the observed number of muon events and N_{BG} is the number of muon events due to the atmospheric neutrino background [76], which is discussed further in Appendix C.

For the IceCube detector we divide the muon events into *upward* and *contained* events, following the treatment of [77]. As we discuss in Appendix B, the former are due to upward going neutrinos interacting outside the detector volume, the latter to neutrinos that interact within the instrumented volume. To evaluate the event rate we track the Sun in the sky at different times of the year, and consider only events detected when the Sun is below the horizon. The distinction between upward and contained events does not apply to DeepCore, which only sees contained events. For DeepCore, IceCube will veto atmospheric muons from above the horizon to a level of one part in 10^6. Therefore, at DeepCore we consider the signal detected throughout the year. We consider a period of 5 yrs of observation. As anticipated in Sec. 3, we rescale the event rates obtained at equilibrium by $\xi \equiv \Gamma_A^{MSSM}/\Gamma_{eq}$.

3.3.1 Event Rates: tau-channel

In Fig. 3.6 we plot the upward and contained event rates at IceCube for our three benchmark DM masses for the $XX \to \tau^-\tau^+$ channel, as a function of the scalar connector mass $m_{\tilde{Y}}$ and the Yukawa couplings. We assume that the masses of the

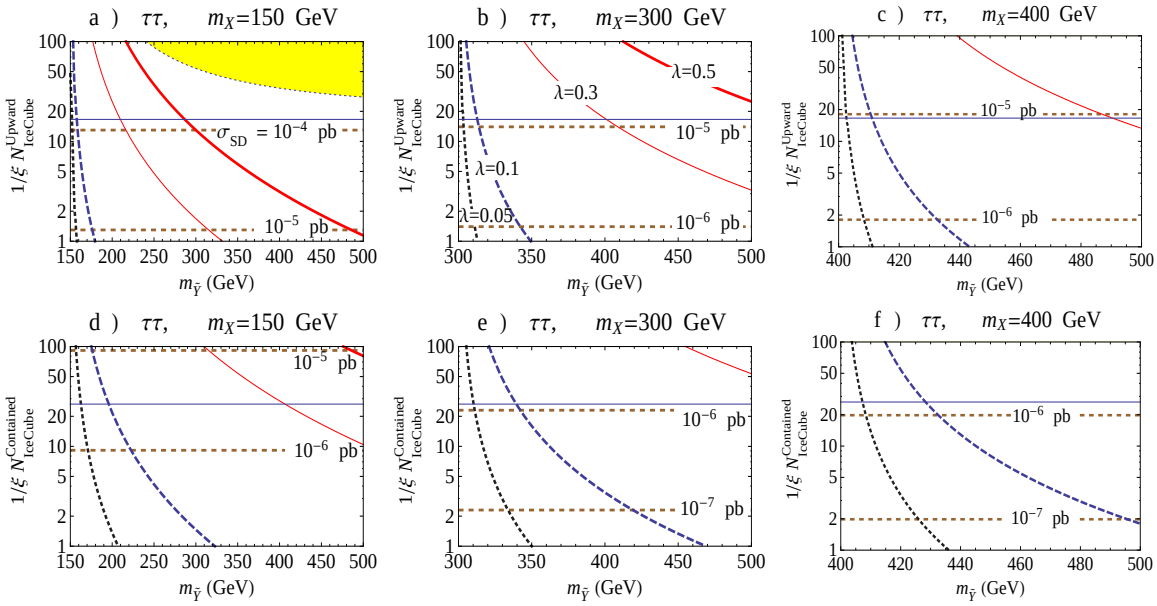

Figure 3.6: Number of upward and contained events in five years of observation at IceCube for three values of m_X as a function of $m_{\tilde{Y}}$ for the $\tau^-\tau^+$-channel for several choices of $\lambda = \lambda_{(L,R)(u,d)}$. Dotted black: $\lambda = 0.05$; dashed blue: $\lambda = 0.1$; solid thin red: $\lambda = 0.3$; solid thick red: $\lambda = 0.5$. The blue horizontal lines represent the number of events needed for a 3σ-discovery in five years of observation. The dashed brown horizontal lines represent σ_{SD} in pb. The yellow band represents values of λ that yield the correct relic abundance.

up-type and down-type squarks $\tilde{Y}$ are degenerate, and that $\lambda \equiv \lambda_{(L,R)(u,d)}$. In Fig. 3.7 we plot the contained event rates at DeepCore for the same channel. The event rates (see Eqs. 35, 37 and 39 of Appendix B) are evaluated for values of the Yukawa couplings which allow calculations in the perturbative regime. The values in pb of SD cross sections that correspond to the event rates are shown as horizontal dashed brown lines, and labeled on the plots. Notice the following features:

- As we show in Appendix C, the atmospheric background to upward events in IceCube is $N_{BG}^{Up} \simeq 6.1$ yr^{-1}, while the background to contained events is $N_{BG}^{Con} \simeq 15.6$ yr^{-1}. The background to contained events at DeepCore is $N_{BG}^{DC} \simeq 2.5$ yr^{-1}. The blue horizontal lines in Figs. 3.6 and 3.7 indicate the number of signal events needed

for a 3σ-detection in five years. We see that a 3σ-detection in upward events at IceCube is possible for reasonable values of λ and $m_{\tilde{Y}}$. The contained event sample offers even better prospects.

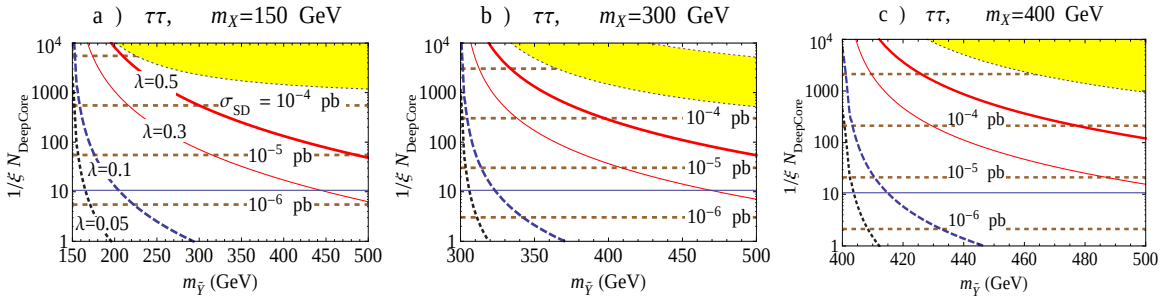

Figure 3.7: Similar to Fig. 3.6 for contained events at DeepCore.

• In Fig. 3.7a we see that DeepCore significantly improves the prospects for observation of events for $m_X = 150$ GeV. A 3σ-detection in this channel can be obtained with Yukawa couplings of about 0.3 without a need for resonant enhancement. If the Yukawa couplings are allowed to assume larger values, the prospects for signal detection become even more robust.

• For DM masses well above E_{thr} the advantages of DeepCore in the τ-channel are less evident. As a matter of fact a 3σ-detection is more likely in the contained events at IceCube. For such high masses the propagator suppression of the SD cross section reduces the flux at the detector and makes the larger effective volume of IceCube advantageous.

One may ask whether it is possible to relate the size of the Yukawa coupling λ responsible for SD scattering to the size of the Yukawa couplings λ_τ that appear in Eq. (3.10), and are responsible for the annihilation to SM particles. This is possible under certain assumptions:

• The yellow bands in Figs. 3.6 and 3.7 indicate the region with 0.1 pb $\leq \sigma_{X\bar{X}\to\tau\bar{\tau}}v \leq 1$ pb, assuming $\lambda'_\tau = \lambda$ and $m_{\tilde{Y}^{lep.}} = m_{\tilde{Y}}$. For this range of $\sigma_{X\bar{X}\to\tau\bar{\tau}}v$ (as-

suming there are light bosons in the hidden sector), annihilation to MSSM particles has a large enough branching fraction to permit observation at neutrino telescopes, while not being so large as to dilute the relic abundance and thwart the WIMPless miracle. Note however, that this constraint is only relevant if DM annihilation to the hidden sector is not chirality/p-wave suppressed.

• If $\lambda'_\tau/\lambda > 1$, the yellow band shifts down to lower values. Such a situation may be desirable in the $\tau^-\tau^+$-channel so that the iso-λ curves pass through the yellow bands, i.e., the relic abundance and observable signals at neutrino telescopes can be simultaneously obtained for more of the parameter space.

• As is clear from inspection of Eq. (3.9) and the first of Eqs. (3.10), the capture rate depends on λ and $m_{\tilde{Y}}$ while the annihilation cross-section to taus depends on λ'_τ and $m_{\tilde{Y}^{lep.}}$. ξ depends on the details of the solar model, particularly on the ratio T/ρ in Eq. (3.13), and on the ratios λ'_τ/λ and $m_{\tilde{Y}}/m_{\tilde{Y}^{lep.}}$. A detailed analysis of these aspects is beyond the scope of this paper.

3.3.2 Event Rates: stau and sneutrino channels

In Figs. 3.8 and 3.9 we compare the performances of IceCube and DeepCore, respectively, for the stau-channel. Figures 3.10 and 3.11 show our results for the sneutrino-channel. The 90% C. L. upper bound placed by Super-Kamiokande [78] on σ_{SD} is indicated on the plots by a thick horizontal pink line. For $m_X = 150$ GeV this bound is $\sigma_{SD}^{Max} \simeq 3.5 \times 10^{-3}$ pb and for $m_X = 300 - 400$ GeV, $\sigma_{SD}^{Max} \simeq 8 \times 10^{-3}$ pb. For the $\tau^-\tau^+$-channel these bounds are off-scale and therefore not visible. The advantages of DeepCore in the observation of neutrino fluxes from low mass DM are evident:

• For our choice of spectra and energy thresholds, DM particles with a 150 GeV (300 GeV) mass do not produce observable events at IceCube in the two sparticle

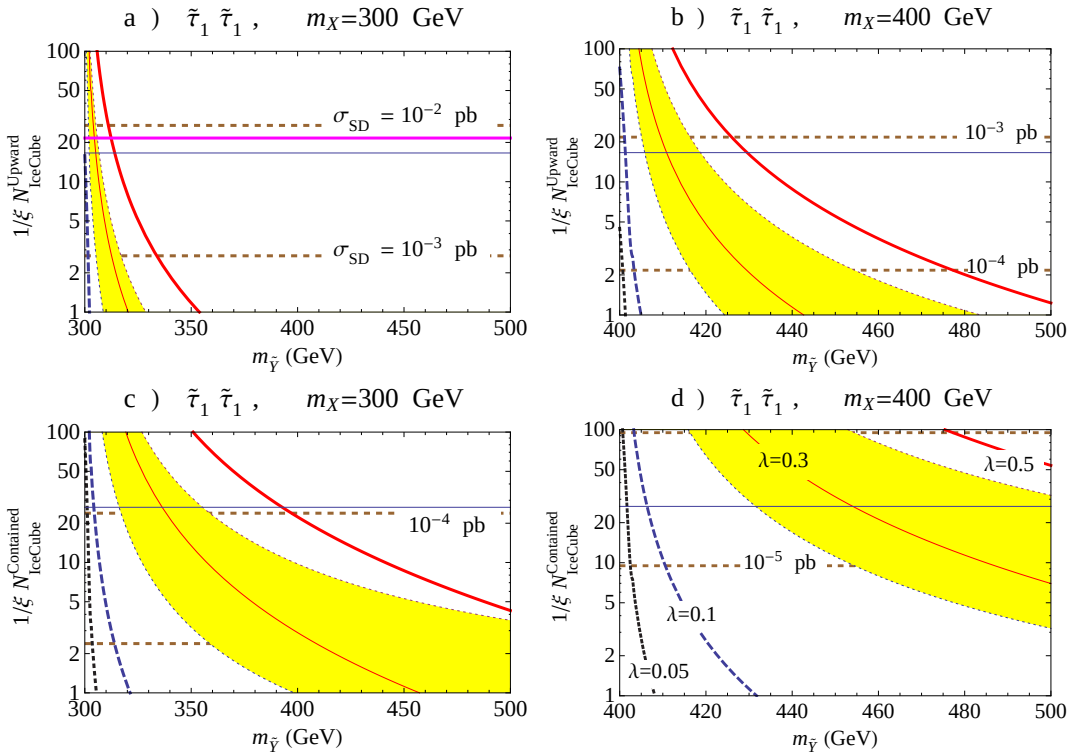

Figure 3.8: Similar to Fig. 3.6 for the $\tilde{\tau}_1^-\tilde{\tau}_1^+$-channel. IceCube is insensitive to this channel for $m_X = 150$ GeV. The thick pink horizontal line represents the Super-K 90% C. L. upper bound on σ_{SD}.

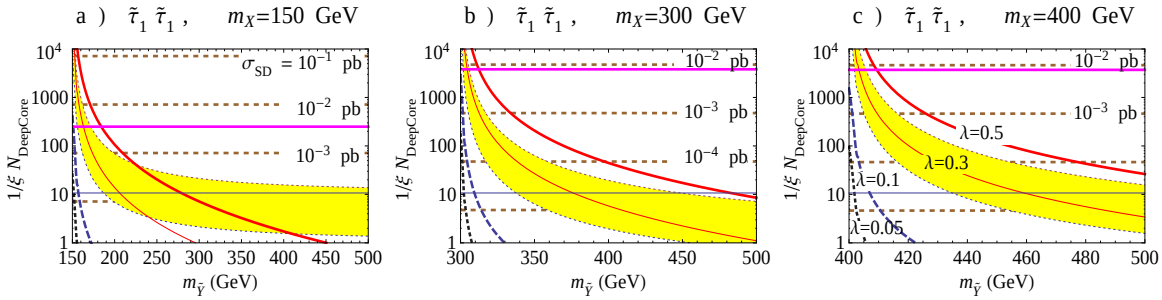

Figure 3.9: Similar to Fig. 3.7 for the $\tilde{\tau}_1^-\tilde{\tau}_1^+$-channel. The thick pink horizontal line represents the Super-K 90% C. L. upper bound on σ_{SD}.

channels (sneutrino-channel). At production, neutrino spectra for annihilation of $m_X = 150$ GeV DM particles become negligible above 60 GeV for the stau-channel and above 40 GeV for the sneutrino-channel. Neutrino spectra originating from $m_X =$

300 GeV DM annihilation into sneutrinos are negligible above 80 GeV. Thus, with a threshold energy $E_{thr} = 100$ GeV no signal is expected for these channels at IceCube.

• As Figs. 3.8a shows, even if observation of upward events at IceCube is possible in the stau-channel for $m_X = 300$ GeV, the region of parameter space allowed is very narrow. It is represented by the strip between the thin blue and thick pink horizontal lines. Similarly, Fig. 3.10a shows that a 3σ-discovery in upward events for $m_X = 400$ GeV in the sneutrino-channel is incompatible with Super-K data, as the thin blue line is above the thick pink line. Figures 3.8c and 3.10b show that, as usual, the contained events offer better detection prospects at IceCube: assuming $\lambda = 0.5$, 3σ-detection is obtained with a connector mass within 31% of $m_X = 300$ GeV in the stau-channel, and within 24% of $m_X = 400$ GeV in the sneutrino-channel.

The performance of DeepCore is much less sensitive to the annihilation channel than IceCube, because the lower energy threshold allows integration of much of the neutrino spectra independent of its shape or features.

• Even for values of m_X that do not allow observation of events at Icecube, DeepCore is able to observe events at 3σ in five years for reasonable values of λ and $m_{\tilde{Y}}$. However, the region of parameter space for which DeepCore is sensitive to the $m_X = 150$ GeV sparticle channels is very narrow, as can be seen in Figs. 3.9a and 3.11a.

• The advantages of DeepCore over IceCube are not substantial for heavy-DM masses in the stau channel, and the detector fares just a little better in the heavy-DM sneutrino channel. Fig. 3.9c (3.11c) shows that 3σ detection of $m_X = 400$ GeV DM in the stau (sneutrino) channel can be obtained with a range of connector masses extended by a mere 3% (18%) with respect to IceCube.

• The yellow bands represent the region of $(m_{\tilde{Y}}, \lambda)$-parameter space such that

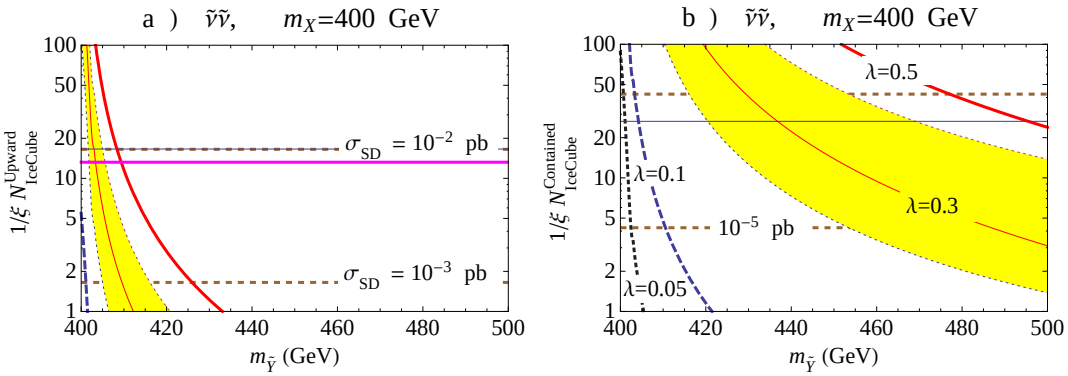

Figure 3.10: Similar to Fig. 3.6 for the $\tilde{\nu}\tilde{\nu}$-channel. IceCube is insensitive to this channel for $m_X = 150$ GeV, 300 GeV. The thick pink horizontal line represents the Super-K 90% C. L. upper bound on σ_{SD}. In a), the solid blue horizontal line is coincident with the dashed brown line representing $\sigma_{SD} = 10^{-2}$ pb.

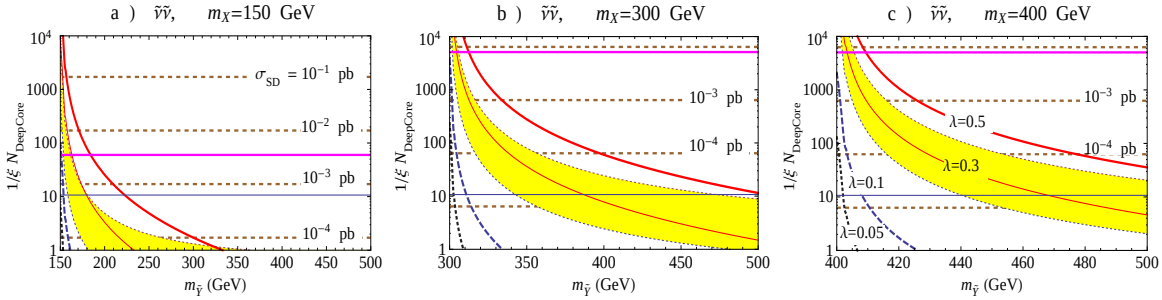

Figure 3.11: Similar to Fig. 3.7 for the $\tilde{\nu}\tilde{\nu}$-channel. The thick pink horizontal line represents the Super-K 90% C. L. upper bound on σ_{SD}.

0.1 pb $\leq \sigma_{X\bar{X}\to\tilde{f}_i\bar{\tilde{f}}_i} v \leq 1$ pb assuming that $\lambda'_i = \lambda$ and $m_{Y^{lep.}} = m_{\tilde{Y}}$.

It has been recently pointed out [79] that DeepCore should be able to identify contained "cascade" events, which originate from CC-interactions of electron- and tau-neutrinos inside the detector, and from NC-interactions of neutrinos of all three flavors. For such events the signal is enhanced with respect to the background at energies $\gtrsim$ 40 GeV, since the signal is predominantly due to the CC-interactions. Specifically, at such energies the flux of atmospheric ν_μ is from one to a few orders of magnitude larger than the flux of ν_e and ν_τ [80]; thus ν_μ give the dominant contribution to the background through NC-interactions, which are weaker than CC-

interactions. This could provide an additional method of detection for neutrinos. However, as noted in [72, 81], the angular sensitivity for cascades is $\sim 50^\circ$, which does not permit tracking of the Sun with the desired accuracy. Consequently, we do not consider cascade events as a potential signal.

3.4 Summary

We investigated the prospects for indirect detection of fermion WIMPless DM at IceCube and DeepCore. We considered a hidden sector Majorana DM particle of mass m_X that couples through Yukawa couplings in the superpotential to a connector of mass m_Y and visible sector particles. These models are especially interesting in the context of IceCube/DeepCore because they exhibit only SD nuclear scattering, for which IceCube/DeepCore is expected to soon provide the greatest experimental sensitivity for $m_X \sim \mathcal{O}$(few 100 GeV).

We focused our attention on DM annihilation to taus, staus and sneutrinos. In order to be captured by the Sun the DM particle needs to couple also to up and down quarks and first generation squarks through the superfield. Annihilation to light fermions does not produce an observable signal because it is chirality suppressed. As for annihilation into squarks, in the GMSB-inspired WIMPless scenario, squarks are generally very heavy and the resulting neutrino spectra are strongly dependent on the features of the sparticle spectrum. Therefore, we assumed that the dominant channels for annihilation are exclusively leptonic. We assumed that if the DM candidate annihilates to SM particles, these are predominantly taus. If it annihilates to supersymmetric particles, these belong to lepton superfields and are the NNLSP, with the lightest neutralino being the NLSP. In the cases of stau and sneutrino annihilation channels we focused our attention on the distinct situations where either the DM

candidate couples predominantly to the third family (staus), or it couples with equal strength to degenerate sneutrinos of all three families. We believe this allows us to consider a range of interesting possibilities.

We propagated the neutrino spectra originated by DM annihilation at the center of the Sun through the solar medium. We took into account energy losses due to NC-interactions, CC-interactions and tau-regeneration. We also implemented neutrino oscillations in the propagation through the Sun.

In order to calculate the event rate at the IceCube detector, we considered upward and contained events, taking into account muon energy losses due to ionization, bremsstrahlung, pair production and photonuclear effects. The technical details of our analyses are provided in the appendices.

We found that it is not possible to obtain 3σ-detection in upward or contained events at IceCube for the stau- and sneutrino-channel for DM masses $m_X \lesssim 150$ GeV with five years of data. Moreover, a 300 GeV DM particle would not produce observable events for the sparticle channels, unless the Yukawa couplings are large or the connector mass is not more than about 30% heavier than the DM mass. Indirect detection of these relatively light DM particles is favored in the tau-channel, due to the broader neutrino spectra produced in this channel. We quantified the improvement DeepCore brings to the detection prospects in all channels, especially for low m_X. In particular, even in the cases mentioned above, where the steep decrease in flux below the detector energy threshold makes signal detection highly unlikely at IceCube, such limitations do not apply to DeepCore. While the performance of the IceCube detector varies significantly between different channels and different DM masses, thus requiring a case by case analysis, we showed that DeepCore can comfortably produce a five year 3σ-detection for any analyzed channel, without strong dependence on the Yukawa couplings or connector masses. We thus find good prospects for probing

models of Majorana fermionic WIMPless DM at IceCube, including the DeepCore extension.

Appendix

.1 Neutrino Propagation

We describe the procedure involving the propagation of neutrinos from the center of the Sun to the Earth, and the detection at IceCube and DeepCore.

Once the neutrinos are produced at the center of the Sun, they need to be propagated through the solar medium, travel to the Earth and be detected at the neutrino telescope. The appropriate formalism involves the density matrix for the neutrino spectra in the flavor basis [82]. We call this ρ, and indicate matrices in boldface.

Neutrinos of energy E_ν can be propagated from a point r to $r + dr$ inside the Sun by solving the Heisenberg equation,

$$\frac{d\rho(E_\nu)}{dr} = -i[\mathbf{H}(E_\nu), \rho(E_\nu)] + \left.\frac{d\rho(E_\nu)}{dr}\right|_{NC} + \left.\frac{d\rho(E_\nu)}{dr}\right|_{CC} + \left.\frac{d\rho(E_\nu)}{dr}\right|_{in}, \tag{17}$$

where $\mathbf{H}$ is the Hamiltonian for neutrino oscillations in matter, the term indicated by *in* is the injection spectrum at the center of the Sun and the other two terms represent the matter effects due to NC- and CC-interactions. The Hamiltonian is

$$\mathbf{H} = \frac{1}{2E_\nu}\mathbf{U}\text{diag}(0, \Delta m^2_{21}, \Delta m^2_{31})\mathbf{U}^\dagger + \text{diag}(\sqrt{2}G_F N_e, 0, 0)\,, \tag{18}$$

where $\mathbf{U}$ is the neutrino mixing matrix as given in [83], N_e is the radius-dependent density of electrons inside the Sun, G_F is the Fermi constant, E_ν is the energy of the

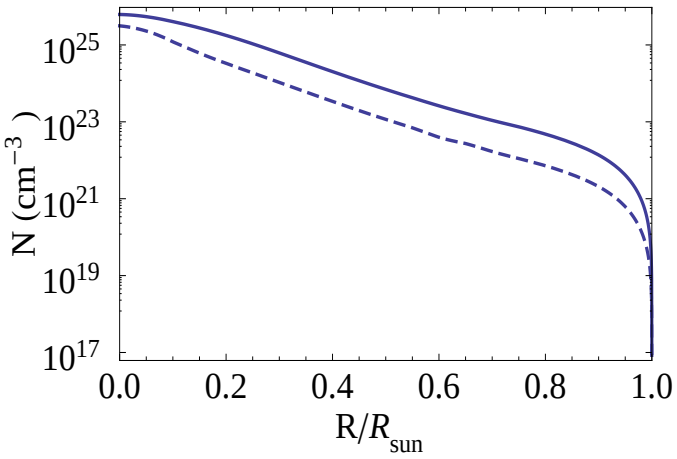

Figure 12: Electron density (solid line) and neutron density (dashed line) as a function of the Sun's radius.

incoming neutrino, and Δm^2_{21} and Δm^2_{31} are the neutrino mass-squared differences, $\Delta m^2_{ij} = m^2_i - m^2_j$. We use the following values: $\Delta m^2_{21} = 8.1 \times 10^{-5}$ eV^2, $\Delta m^2_{31} = 2.2 \times 10^{-3}$ eV^2, $\theta_{12} = 33.2°$, $\theta_{23} = 45°$, $\theta_{13} = 0$. It has been shown in [82, 84] that the oscillation results are not significantly changed if θ_{13} is small but nonzero. The density profile of the Sun is shown in Fig. 12 [85].

The injection term is

$$\left.\frac{d\rho_{ij}}{dr}\right|_{in}(E_\nu) = \delta(r)\delta_{ij}\frac{dN}{dE_\nu}\,. \tag{19}$$

It expresses the number of neutrinos and antineutrinos produced in DM-annihilation at the center of the Sun as a function of energy. It is diagonal in the flavor basis.

In considering the NC and CC terms, we introduce the following quantity which depends on the deep inelastic scattering (DIS) total cross sections σ:

$$\mathbf{\Gamma}_{NC(CC)}(E_\nu, E') = N_p(r)\mathrm{diag}[\sigma(\nu_l p \to \nu'_l(l)+\mathrm{any})]+N_n(r)\mathrm{diag}[\sigma(\nu_l n \to \nu'_l(l)+\mathrm{any})]\,, \tag{20}$$

where $N_p(r)(= N_e(r))$ and $N_n(r)$ are the proton and neutron densities inside the Sun, plotted in Fig. 12, E_ν is the incoming neutrino energy, E' the outgoing neutrino (charged lepton) energy and l labels flavor. Then, the neutral current term is given by:

$$\left.\frac{d\rho(E_\nu)}{dr}\right|_{NC} = -\rho(E_\nu)\int_0^{E_\nu}\frac{d\mathbf{\Gamma}_{NC}}{dE'_\nu}(E_\nu, E'_\nu)dE'_\nu + \int_{E_\nu}^{\infty}\frac{d\mathbf{\Gamma}_{NC}}{dE_\nu}(E'_\nu, E_\nu)\rho(E'_\nu)dE'_\nu\,. \quad (21)$$

The CC term is defined in a similar way but it is more complicated for two reasons. Firstly, the CC-DIS cross sections are not the same for all flavors of neutrinos. As a matter of fact the ν_τ-cross sections are suppressed near threshold by the kinematical effects of m_τ. Secondly, one needs to take into account the effects of tau regeneration that couple the propagation of different flavors (different elements of the density matrix) and elements of the neutrino and antineutrino density matrices.

Tau regeneration is an important effect that leads to a reinjection of the neutrinos produced by the decay of the taus that are CC-created by neutrinos of higher energies. The taus produced by energetic neutrinos undergoing CC interactions can decay promptly through various channels, for example $\tau^- \to \nu_\tau + \text{any}$, $\tau^- \to e^-\bar{\nu}_e\nu_\tau$ and $\tau^- \to \mu^-\bar{\nu}_\mu\nu_\tau$, and similarly for the antiparticles. These processes provide additional sources of energetic neutrinos that reenter the flux with lower energies. The probabilities of reinjection are encoded in four functions $f_{\nu_\tau\to\nu_\tau}(u)$, $f_{\bar{\nu}_\tau\to\bar{\nu}_\tau}(u)$, $f_{\nu_\tau\to\bar{\nu}_{e,\mu}}(u)$, $f_{\bar{\nu}_\tau\to\nu_{e,\mu}}(u)$, which depend on the branching ratios of the above channels and on $u \equiv E_\nu^{out}/E_\nu^{in}$, where E_ν^{in} is the energy of the tau-neutrino undergoing CC-scattering, and E_ν^{out} is the energy of the lower energy neutrinos produced by tau decay [82]. The

charged current contribution to the Heisenberg equation is therefore,

$$\left.\frac{d\rho(E_\nu)}{dr}\right|_{CC} = -\frac{\{\mathbf{\Gamma}_{CC},\rho\}}{2} + \int_{E_\nu}^{\infty}\frac{dE_\nu^{in}}{E_\nu^{in}}\left[\mathbf{\Pi}_\tau\rho_{\tau\tau}(E_\nu^{in})\Gamma^\tau_{CC}(E_\nu^{in})f_{\nu_\tau\to\nu_\tau}\left(\frac{E_\nu}{E_\nu^{in}}\right)\right.$$
$$\left. + \mathbf{\Pi}_{e,\mu}\bar{\rho}_{\tau\tau}(E_\nu^{in})\bar{\Gamma}^\tau_{CC}(E_\nu^{in})f_{\bar{\nu}_\tau\to\nu_{e,\mu}}\left(\frac{E_\nu}{E_\nu^{in}}\right)\right], \quad (22)$$

$$\left.\frac{d\bar{\rho}(E_\nu)}{dr}\right|_{CC} = -\frac{\{\bar{\mathbf{\Gamma}}_{CC},\bar{\rho}\}}{2} + \int_{E_\nu}^{\infty}\frac{dE_\nu^{in}}{E_\nu^{in}}\left[\mathbf{\Pi}_\tau\bar{\rho}_{\tau\tau}(E_\nu^{in})\bar{\Gamma}^\tau_{CC}(E_\nu^{in})f_{\bar{\nu}_\tau\to\bar{\nu}_\tau}\left(\frac{E_\nu}{E_\nu^{in}}\right)\right.$$
$$\left. + \mathbf{\Pi}_{e,\mu}\rho_{\tau\tau}(E_\nu^{in})\Gamma^\tau_{CC}(E_\nu^{in})f_{\nu_\tau\to\bar{\nu}_{e,\mu}}\left(\frac{E_\nu}{E_\nu^{in}}\right)\right], \quad (23)$$

where $\mathbf{\Pi}_e = \mathrm{diag}(1,0,0)$ are projectors, and similar expressions apply to the other flavors. As is clear from the last term on the right-hand side of Eqs. (22) and (23), tau regeneration effects couple the two sets of equations. The regeneration probability functions are given by [84],

$$f_{\nu_\tau\to\nu_\tau}(u) = N\int_u^1\frac{dz}{z}\left(1+\frac{z^2}{5}\right)\sum_{i=1}^{6}\mathrm{Br}_i\left(g_{0i}\left(\frac{u}{z}\right)-g_{1i}\left(\frac{u}{z}\right)\right), \quad (24)$$

$$f_{\bar{\nu}_\tau\to\bar{\nu}_\tau}(u) = N\int_u^1\frac{dz}{z}\left(\frac{1}{5}+z^2\right)\sum_{i=1}^{6}\mathrm{Br}_i\left(g_{0i}\left(\frac{u}{z}\right)-g_{1i}\left(\frac{u}{z}\right)\right), \quad (25)$$

$$f_{\nu_\tau\to\bar{\nu}_{e,\mu}}(u) = N\int_u^1\frac{dz}{z}\left(1+\frac{z^2}{5}\right)0.18\left(\tilde{g}_0\left(\frac{u}{z}\right)-\tilde{g}_1\left(\frac{u}{z}\right)\right), \quad (26)$$

$$f_{\bar{\nu}_\tau\to\nu_{e,\mu}}(u) = N\int_u^1\frac{dz}{z}\left(\frac{1}{5}+z^2\right)0.18\left(\tilde{g}_0\left(\frac{u}{z}\right)-\tilde{g}_1\left(\frac{u}{z}\right)\right), \quad (27)$$

where $z = E_\tau/E_\nu^{in}$ and N normalizes the equations so that their integral is either 1 ($\nu_\tau \to \nu_\tau$ and $\bar{\nu}_\tau \to \bar{\nu}_\tau$), or 0.18 ($\nu_\tau \to \bar{\nu}_{e,\mu}$ and $\bar{\nu}_\tau \to \nu_{e,\mu}$). The functions g_{0i} and g_{1i} are, respectively, the unpolarized and polarized energy spectra of the τ-neutrinos originating from the taus in the fragmentation frame, for each final state. The functions $\tilde{g}_0$ and $\tilde{g}_1$ are the unpolarized and polarized energy spectra of the $\bar{\nu}_{e,\mu}$ from decay of the τ. The explicit forms of g_{0i} and g_{1i} are given in Table I of [86],

and those of $\tilde{g}_0$ and $\tilde{g}_1$ are given in Ref. [87]. The branching fractions Br_i refer to the six possible final states: $\tau^- \to e^- \bar{\nu}_e \nu_\tau$ (Br_1 =0.18), $\tau^- \to \mu^- \bar{\nu}_\mu \nu_\tau$ (Br_2 =0.18), $\tau^- \to \pi^- \nu_\tau$ (Br_3 =0.12), $\tau^- \to a_1 \nu_\tau$ (Br_4 =0.13), $\tau^- \to \rho \nu_\tau$ (Br_5 =0.26), $\tau^- \to \nu_\tau +$ any (Br_6 =0.13).

Once the neutrinos reach the surface of the Sun, the propagation to the Earth is obtained by the following averaging procedure: we rotate the density matrix to the mass basis; drop the off-diagonal terms and rotate it back to the flavor basis. With our choice of neutrino parameters, the averaging should wash out any observable modulation.

.2 Muon Rates

Upward Events at IceCube

When a muon generated via CC-interactions travels through the rock and ice beneath the detector it loses energy due to ionization, bremsstrahlung, pair production and photonuclear effects [88]. The average energy loss of the muons that travel a distance dz in a medium of density ρ_{med} is given by:

$$\left\langle \frac{dE}{dz} \right\rangle = -(\alpha + \beta(E)E)\rho_{med}(z)\,, \tag{28}$$

where $\alpha = 3.0 \times 10^{-3}$ GeV cm^2/g is related to ionization, while $\beta(E)$ takes into account bremsstrahlung, pair production and photonuclear effects. We take $\beta = 3.0 \times 10^{-6}$ cm^2/g and $\rho_{med} = \rho_{ice} = 0.92$ g/cm^3. The results from Muon Monte Carlo [89] are reproduced by choosing these values of α and β [90]. Equation (28) can then be easily solved to obtain the final energy $E_{\mu f}$, given initial energy $E_{\mu i}$:

$$E_{\mu f} = -\frac{\alpha}{\beta} + e^{-\beta\rho_{ice}z}\left(E_{\mu i} + \frac{\alpha}{\beta}\right)\,. \tag{29}$$

The average range covered by the muon between energies $E_{\mu i}$, $E_{\mu f}$ is then,

$$R_\mu(E_{\mu i}, E_{\mu f}) = \frac{1}{\beta\rho_{ice}} \ln\left(\frac{\alpha + \beta E_{\mu i}}{\alpha + \beta E_{\mu f}}\right)\,. \tag{30}$$

Thus, the muon flux at the detector is obtained by a convolution of the following: the probability of the incoming neutrino to CC-scatter with a nucleus in ice; the average range over which energy losses force the muon energy below the detector threshold; the muon probability of surviving its own decay length. This last effect

can be parametrized by the survival probability,

$$P_{sur}(E_{\mu i}, E_{\mu f}) = \left[\frac{E_{\mu f}(\alpha + \beta E_{\mu i})}{E_{\mu i}(\alpha + \beta E_{\mu f})}\right]^{\frac{m_\mu}{c\tau\alpha\rho_{ice}}} , \tag{31}$$

which is a solution to the differential equation,

$$\frac{dP_{sur}}{dE_{\mu f}} = \frac{P_{sur}}{E_{\mu f} c\tau \rho_{ice}(\alpha + \beta E_{\mu f})/m_\mu} , \tag{32}$$

where τ is the muon lifetime and m_μ its mass. Folding these effects together gives the spectrum of muon events,

$$\begin{aligned} \frac{d\Phi_\mu}{dE_{\mu f}} &= \int_0^{R_\mu(m_X, E_{\mu f})} dz\, e^{\beta\rho_{ice} z} P_{sur}(E_{\mu i}(E_{\mu f}, z), E_{\mu f}) \\ &\times \int_{E_{\mu i}(E_{\mu f}, z)}^{m_X} dE_\nu \left[\frac{d\Phi_\nu}{dE_\nu}\left(\frac{d\sigma^{CC}_{\nu p}}{dE_{\mu i}}(E_\nu)\rho_p + \frac{d\sigma^{CC}_{\nu n}}{dE_{\mu i}}(E_\nu)\rho_n\right)\right. \\ &+ \left.\text{(a corresponding contribution for } \bar{\nu})\right] , \end{aligned} \tag{33}$$

where $E_{\mu i}(E_{\mu f}, z)$ is obtained by inverting Eq. (29), $d\sigma^{CC}/dE_\mu(E_\nu)$ are the differential CC-cross sections to protons (νp) and neutrons (νn), $\rho_p \sim 5/9\ N_A$ cm^{-3} and $\rho_n \sim 4/9\ N_A$ cm^{-3} are the number densities of nucleons in ice expressed in terms of Avogadro's number N_A, and $d\Phi_\nu/dE_\nu$ is the neutrino spectrum at Earth, depicted in our specific cases in the third column of Figs. 3.3, 3.4 and 3.5.

The event rate for upward events is obtained by convolving Eq. (33) with the muon *effective area* of the detector, $A_{eff}(E_{\mu f})R(\cos\theta)$, which is constituted by a zenith angle-independent part, shown in Fig. 13a, and a factor $R(\cos\theta) = 0.92 - 0.45\cos\theta$ that accounts for the rock bed beneath the ice [91]. We take the average of the effective area over the time of the year that the Sun spends below the horizon, namely between the March and September equinoxes. We define the zenith angle θ_z at the South Pole

to be the angle centered at the detector with $\theta_z = 0°$ indicating the vertical direction in the sky. θ_z can be parametrized in terms of the time of the year f_y (where $f_y = 0, 1/2$ correspond to the March and September equinoxes, respectively), and the tilt of the Earth axis with respect to the perpendicular to the ecliptic plane, $\theta_t = 23°26'$:

$$\theta_z(f_y) = \frac{\pi}{2} + \theta_t \sin(2\pi f_y)\,. \tag{34}$$

The event rate reads,

$$N^{Up}_{events} = \xi\Gamma_{eq}\int_0^{m_X} \frac{d\Phi_\mu}{dE_{\mu f}}\langle A_{eff}(E_{\mu f})R(\cos\theta_z)\rangle dE_{\mu f}, \tag{35}$$

where ξ and Γ_{eq} are the quantities introduced in Sec. 3.2.1. $\langle A_{eff}(E_{\mu f})R(\cos\theta_z)\rangle$ is the average over the portion of the solid angle (θ_z, ϕ) that corresponds to the time the Sun spends below the horizon.

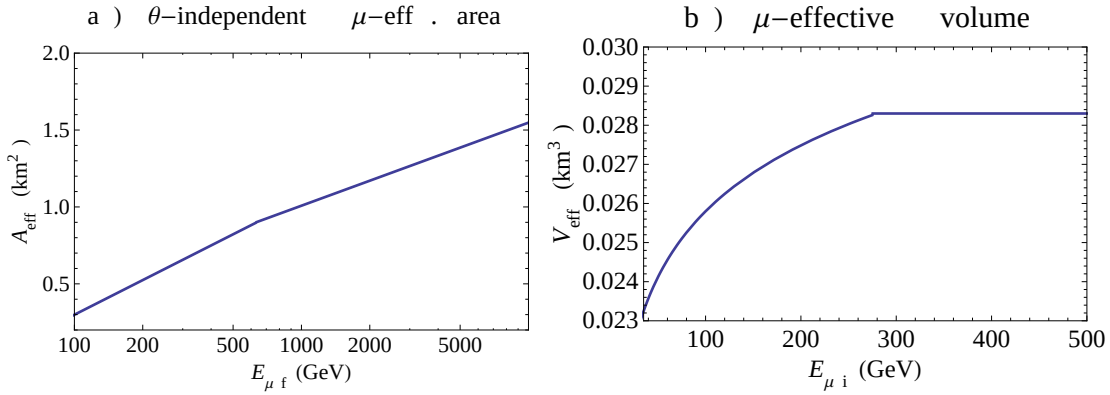

Figure 13: a) The IceCube muon effective area with zenith angle dependence factored out. b) Muon effective volume for DeepCore.

Contained Events at IceCube

For neutrinos that interact within the detector volume, the resulting muons do not lose an appreciable fraction of their energies. Following notation similar to the previous subsection (except that we identify $E_\mu \equiv E_{\mu i}$ since the muons do not propagate) the muon flux for contained events is given by,

$$\frac{d\Phi_\mu}{dE_\mu} = L \int_{E_\mu}^{m_X} dE_\nu \left[\frac{d\Phi_\nu}{dE_\nu} \left(\frac{d\sigma_{\nu p}^{CC}}{dE_\mu}(E_\nu)\rho_p + \frac{d\sigma_{\nu n}^{CC}}{dE_\mu}(E_\nu)\rho_n \right) + (\nu \to \bar{\nu}) \right] , \tag{36}$$

where $L \sim 1$ km is the size of the IceCube detector. The event rate reads,

$$N_{events}^{C} = \xi \Gamma_{eq} \int_{E_{thr}}^{m_X} \frac{d\Phi_\mu}{dE_\mu} (1 \text{ km}^2) dE_\mu \, , \tag{37}$$

where $E_{thr} = 100$ GeV is the energy threshold of the IceCube detector. As mentioned above, we only consider events observed between the March and September equinoxes.

Events at DeepCore

The great advantage of DeepCore with respect to IceCube is that the outer instrumented volume of IceCube will serve as a veto to atmospheric muon events up to one part in 10^6 [72], so that data can be collected throughout the year, i.e., even when the Sun is above the horizon. The rate for contained events at DeepCore can be calculated by convolving Eq. (36) with the muon *effective volume* $V_{eff}(E_{\mu i})$. In the most optimistic estimates the effective volume is constant for muon energies above ~ 300 GeV, and drops significantly at lower energies [74]. As explained in Sec. 3.2.3, for DeepCore we consider the interval $E_{\mu i} > E_{min} = 35$ GeV. We find that in this

interval the effective volume in km^3 can be parametrized by

$$V_{eff}(E_{\mu i}) = (0.0056 \log E_{\mu i} + 0.0146)\Theta(275 - E_{\mu i}) + 0.0283\Theta(E_{\mu i} - 275)\,, \qquad (38)$$

where Θ is the Heaviside step function and $E_{\mu i}$ is in GeV. The effective volume is plotted in Fig. 13b.

After convolution one gets

$$N_{events}^{DC} = \xi\Gamma_{eq}\int_{E_{min}}^{m_X} \frac{1}{L}\frac{d\Phi_\mu}{dE_\mu}V_{eff}(E_\mu)dE_\mu\,. \qquad (39)$$

.3 Atmospheric Background

The angle-dependent flux of atmospheric neutrinos $d\Phi_\nu^{atm}/(dE_\nu d\cos\theta)$ is given in [76]. These neutrinos interact with the medium surrounding the detector and produce muons that constitute the background. As in the case of neutrinos from annihilation, the atmospheric background can be divided in upward and contained events.

By following the notation introduced in the previous subsections we can write the angular dependence of the upward background flux for IceCube as

$$\begin{aligned}\frac{d\Phi_\mu^{atm}}{dE_{\mu f} d\cos\theta_z(f_y)} &= \int_0^{R_\mu(E_{Max},E_{\mu f})} dz e^{\beta\rho_{ice}z} P_{sur}(E_i(E_{\mu f},z),E_{\mu f}) \\ &\times \int_{E_i(E_{\mu f},z)}^{E_{Max}} dE_\nu \left[\frac{d\Phi_\nu^{atm}}{dE_\nu d\cos\theta_z(f_y)}\left(\frac{d\sigma_{\nu p}^{CC}}{dE_i}(E_\nu)\rho_p + \frac{d\sigma_{\nu n}^{CC}}{dE_i}(E_\nu)\rho_n\right)\right. \\ &+ \left.(\nu\to\bar{\nu})\right] , \end{aligned} \tag{40}$$

where $E_{Max} \sim 10^4$ GeV is the maximum energy above which the rapidly falling atmospheric flux becomes negligible. The angle-dependent flux, Eq. (40), is integrated over a cone of solid angle $d\Omega = \pi(d\theta)^2$, where the opening angle (half the apex angle) $d\theta \sim 1^\circ$, consistent with the IceCube angular sensitivity [72, 77]. The cone tracks the Sun according to Eq. (34), for the fraction of the year over which the Sun is below the horizon. The number of upward background events for IceCube can be calculated by folding in the effective area $A_{eff}(E_{\mu f})R(\cos\theta_z)$. We find $N_{BG}^{Up} \simeq 6.1$ yr^{-1} where, again, data is taken only between the March and September Equinoxes.

Contained events are those obtained by muon-neutrinos undergoing charged current interactions within the detector volume, thus the angular dependence of the flux

is given by

$$\frac{d\Phi_\mu^{atm}}{dE_\mu d\cos\theta_z(f_y)} = L\int_{E_\mu}^{E_{Max}} dE_\nu \left(\rho_p \frac{d\sigma_\nu^p(E_\nu,E_\mu)}{dE_\mu} + \rho_n \frac{d\sigma_\nu^n(E_\nu,E_\mu)}{dE_\mu} + \right) \frac{d\Phi_\nu^{atm}}{dE_\nu d\cos\theta_z(f_y)} + (\nu \to \bar{\nu})\,. \quad (41)$$

The number of contained background events in a cone of 1° opening for time of exposure limited to the period between March and September is obtained, as in Eq. (37), by convolving with a constant 1 km^2 area. We get $N_{BG}^{Con} \simeq 15.6$ yr^{-1}.

The number of background events for DeepCore over the whole year, obtained by convolving with $V_{eff}(E_{\mu i})/L$, is $N_{BG}^{DC} \simeq 2.5$ yr^{-1}.

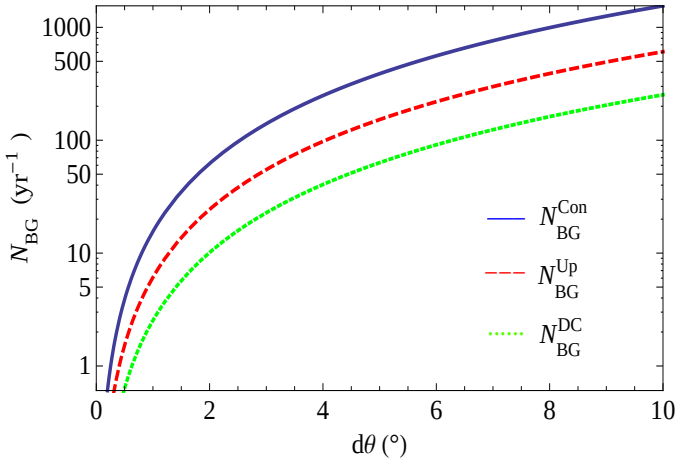

Figure 14: Number of background events per year as a function of the opening angle $d\theta$.

In Fig. 14 we show the dependence of N_{BG}^{Up}, N_{BG}^{Con} and N_{BG}^{DC} on the opening angle $d\theta$. The thin blue horizontal lines shown in Figs. 6-11 represent the five-year 3σ-discovery reach for $d\theta = 1°$. While the angular resolution is expected to be best for directions close to the horizon (and the Sun does not stray more than 23°26' from the horizon at the South Pole), in case the angular resolution of the IceCube and DeepCore detectors do not meet expectations, the background event rates can

be obtained from Fig. 14. Then, for a 3σ-detection, $N_\mu = 3\sqrt{N_{BG}}$ can be trivially recalculated.

Bibliography

[1] P. Langacker, *In *Langacker, P. (ed.): Precision tests of the standard electroweak model* 3-11*

[2] G. Jungman, M. Kamionkowski and K. Griest, Phys. Rept. **267**, 195 (1996) [arXiv:hep-ph/9506380].

[3] J. L. Feng and J. Kumar, Phys. Rev. Lett. **101**, 231301 (2008) [arXiv:0803.4196 [hep-ph]].

[4] J. L. Feng, J. Kumar and L. E. Strigari, Phys. Lett. B **670**, 37 (2008) [arXiv:0806.3746 [hep-ph]]; J. L. Feng, H. Tu and H. B. Yu, JCAP **0810**, 043 (2008) [arXiv:0808.2318 [hep-ph]].

[5] J. L. Feng, J. Kumar, J. Learned and L. E. Strigari, JCAP **0901**, 032 (2009) [arXiv:0808.4151 [hep-ph]].

[6] J. L. Feng, H. Tu and H. B. Yu, JCAP **0810**, 043 (2008) [arXiv:0808.2318 [hep-ph]].

[7] J. L. Feng, M. Kaplinghat, H. Tu and H. B. Yu, JCAP **0907**, 004 (2009) [arXiv:0905.3039 [hep-ph]].

[8] H. Baer and X. Tata, "Weak scale supersymmetry: From superfields to scattering events," *Cambridge, UK: Univ. Pr. (2006) 537 p*

[9] J. Wess and B. Zumino, Nucl. Phys. B **70**, 39 (1974).

[10] C. Amsler *et al.* [Particle Data Group], Phys. Lett. B **667**, 1 (2008).

[11] G. R. Farrar and P. Fayet, Phys. Lett. B **76**, 575 (1978).

[12] S. Dimopoulos and L. J. Hall, Phys. Lett. B **207**, 210 (1988).

[13] V. D. Barger, G. F. Giudice and T. Han, Phys. Rev. D **40**, 2987 (1989).

[14] H. K. Dreiner and G. G. Ross, Nucl. Phys. B **365**, 597 (1991).

[15] R. Barbier *et al.*, Phys. Rept. **420**, 1 (2005) [arXiv:hep-ph/0406039].

[16] S. Dimopoulos, S. Raby and F. Wilczek, Phys. Lett. B **112**, 133 (1982).

[17] G. Bhattacharyya and P. B. Pal, Phys. Rev. D **59**, 097701 (1999) [arXiv:hep-ph/9809493].

[18] L. J. Hall and M. Suzuki, Nucl. Phys. **B231**, 419 (1984).

[19] I. H. Lee, Phys. Lett. B **138**, 121 (1984).

I. H. Lee, Nucl. Phys. B **246**, 120 (1984).

[20] S. Dawson, Nucl. Phys. B **261**, 297 (1985).

[21] A. Sirlin, Phys. Rev. D **22**, 971 (1980).

[22] W. J. Marciano and A. Sirlin, Phys. Rev. Lett. **56**, 22 (1986).

W. J. Marciano and A. Sirlin, Phys. Rev. Lett. **61**, 1815 (1988).

[23] The *on shell* and $\overline{MS}$ renormalization schemes are widely used and references can be found in [10]. For the NOV scheme, the original reference is: V. A. Novikov, L. B. Okun and M. I. Vysotsky, Nucl. Phys. B **397**, 35 (1993).

[24] W. J. Marciano and J. L. Rosner, Phys. Rev. Lett. **65**, 2963 (1990) [Erratum-ibid. **68**, 898 (1992)].

S. Fanchiotti, B. A. Kniehl and A. Sirlin, Phys. Rev. D **48**, 307 (1993) [arXiv:hep-ph/9212285].

[25] H. K. Dreiner, M. Kramer and B. O'Leary, Phys. Rev. D **75**, 114016 (2007) [arXiv:hep-ph/0612278].

[26] P. Vilain *et al.* [CHARM-II Collaboration], Phys. Lett. B **335**, 246 (1994).

[27] F. Reines, H. Gurr and H. Sobel, Phys. Rev. Lett. **37**, 315 (1976).

[28] L. Auerbach *et al.* (LSND Collaboration), Phys. Rev. D **63**, 112001 (2001).

[29] C. Amsler *et al.* (Bugey Collaboration)., Phys. Lett. B **545**, 57 (2002).

[30] J. Barranco, O. Miranda, C. Moura and J. Valle, Phys. Rev. D **73**, 113001 (2006).

[31] J. Barranco, O. Miranda, C. Moura and J. Valle, Phys. Rev. D **77**, 093014 (2008).

[32] A. Bolanos, O. G. Miranda, A. Palazzo, M. A. Tortola and J. W. F. Valle, Phys. Rev. D **79**, 113012 (2009) [arXiv:0812.4417 [hep-ph]].

[33] W. J. Marciano and Z. Parsa, J. Phys. G **29**, 2629 (2003) [arXiv:hep-ph/0403168].

[34] F. T. Avignone, Phys. Rev. D **2**, 2609 (1970).

[35] For a complete account of the definition of mSUGRA and its mass spectrum, see Reference [8], Chap. 9 pp. 204-214.

[36] A. Heister *et al.* [ALEPH Collaboration], Eur. Phys. J. C **28**, 1 (2003).

P. Abreu *et al.* [DELPHI Collaboration], Eur. Phys. J. C, **17**, 53, (2000).

M. Acciarri *et al.* [L3 Collaboration], Phys. Lett. B **470**, 268 (1999).

G. Abbiendi *et al.* [OPAL Collaboration], Eur. Phys J. C **18** 253 (2000).

[37] T. Adams *et al.* [NuSOnG Collaboration], Int. J. Mod. Phys. A **24**, 671 (2009) [arXiv:0803.0354 [hep-ph]].

[38] R. N. Mohapatra, Phys. Rev. D **34**, 3457 (1986).

K. S. Babu and R. N. Mohapatra, Phys. Rev. Lett. **75**, 2276 (1995) [arXiv:hep-ph/9506354].

M. Hirsch, H. V. Klapdor-Kleingrothaus and S. G. Kovalenko, Phys. Rev. Lett. **75**, 17 (1995).

[39] L. Wolfenstein, Phys. Rev. Lett. **51**, 1945 (1983).

[40] F. Halzen and A. D. Martin, "Quarks And Leptons: An Introductory Course In Modern Particle Physics," *New York, Usa: Wiley (1984) 396p*

[41] E. A. Paschos, "Electroweak theory," *Cambridge, UK: Univ. Pr. (2007) 245 p*

[42] M. Chemtob and G. Moreau, Phys. Rev. D **59**, 116012 (1999) [arXiv:hep-ph/9806494].

[43] C. S. Wood, S. C. Bennett, D. Cho, B. P. Masterson, J. L. Roberts, C. E. Tanner and C. E. Wieman, Science **275**, 1759 (1997).

[44] J. Guena, M. Lintz and M. A. Bouchiat, Phys. Rev. A **71**, 042108 (2005) [arXiv:physics/0412017].

[45] G. Altarelli, G. F. Giudice and M. L. Mangano, Nucl. Phys. B **506**, 29 (1997) [arXiv:hep-ph/9705287].

[46] Since we take ratios of decay rates and we assume universality, we do not deal with hadronization effects in this paper. Discrepancies between experimental measurements of the D_s decay constant and the related lattice calculations can be used to place bounds on some λ' couplings. See, for example, A. Kundu and S. Nandi, Phys. Rev. D **78**, 015009 (2008) [arXiv:0803.1898 [hep-ph]].

[47] G. Wikstrom and J. Edsjo, JCAP **0904**, 009 (2009) [arXiv:0903.2986 [astro-ph.CO]].

[48] D. Hooper, F. Petriello, K. M. Zurek and M. Kamionkowski, Phys. Rev. D **79**, 015010 (2009) [arXiv:0808.2464 [hep-ph]]; J. L. Feng, J. Kumar, J. Learned and L. E. Strigari, arXiv:0808.4151 [hep-ph]; J. Kumar, J. G. Learned and S. Smith, Phys. Rev. D **80**, 113002 (2009) [arXiv:0908.1768 [hep-ph]]; V. Niro, A. Bottino, N. Fornengo and S. Scopel, Phys. Rev. D **80**, 095019 (2009) [arXiv:0909.2348 [hep-ph]].

[49] A. Bottino, F. Donato, N. Fornengo and S. Scopel, Phys. Rev. D **69**, 037302 (2004) [arXiv:hep-ph/0307303]; P. Gondolo and G. Gelmini, Phys. Rev. D **71**, 123520 (2005) [arXiv:hep-ph/0504010]; R. Bernabei *et al.*, Eur. Phys. J. C **53**, 205 (2008) [arXiv:0710.0288 [astro-ph]]; F. Petriello and K. M. Zurek, JHEP **0809**, 047 (2008) [arXiv:0806.3989 [hep-ph]]; A. Bottino, F. Donato, N. Fornengo and S. Scopel, Phys. Rev. D **78**, 083520 (2008) [arXiv:0806.4099 [hep-ph]]. S. Chang, A. Pierce and N. Weiner, arXiv:0808.0196 [hep-ph]; C. Savage, G. Gelmini, P. Gondolo and K. Freese, JCAP **0904**, 010 (2009) [arXiv:0808.3607 [astro-ph]].

[50] M. Fairbairn and T. Schwetz, JCAP **0901**, 037 (2009) [arXiv:0808.0704 [hep-ph]].

[51] Z. Ahmed *et al.* [The CDMS-II Collaboration], arXiv:0912.3592 [astro-ph.CO].

[52] C. E. Aalseth *et al.* [CoGeNT Collaboration], arXiv:1002.4703 [astro-ph.CO].

[53] A. Bottino, F. Donato, N. Fornengo and S. Scopel, arXiv:0912.4025 [hep-ph]; A. L. Fitzpatrick, D. Hooper and K. M. Zurek, arXiv:1003.0014 [hep-ph]; D. Feldman, Z. Liu and P. Nath, arXiv:1003.0437 [hep-ph]; E. Kuflik, A. Pierce and K. M. Zurek, arXiv:1003.0682 [hep-ph].

[54] G. Bertone, D. G. Cerdeno, J. I. Collar and B. C. Odom, Phys. Rev. Lett. **99**, 151301 (2007) [arXiv:0705.2502 [astro-ph]]; V. Barger, W. Y. Keung and G. Shaughnessy, Phys. Rev. D **78**, 056007 (2008) [arXiv:0806.1962 [hep-ph]]; G. Belanger, E. Nezri and A. Pukhov, Phys. Rev. D **79**, 015008 (2009) [arXiv:0810.1362 [hep-ph]]; T. Cohen, D. J. Phalen and A. Pierce, arXiv:1001.3408 [hep-ph]; P. Agrawal, Z. Chacko, C. Kilic and R. K. Mishra, arXiv:1003.1912 [hep-ph]; P. Agrawal, Z. Chacko, C. Kilic and R. K. Mishra, arXiv:1003.5905 [hep-ph].

[55] J. Braun and D. Hubert for the IceCube Collaboration, arXiv:0906.1615 [astro-ph.HE].

[56] E. Aprile *et al.* [XENON100 Collaboration], arXiv:1005.0380 [astro-ph.CO].

[57] M. Dine and A. E. Nelson, Phys. Rev. D **48**, 1277 (1993) [arXiv:hep-ph/9303230]; M. Dine, A. E. Nelson, Y. Nir and Y. Shirman, Phys. Rev. D **53**, 2658 (1996) [arXiv:hep-ph/9507378].

[58] Ya. B. Zeldovich, Adv. Astron. Astrophys. **3**, 241 (1965); H.Y. Chiu, Phys. Rev. Lett. **17**, 712 (1966); G. Steigman, Ann. Rev. Nucl. Part. Sci. **29**, 313 (1979); R.J. Scherrer and M.S. Turner, Phys. Rev. D **33**, 1585 (1986).

[59] H. J. He, N. Polonsky and S. f. Su, Phys. Rev. D **64**, 053004 (2001) [arXiv:hep-ph/0102144]; J. Alwall *et al.*, Eur. Phys. J. C **49**, 791 (2007) [arXiv:hep-ph/0607115]; G. D. Kribs, T. Plehn, M. Spannowsky and T. M. P. Tait, Phys. Rev. D **76**, 075016 (2007) [arXiv:0706.3718 [hep-ph]]; R. Fok and G. D. Kribs, Phys. Rev. D **78**, 075023 (2008) [arXiv:0803.4207 [hep-ph]]; B. Holdom, W. S. Hou, T. Hurth, M. L. Mangano, S. Sultansoy and G. Unel, PMC Phys. A **3**, 4 (2009) [arXiv:0904.4698 [hep-ph]]; M. Hashimoto, arXiv:1001.4335 [hep-ph].

[60] V. M. Abazov *et al.* [D0 Collaboration], Phys. Rev. Lett. **97**, 171806 (2006) [arXiv:hep-ex/0608013]; T. Aaltonen *et al.* [CDF Collaboration], Phys. Rev. D **76**, 072010 (2007) [arXiv:0707.2567 [hep-ex]].

[61] J. Alwall, J. L. Feng, J. Kumar and S. Su, arXiv:1002.3366 [hep-ph].

[62] T. Aaltonen *et al.* [The CDF Collaboration], arXiv:0912.4691 [hep-ex].

[63] G. K. Mallot, in *Proc. of the 19th Intl. Symp. on Photon and Lepton Interactions at High Energy (LP99), 9-14 August 1999, Stanford, California*, edited by J.A. Jaros and M.E. Peskin (World Scientific, Singapore, 2000), pp 521-537 [arXiv:hep-ex/9912040].

[64] J. R. Ellis, K. A. Olive and C. Savage, Phys. Rev. D **77**, 065026 (2008) [arXiv:0801.3656 [hep-ph]].

[65] M. A. Shifman, A. I. Vainshtein and V. I. Zakharov, Phys. Lett. B **78**, 443 (1978).

[66] K. Griest and D. Seckel, Nucl. Phys. B **283**, 681 (1987) [Erratum-ibid. B **296**, 1034 (1988)].

[67] J. Ellis, K. A. Olive, C. Savage and V. C. Spanos, arXiv:0912.3137 [hep-ph].

[68] A. Gould, Astrophys. J. **321**, 571 (1987); Astrophys. J. **388**, 338 (1992).

[69] T. Sjostrand, S. Mrenna and P. Z. Skands, JHEP **0605**, 026 (2006) [arXiv:hep-ph/0603175].

[70] S. Dimopoulos, S. D. Thomas and J. D. Wells, Nucl. Phys. B **488**, 39 (1997) [arXiv:hep-ph/9609434].

[71] M. Blennow, J. Edsjo and T. Ohlsson, JCAP **0801**, 021 (2008) [arXiv:0709.3898 [hep-ph]].

[72] E. Resconi [IceCube Collaboration], Nucl. Instrum. Meth. A **602**, 7 (2009) [arXiv:0807.3891 [astro-ph]].

[73] O. Schulz [IceCube Collaboration], AIP Conf. Proc. **1085**, 783 (2009).

[74] T. DeYoung, private communication.

[75] D. Grant, private communication.

[76] M. Honda, T. Kajita, K. Kasahara, S. Midorikawa and T. Sanuki, Phys. Rev. D **75**, 043006 (2007) [arXiv:astro-ph/0611418].

[77] A. E. Erkoca, M. H. Reno and I. Sarcevic, Phys. Rev. D **80**, 043514 (2009) [arXiv:0906.4364 [hep-ph]].

[78] S. Desai *et al.* [Super-Kamiokande Collaboration], Phys. Rev. D **70**, 083523 (2004) [Erratum-ibid. D **70**, 109901 (2004)] [arXiv:hep-ex/0404025].

[79] S. K. Mandal, M. R. Buckley, K. Freese, D. Spolyar and H. Murayama, Phys. Rev. D **81**, 043508 (2010) [arXiv:0911.5188 [hep-ph]].

[80] T. Stanev, Phys. Rev. Lett. **83**, 5427 (1999) [arXiv:astro-ph/9907018].

[81] E. Middell, J. McCartin and M. D'Agostino [IceCube Collaboration], in the proceedings of The 31st International Cosmic Ray Conference (ICRC 2009), 7-15 July 2009, Lodz, Poland, 2009.

[82] M. Cirelli, N. Fornengo, T. Montaruli, I. Sokalski, A. Strumia and F. Vissani, Nucl. Phys. B **727**, 99 (2005) [Erratum-ibid. B **790**, 338 (2008)] [arXiv:hep-ph/0506298].

[83] C. Amsler *et al.* [Particle Data Group], Phys. Lett. B **667**, 1 (2008).

[84] V. Barger, W. Y. Keung, G. Shaughnessy and A. Tregre, Phys. Rev. D **76**, 095008 (2007) [arXiv:0708.1325 [hep-ph]].

[85] J. N. Bahcall, M. H. Pinsonneault and S. Basu, Astrophys. J. **555**, 990 (2001) [arXiv:astro-ph/0010346].

[86] S. I. Dutta, M. H. Reno and I. Sarcevic, Phys. Rev. D **62**, 123001 (2000) [arXiv:hep-ph/0005310].

[87] P. Lipari, Astropart. Phys. **1**, 195 (1993).

[88] P. Lipari and T. Stanev, Phys. Rev. D **44**, 3543 (1991).

[89] D. Chirkin and W. Rhode, arXiv:hep-ph/0407075.

[90] Y. Gao, private communication.

[91] M. C. Gonzalez-Garcia, F. Halzen and S. Mohapatra, Astropart. Phys. **31**, 437 (2009) [arXiv:0902.1176 [astro-ph.HE]].